LBNL-42352

ERNEST ORLANDO LAWRENCE
BERKELEY NATIONAL LABORATORY

Gas Phase Chromatography of Some Group 4, 5, and 6 Halides

Eric Robert Sylwester

Nuclear Science Division

October 1998

Ph.D. Thesis

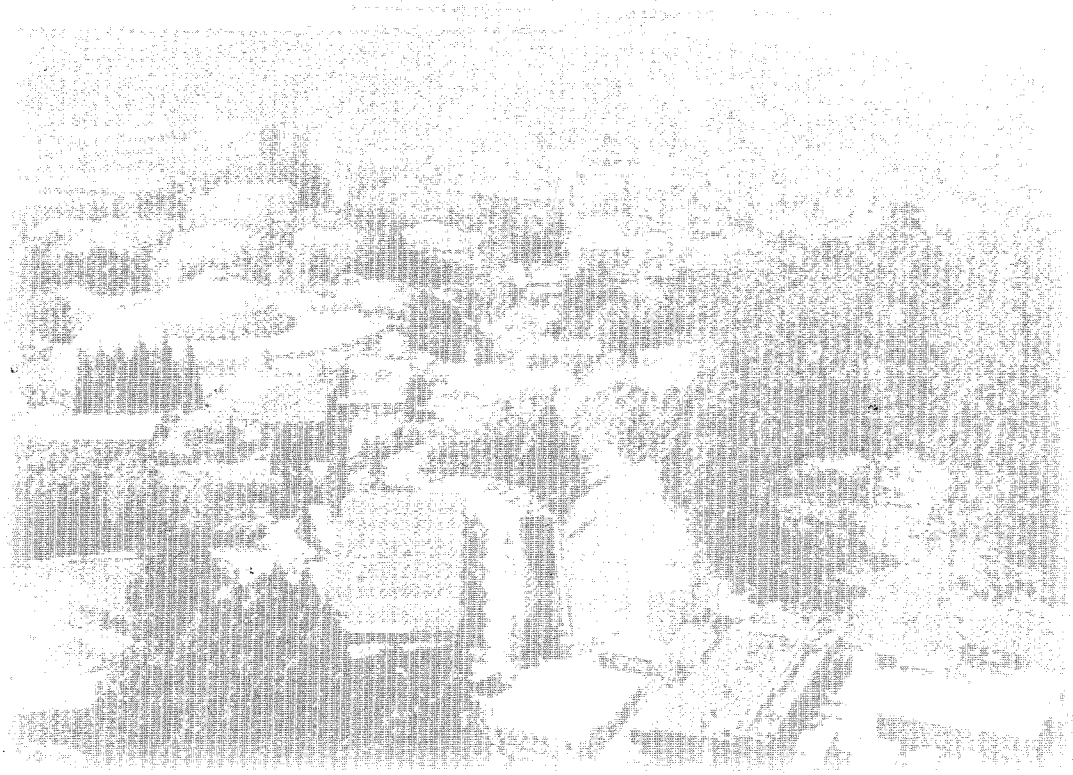

DISCLAIMER

Portions of this document may be illegible in electronic image products. Images are produced from the best available original document.

LBNL-42352

Gas Phase Chromatography of some Group 4, 5, and 6 Halides

Eric Robert Sylwester

Ph.D Thesis

Department of Chemistry
University of California
Berkeley, CA 94720

and

Nuclear Science Division
Lawrence Berkeley National Laboratory
Berkeley, CA 94720

This research was supported in part by the Office of Energy Research, Office of Basic Energy Sciences, Division of Chemical Sciences, US Department of Energy, under Contract DE-AC03-76SF00098

Gas Phase Chromatography of some Group 4, 5, and 6 Halides

by

Eric Robert Sylwester

B.S. (The College of William and Mary) 1991

A dissertation submitted in partial satisfaction of the requirements for the degree of

Doctor of Philosophy in Nuclear Chemistry

in the

Graduate Division

of the

University of California, Berkeley

Committee in charge:

Professor Emeritus Darleane C. Hoffman, Chair
Professor Stanley Prussin
Professor Emeritus John Rassmussen

Fall 1998

Gas Phase Chromatography of Some Group 4, 5, and 6 Halides

by

Eric Robert Sylwester

Abstract

Gas Phase Chromatography of some Group 4, 5, and 6 Halides.

by

Eric Robert Sylwester

Doctor of Philosophy in Chemistry

University of California at Berkeley

Professor Darleane C. Hoffman, Chair

Gas phase chromatography using The Heavy Element Volatility Instrument (HEVI) and the On Line Gas Apparatus (OLGA III) was used to determine volatilities of $ZrBr_4$, $HfBr_4$, $RfBr_4$, $NbBr_5$, $TaOBr_3$, $HaCl_5$, WBr_6, FrBr, and $BiBr_3$.

Short-lived isotopes of Zr, Hf, Rf, Nb, Ta, Ha, W, and Bi were produced via compound nucleus reactions at the 88-Inch Cyclotron at Lawrence Berkeley National Laboratory and transported to the experimental apparatus using a He gas transport system. The isotopes were halogenated, separated from the other reaction products, and their volatilities determined by isothermal gas phase chromatography.

Adsorption Enthalpy (ΔH_a) values for these compounds were calculated using a Monte Carlo simulation program modeling the gas phase chromatography column. All bromides showed lower volatility than molecules of similar molecular structures formed as chlorides, but followed similar trends by central element. Tantalum was observed to form the oxybromide, analogous to the formation of the oxychloride under the same conditions. For the group 4 elements, the following order in volatility and ΔH_a was observed: $RfBr_4 > ZrBr_4 > HfBr_4$. The ΔH_a values determined for the group 4, 5, and 6 halides are in general agreement with other experimental data and theoretical predictions. Preliminary experiments were performed on Mo-bromides.

A new measurement of the half-life of ^{261}Rf was performed. ^{261}Rf was produced via the ^{248}Cm(^{18}O, 5n) reaction and observed with a half-life of 74^{+7}_{-6} seconds, in excellent agreement with the previous measurement of 78^{+11}_{-6} seconds. We recommend a new half-life of 75±7 seconds for ^{261}Rf based on these two measurements.

Preliminary studies in transforming HEVI from an isothermal (constant temperature) gas phase chromatography instrument to a thermochromatographic (variable temperature) instrument have been completed. Thermochromatography is a technique that can be used to study the volatility and ΔH_a of longer-lived isotopes off-line. Future work will include a comparison between the two techniques and the use of

thermochromatography to study isotopes in a wider range of half-lives and molecular structures.

Table of Contents

List of Figures

List of Tables

Acknowledgements

I would like to thank my advisor, Dr. Darleane Hoffman, for her unwavering support throughout my (long) time in her group. I would also like to thank Dr. Ken Gregorich and Diana Lee for their invaluable help in the numerous details of my cyclotron experiments, ranging from set-up to the data acquisition and analyses, and everything else in between.

I am indebted to the members of the Hoffman research group for their assistance during the experiments, and to Heinz Gäggeler and Andreas Türler for their advice and collaborative work with OLGAs II and III.

Finally, I would like to thank my friends and family for their patience and continual moral support during the last year.

Gas Phase Chromatographpy of Bromides and Chlorides of Transactinides and their Group 4, 5, and 6 Homologs

1. Introduction

The discovery and investigation of new elements is one of the oldest and yet most challenging and important areas of study in the field of chemistry. After the discovery of artificial radiation in 1935 and nuclear fission in 1939, chemists began extending the known periodic table of the elements via the creation of new elements beyond uranium, unstable and having half-lives which vary from millions of years to microseconds or less[1]. By 1974, the elements through seaborgium had been discovered. The importance of some of these discoveries on modern society is obvious; the impact of plutonium alone on society has been enormous. Less obvious, but of far more importance to modern science, is the contribution of these discoveries to our basic knowledge of the structure of the atom. By creating and investigating new elements we not only determine the specific properties of these new elements, we also investigate the periodic trends in the properties of these elements, which were represented by Dmitri Mendeleev in his periodic table of 1869 [Hudson 92, Moore 39]. The elements through 112 are now known, and the periodic table as of early 1998 [D Hoffman 98] is shown in Figure 1-1. Figure 1-2 shows the known isotopes of the transactinides as of mid-1997 [D Hoffman 97] and Table 1-1 shows the names approved[2] by the International Union of Pure and Applied Chemistry

---

[1] For a review of the discovery of the elements from Np through 110, see G.T. Seaborg's book "The Elements Beyond Uranium" and referenced in this work as [Seaborg 90]. The discovery experiments for elements 111 and 112 are given in [S Hofmann, 95, 96], respectively.

[2] The names used in this document and in Figures 1-1 and 1-2 for the tranuranium elements are those approved by IUPAC in August, 1997, except that we will continue to use hahnium (Ha) for element 105.

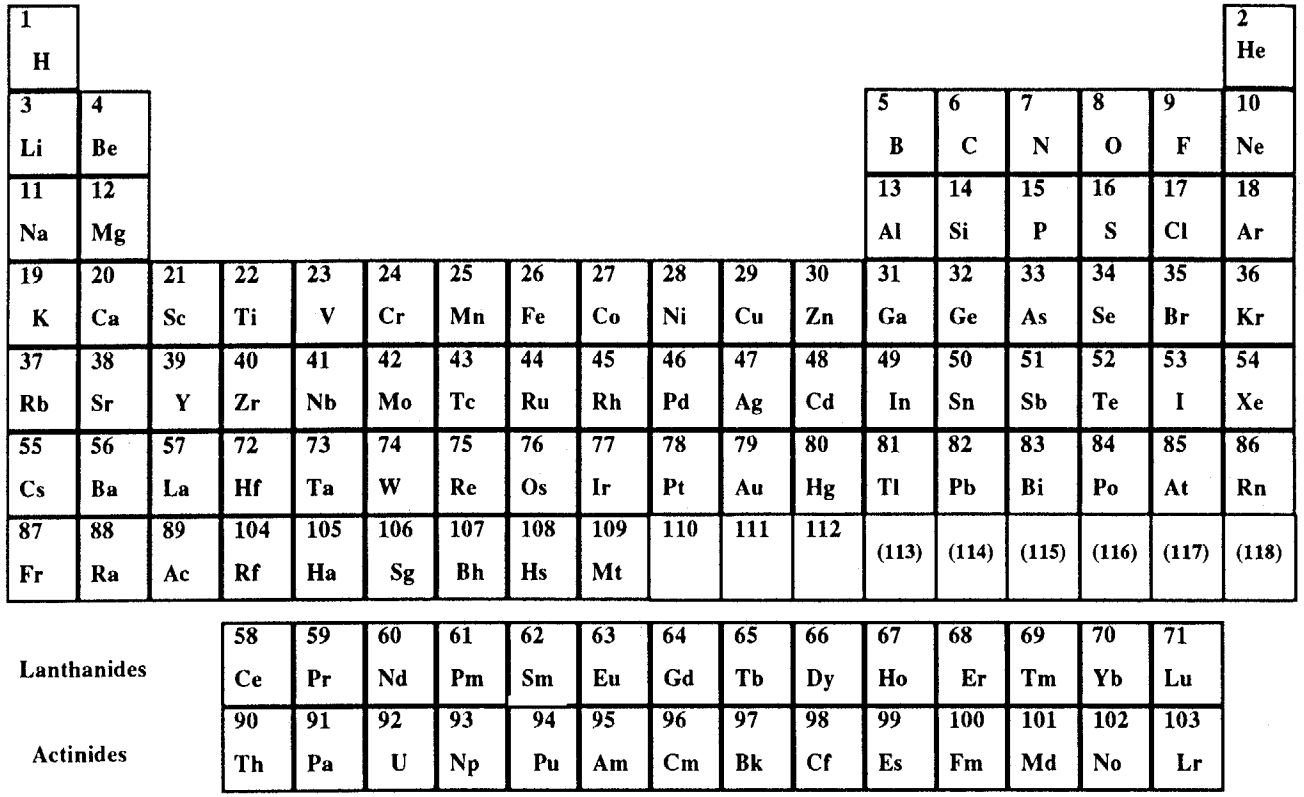

Figure 1-1: Periodic Table of the Elements as of April, 1998.

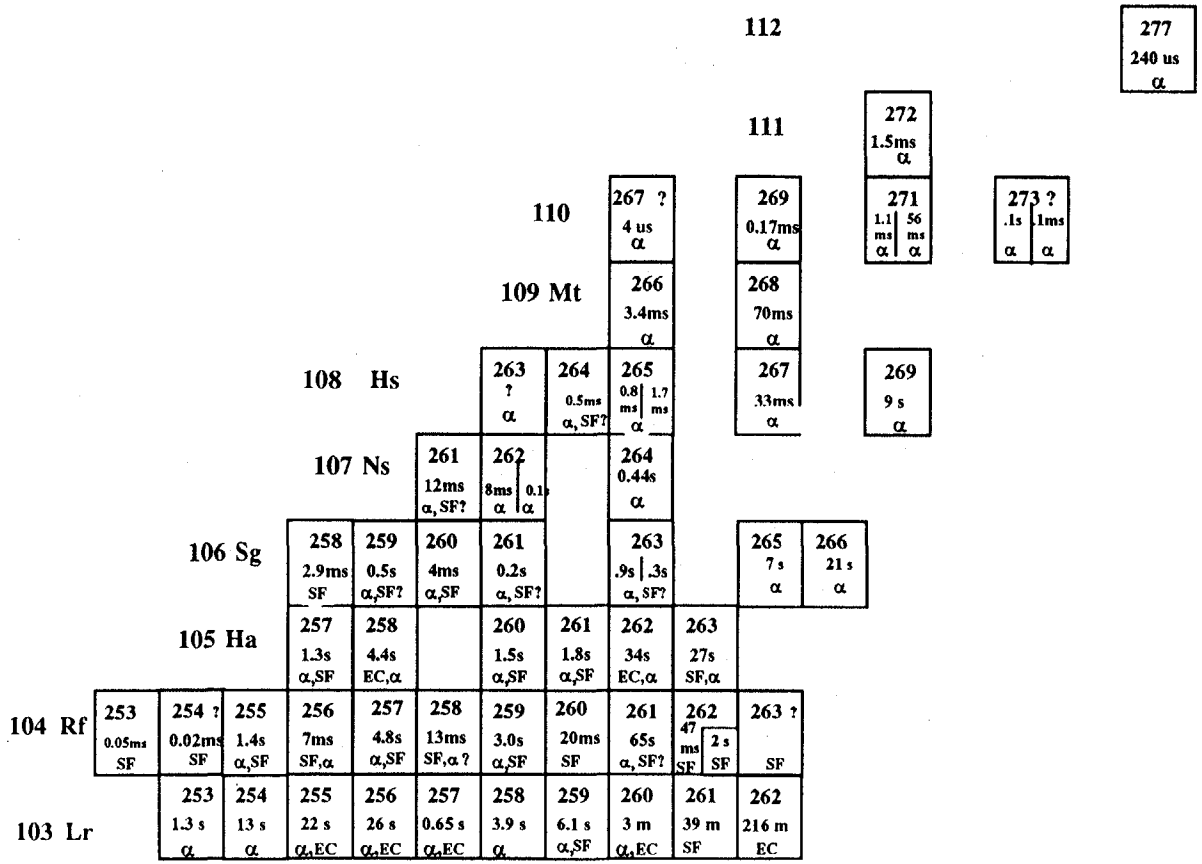

Figure 1-2: Chart of the Nuclides for the transactinide elements as of mid-1997.
Reproduced from [D Hoffman 97].

Table 1-1 Names approved by IUPAC for the elements 101-109 August 31, 1997

Element	Name	Symbol
101	Mendelevium	Md
102	Nobelium	No
103	Lawrencium	Lr
104	Rutherfordium	Rf
105	Dubnium	Db
106	Seaborgium	Sg
107	Bohrium	Bh
108	Hassium	Hs
109	Meitnerium	Mt

(IUPAC) for elements 101 through 109 in 1997. By aligning the known elements according to their properties, Mendeleev hoped to use the trends in their properties- either down the rows or across the columns- to predict the chemical properties of as yet unknown or unstudied elements.

Today, by testing our theories concerning the underlying physical basis for these trends, we increase our ability to predict the properties of new elements before they are discovered and to more accurately predict the chemical properties and behavior of the older, more familiar elements. Not surprisingly, the periodic table of the elements reflects some of the general structure of the atom. The rows and columns of the modern periodic table represent the electronic shell structure of the atoms listed. Electronic shell structure determines the oxidation states and bonding characteristics of the atom, which is the basis of its chemistry.

When the production of the transuranium elements was first undertaken in 1940 and 1941, their chemical properties were used to determine whether the isotope created was that of a new element or merely a new isotope of an already existing element [Seaborg 46,90, McMillan 40]. The electronic shell structure of new atoms is still of the utmost importance to researchers, not only for the value of scientific discovery, but also for the ability to use this information as a method of identifying and separating newly created elements from new isotopes of previously discovered elements.

However, predicting the electronic structure of the transactinides is especially difficult because of the presence of *relativistic effects*. These effects are the changes occuring in the structure of an atom which arise from the differences in the rest mass (m_0; 5.486×10^{-4} amu) of the electrons, and the actual mass of the electrons given by Einstein's theory of relativity:

$$m = \frac{m_0}{\left(1 - (v/c)\right)^2} \qquad (1)$$

Where m_0 is the rest mass and v is the speed of the electron. The increase in mass will cause the inner s and p shells of the atom to contract. Due to the requirement that the wave functions of these shells must be orthogonal with the lower ones, this will in turn cause a contraction in all the s-shell and $p_{1/2}$-shell electrons, including the valence shell electrons.

As an example, we can look at the simplest case, hydrogen. An increase in the electron mass in hydrogen will have a direct effect on the Bohr radius, a_0, which can be seen to decrease:

$$a_o = (4\pi\varepsilon_o)(\eta^2/me^2) \tag{2}$$

Fricke and Greiner first discussed the possible influence of relativistic effects on the properties of the atom in 1969 [Fricke 69]. Pitzer was also responsible for some of the early theoretical work on relativistic effects, and even predicted they might cause elements 112 and 114 to behave as pseudo-noble gasses rather than like the other group 12 and 14 elements [Pitzer 75]. Pyykkö [Pyykkö 84, 86, 88] and others [Grant 70, 86, Lindgren 74, Malli 83, Kelly 86] have studied the theoretical limits of these relativistic contractions on the electrons in the other shells (p, d, f), and have calculated the effects caused by the contraction of the inner shell electrons on the outer shell electrons. An example of the results of some of these calculations by Glebov [Glebov 89] for Rutherfordium (element 104) is shown in Figure 1-3.

The extent to which these relativistic effects actually change the predicted electronic shell structure and the energies of the valence electrons of the heaviest elements is still under debate, as is the effect these changes would have on the other properties of the atom. Pyykkö has provided a comprehensive discussion of the

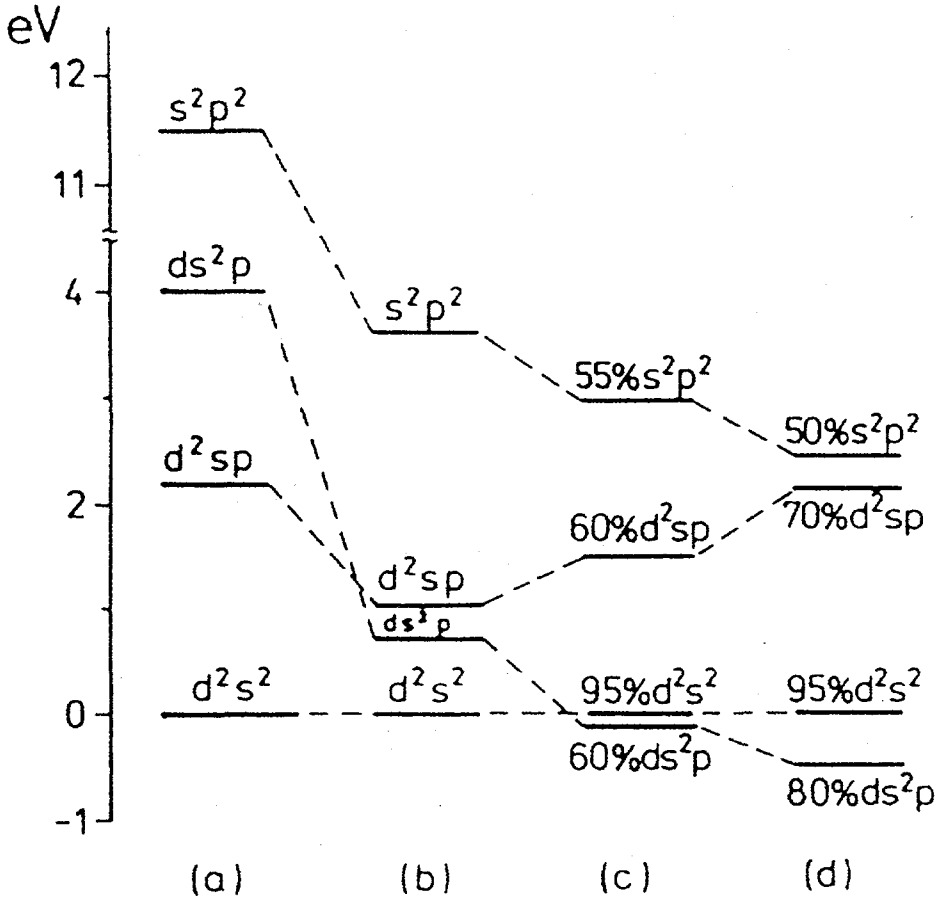

Figure 1-3: Level structure of element 104, for the shells outside the Ra + $5f^{14}$ core, for the 4 valence electrons $6d^2$, 7s, and 7p, calculated for both relativistic and non-relativistic configurations. Reproduced from [Glebov 89]

properties that are affected by the presence of relativistic effects [Pyykkö 88]. He states:

> "Thus the main effects on atomic orbitals are (1) the relativistic radial contraction and energetic stabilization of the s and p shells, (2) the well-known spin-orbit splitting, and (3) the relativistic radial expansion and energetic de-stabilization of the (outer) d and all f shells. All three effects are of the same order of magnitude and grow roughly like Z^2."

More recently, theorists have studied the specific effects of the electronic structure on the molecular orbitals formed in transactinide compounds and on the gas phase properties of the group 4, 5, and 6 halides, oxyhalides and related species [Pershina 92a-c, 94a-d, 95, 96a-b, Ionova 92, Malli 96]. The theoretical basis for calculating relativistic effects on electronic shell structure, how that structure is then related to molecular properties, and some examples are given in section 3.3. See [Pershina 96a] for a comprehensive review of the methods used in calculating relativistic effects, and the current predictions of elemental and molecular properties.

Determining the volatilities of the transactinide compounds, specifically the halides and oxyhalides, by on-line gas phase chromatography is one method we can use to study the chemical properties of the heaviest elements. The information we gain can be compared to the theoretical electronic structure predicted by relativistic molecular orbital calculations to improve our theoretical understanding of the extent of these effects, which in turn can be used to predict chemical properties of new elements as well as new properties of the known elements.

1.1 Previous Experimental Work

Studies of the gas phase properties of the tranactinides and their homologs first began in the late 1960s and early 1970s. Ivo Zvara et al. [Zvara 66, 69,70, 76, Belov 75] used a quartz chromatography column with a temperature profile that decreased linearly over the length of the column to retain the volatile halide species at a specific position on the column related to the volatility of the compound. This form of gas phase chromatography is called thermochromatography to distinguish it from the operation of a column at a constant temperature, called iso-thermal chromatography.

In Zvara's studies the column was lined with mica plates. The deposited isotopes decayed in position leaving spontaneous fission (SF) tracks in the mica. The position of the tracks within the column was then used to determine the temperature at which the compound is no longer volatile. The measurement of SF activity on the mica was used to detect and presumably identify the transactinide $^{261}105$.

A schematic of Zvara's experimental apparatus with the temperature profile of the column and the results of an experiment on ^{90}Nb and $^{261}105$ (here called Nilsbohrium) are shown in Figure 1-4. The 1.8-sec $^{261}105$ was presumably produced via the reaction ^{243}Am(^{22}Ne, 4n)$^{261}105$ at a beam energy of 119 MeV [Zvara 76]. This method suffers from some obvious difficulties. Detection and identification of the isotope under study is accomplished only by the study of the tracks left by fission fragments produced in the decay. Most of the heavy element production reactions produce a much larger number of lighter isotopes in comparison to the compound nucleus reaction desired, and the method cannot identify the exact element or isotope which produced the tracks. Because the isotopes decay via spontaneous fission, the use of parent-daughter relationships normally

utilized in alpha decay chains for determination of the Z and A of the observed activity is no longer possible. No decay data are obtained, so the half-life of the isotope cannot be determined. Furthermore, analysis of the data using Monte Carlo methods for the determination of volatility and adsorption enthalpies depends on either knowing the half-life beforehand or assuming some value for the half-life. In the case of strong gamma emitters with relatively long half-lives (minutes or longer), it is possible to remove the column and determine the position of the isotope being studied by using position-sensitive gamma spectroscopy. In fact, thermo-chromatography is more suitable than isothermal chromatography for long-lived isotopes due to the relationship between retention time and half-life in the latter.

Rudolph and Bachman [Rudolph 79b, 80] first began using isothermal gas phase chromatography in combination with tracer amounts of radioisotopes in 1979. Their apparatus was used to study compounds not only by radioactive labeling of a carrier, but also by using isotopes produced on-line and carried directly to the chromatography column by a gas jet system. In both cases the operation principle is the same as that described later for the Heavy Element Volatility Instrument (HEVI) [Kadkhodayan 92] and the On-Line Gas Apparatus (OLGA) OLGA III [Gäggeler 91]; the compound being studied is carried into a chromatography column where it interacts with the surface. By measuring the yield as a function of the temperature of the column, volatility and retention time can be determined. Retention time is then used to calculate the adsorption enthalpy, ΔH_a. In these early studies [Rudolph 79b, 80], Nb, Mo, Tc, Zr, and Te in metallic, chloride, and oxychloride forms were studied on a variety of surfaces including SiO_2, NaCl, $CaCl_2$, and $MgCl_2$. The differences in technique between these early studies and the later on-line studies using the OLGA and HEVI systems include the use of

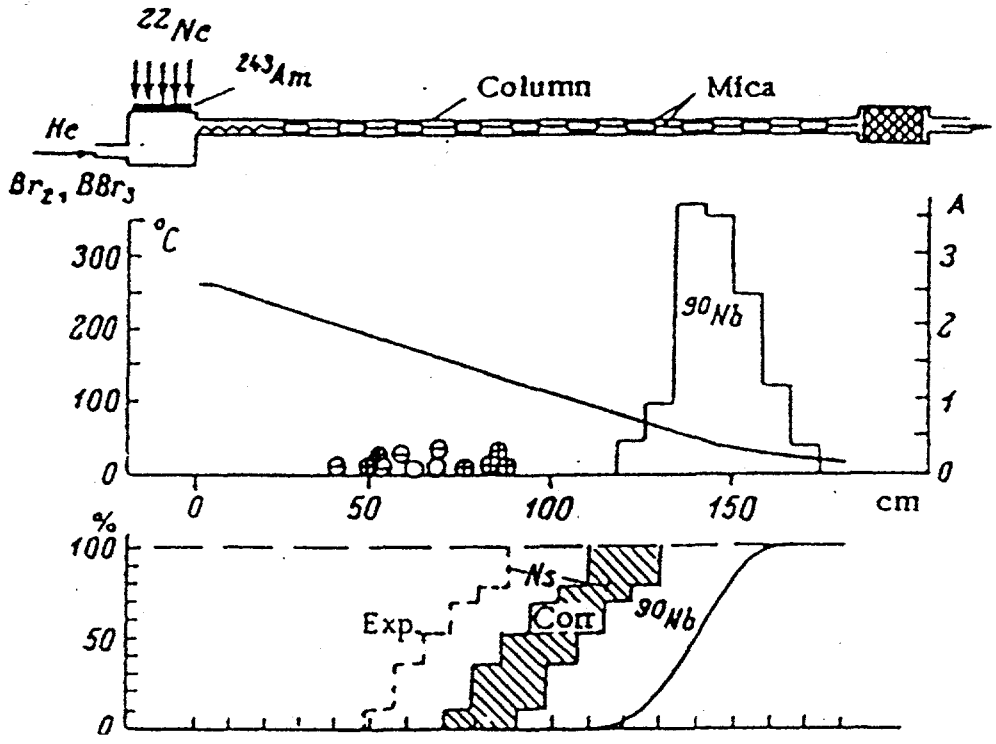

Figure 1-4: Experimental apparatus, column profile, and results of Zvara's thermo-chromatography experiments. Taken from [Zvara 76]:

"Top: Scheme of the experimental apparatus. Middle: variation of temperature along the chromatorgraphic column (sloped line, left- hand scale), a summary distribution of traces of fission fragments of a spontaneously fissioning isotope of 105 (here, nilsbohriumn, Ns) according to three individual experiments (circles) and a histogram of the distribution of niobium-90 along the column (right-hand scale). Bottom: integral distribution of nilsbohrium and niobium. The dotted line is the experimental histogram of element 105. The shaded zone shows the limits of the "corrected" position of the histogram for element 105 based on the differences in half-life between ^{90}Nb and the expected half-life of 105."

radionuclide tracers rather than on-line production of the isotopes being studied at an accelerator or reactor, and the use of quartz, graphite, and coated quartz particles for packing the column as a means of changing the adsorbate (surface).

In 1986 Brüchle et al. [Brüchle 86] developed OLGA, which was designed to continuously separate the volatile products of the superheavy elements. OLGA was only capable of studying non-corrosive oxide and hydroxide compounds of the produced radioisotopes, and no superheavy elements were found. OLGA was replaced in 1991 with OLGA II [Gäggeler 91, Jost 91], which was designed specifically to separate and study the volatile halides of the transactinides and their homologs. OLGA II was designed with a moving magnetic tape detection system which allowed for the suppression of long-lived contaminants. This tape system also permitted the mounting of x-ray and gamma-ray detectors in two of the six detector positions (see Figure 1-5) in addition to the surface barrier detectors usually installed for alpha spectroscopy. The total efficiency of the whole OLGA II system is reported to be 60% (for long-lived isotopes, $t_{1/2} >>$ minutes). A recluster chamber placed immediately after the chromatography column is used in order to reattach the volatile compounds to aerosol particles, and to cool the gas flowing out of the column before it contacts either the gas jet capillary or the detection apparatus. The aerosol can then be transported to the detection system by a He gas jet. The reclustering time for the volatile compounds was estimated to be approximately 20 seconds, which set a limit on the half-life of the isotopes OLGA II could be used to study. This system was used to study the volatility of a mixture of Zr, Nb, Hf, Ta, Po, Rf, Ha bromides, chlorides, and oxychlorides [Türler 91b, 96a]. Figure 1-5 shows a schematic of OLGA II. A comparison of the results for OLGA II and III with the results of the research presented in this work is given in section 5.

HEVI was developed in 1989 by B. Kadkhodayan and A. Türler to study the volatilities of halides of the heaviest elements and their lighter homologs [Kadkhodayan 93, 93a]. It is an isothermal (single temperature) gas chromatography instrument that can separate short-lived isotopes based on their volatilities. This instrument was similar in operation principle and design to OLGA II but had a number of improvements. First, temperature profiles taken for each temperature to be studied showed a variation of at most 5° C throughout the column for any individual temperature. OLGA and OLGA II had shown variations in the temperature profiles with column length, ranging from 10° at low temperatures up to over 100° C at column temperatures of 600-700° C! The column length was increased, from 30 cm in OLGA II to 54 cm in HEVI. A controlled gas flow system for HEVI prevents salt buildup in the column, making the surface both more uniform and the results from multiple experiments more reproducible. Further details on HEVI are given in Section 3 of this work and in [Kadkhodayan 93].

The results of previous experiments performed with HEVI [Kadkhodayan 96] are given in Table 1-2, below. These results show that for the chlorides, the transactinide Rf resembles the light homolog Zr more than the heavier homolog Hf. It is volatile at a lower temperature and has a correspondingly higher adsorption enthalpy. Ha also showed properties similar to its lighter homolog Nb rather than the heavier homolog Ta; both Ha and Nb have the tendency to form volatile pentachlorides while Ta was observed to form the much less volatile oxychloride compound $TaOCl_3$ under the same experimental conditions.

In addition to forming previously unknown transactinide compounds and measuring their volatilities, this research supported Pershina's predictions of a change in electronic structure for the transactinide elements due to relativistic effects, which would

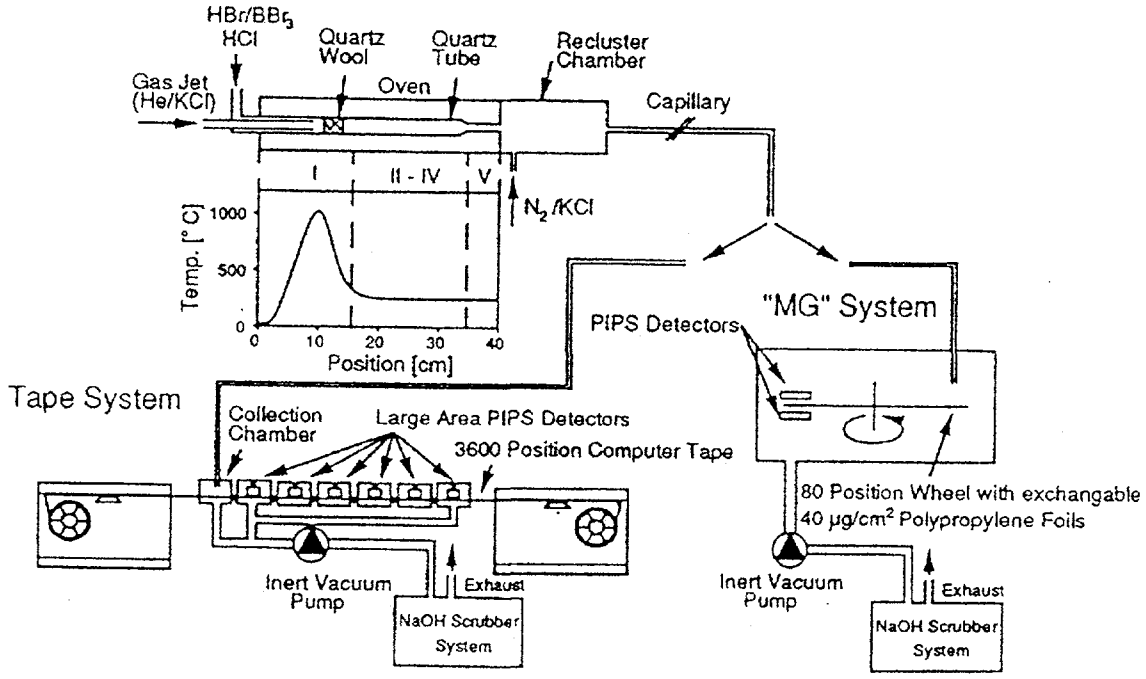

Figure 1-5: Schematic of OLGA II including the two separate detection systems used for experiments.

result in more volatile compounds [Pershina 97].

Preliminary work on the bromides of Nb and Zr also agreed with her predictions, which the observation that the bromides are less volatile than the chlorides. However, more data on the transactinide bromides were needed to determine if the same trends were observed as in the chloride compounds. In addition, HEVI had only been used to study the group 4 and 5 elements, although at the time the tranactinides through 109 were known. We wished to extend the studies to Sg since it has isotopes with half-lives long enough for study (see Figure 1.2) by this method.

The current research has then two primary goals. The first is to extend the measurement of the volatilities of the transactinides for comparison with their lighter homologs in the periodic table. This will allow us to investigate deviations in periodic properties of the elements to assess the presence and extent of relativistic effects in the tranactinides. The second goal is to improve the equipment and methods used to separate the volatile halides of the short-lived transactinides, with an eye towards making HEVI. capable of studying isotopes with a wider range of half-lives.

Table 1-2: Results of previous Gas Phase Chromatography Experiments with HEVI. From [Kadkhodayan 96]

Compound	Volatility (°C)	Adsorption Enthalpy, ΔH_a (kJ/mol)
$BiCl_3$	100-150	-69±4
$PoCl_4$	150-200	-74±5
$ZrCl_4$	100-150	-69±6
$HfCl_4$	200-250	-96±5
$RfCl_4$	100-150	-77±6
$NbCl_5$	100-150	-70±5
$HaCl_5$	100-250	-73±10
$TaOCl_3$	550-600	-153±11
$ZrBr_4$	200-250	-91±6
$NbBr_5$	200-250	-89±5

1.2 Determination of Volatility

The determination of the chemical properties of the transactinides is especially difficult due to the short half-lives of these elements, as shown in Figure 1-2, and due to the small production cross-sections. The longest-lived transactinide known is ^{261}Rf, with a half-life of 78 seconds [Kadkhodayan 96]. The longest-lived isotopes of Sg are ^{265}Sg and ^{266}Sg, with initially reported half-lives of 2-30 seconds and 10-30 seconds respectively [Lazarev 94]. These isotopes were produced via the ^{248}Cm(^{22}Ne, xn) reaction at bombarding energies of 116 and 121 MeV with cross-sections of approximately 260 pb (^{265}Sg at 116 MeV) and 70 pb (^{266}Sg, both energies). Six alpha-SF correlations and four alpha-alpha correlations, as well as one triple alpha correlation, were seen during a total irradiation time of approximately 12 days. More recent experiments with ^{265}Sg and ^{266}Sg [Schädel 97, Türler 97] have yielded better estimations of the half-lives of these isotopes, which are currently reported to be $7.4^{+3.3}_{-2.7}$ seconds and 21^{+25}_{-7} seconds, respectively [Gäggeler 97].

Any method used for determining the chemical properties of these elements must be able to overcome these difficulties. The method must be highly efficient in order to cope with the atom-at-a-time nature of production due to the small production cross-sections and short half-lives. The detection apparatus must be capable of detecting single atoms. Finally, any experimental procedure must be fast enough to be performed on a time scale similar to or shorter than the half-life of the isotope being studied.

HEVI (shown in Figure 3-1 in Section 3) is an instrument which fulfills all of these requirements. The time for transport from the production site to the instrument by the gas

jet is approximately 0.5 second, while the residence time of the non-volatile products in HEVI is approximately 20 seconds. The chemical efficiency of HEVI approaches 80%, and the total efficiency of the system (including gas jet) is between 50% and 80%. The products are detected by α-, SF, and γ-spectroscopy.

An experiment is performed which measures the relative yield of a volatile halide of the isotope under study at a specific temperature. First, a *yield check* measurement is made by sending the gas jet containing the isotopes under study directly to the detection apparatus. Two *gas chromatography* measurements are then taken in which the gas jet is directed through HEVI and chemistry is performed. A final yield check is taken, and the relative yield for that temperature is calculated based on the ratio of the activity measured after the gas chromatography system to the activity measured in the yield check, taking into account the variations in beam current, time of collection, and flow rate of the gas jet.

By performing multiple experiments at different temperatures, a graph of the yield of a particular species vs. temperature may be constructed, showing the volatility of the species. Volatilities are usually reported as a *volatility temperature*, which is the temperature at which the yield of the compound is 50% of the maximum chemical yield observed.

This method has been used in the past with multiple generations of equipment [Gäggeler 91, Kadkhodayan 92, Eichler 94, Türler 94] to successfully determine the volatilities of the group 4, 5, and 6 chlorides including the transactinides Rf, Ha and Sg.

1.3 Determination of Adsorption Enthalpy

By using a Monte Carlo simulation program [Türler 91a] to model the behavior of the volatile species in the column, the adsorption enthalpy can be determined. The retention time of the molecule in the column can be deduced from measurement of the relative chemical yield of the species as a function of the known half-life of the radioisotope being measured. When the chemical yield of the molecule under study reaches 50%, the retention time in the column is equal to the half-life of the radioactive isotope. Based on the volatility temperature, retention time, and the specific details of the column, adsorption enthalpy can be calculated [Rudolph 78a, 79a, Eichler 82, Zvara 85]. The details of the modeling of the column, the behavior of the halides, and the Monte Carlo simulation that is used to determine adsorption enthalpy are given in Section 2.1.

This adsorption enthalpy may then be compared with both on-line and off-line determinations of adsorption enthalpies for compounds which are expected to have similar electronic structures. These are primarily the lighter homologs of the same group in the periodic table as the transactinide in question, but may also include some of the actinides which are expected to have the same oxidation states. This comparison accomplishes two purposes: it can be used to check the results of the method with the results of previous experiments in order to eliminate or uncover systematic errors in the present experiment, and it can be used to determine the extent of relativistic effects in the transactinides. A comparison of the experimental data with the results of theoretical calculations of adsorption enthalpy, based on multi-configurational Dirac-Fock (MCDF) calculations of electronic level structure, can be used to determine the expected electronic level structure of the transactinide under study and to predict deviations due to relativistic effects.

2. Theory

Three theoretical problems must be addressed in the on-line gas chromatography experiments described here. 1) How to compare the data from HEVI with experimental data from other systems such as OLGA I, II, and III. 2) The relationship between the observed data and the atomic characteristics of the transactinide elements must be understood. 3) Finally, a theoretical model of the electronic structure of the transactinides must be developed which accounts for the observed data on volatility and which can predict the behavior of the other volatile halide species.

In order to compare the graphical results of the gas chromatography experiments used here (for example- see Section 5.2) with the results of other experiments, it is useful to arrive at some method of calculating thermodynamic properties based on the observed volatility data. The *adsorption enthalpy* (ΔH_a) of a molecule is one such property. It is the measure of the energy of electrostatic interaction of a molecule in the gas state with a specific surface [Atkins 86], and is ideally suited for comparison of the HEVI volatility data with the results of other gas chromatographic experiments.

The method most currently used in on-line gas chromatography of short-lived atoms to arrive at adsorption enthalpy is to model the passage of a molecule along the column using a Monte Carlo simulation. This model takes into account the physical characteristics of the molecule and the gas chromatograph to calculate an expected yield curve (the % of molecules passing through the column before they decay as a function of temperature) for a given value of adsorption enthalpy. Fitting the calculated curves to the experimental data gives a best estimate for the value of adsorption enthalpy. The Monte Carlo simulation used in this work is described in Section 2.1.

Observed volatilities can be used to arrive at electronic data on the transactinides through the equilibrium vapor pressure, P_{mm}. P_{mm} has been shown experimentally [Türler 96a, b] to correlate with the volatilities observed in OLGA III, and at the same time may be calculated from the polarizabilities of interacting gas molecules, which can itself be calculated using molecular orbital (MO) theory. Section 2.2 gives details of the application of this method to the data.

Once it is possible to draw a connection between the observed volatility and the expected electronic structure of the atom under study, it is necessary to develop a theoretical basis for this electronic structure in order to make further predictions on the properties of the transactinides. This theoretical basis already exists. Section 2.3 outlines the current refinements.

2.1 Monte Carlo Modeling of Gas Phase Chromatography

A Monte Carlo simulation program has been used to calculate adsorption enthalpy values based on the observed volatilities. It is based on a model of thermo-chromatographic adsorption of a molecule on a surface as given in Zvara 85. The time spent by a compound in the column is dependent on the following factors:

- the mean displacement along the column between (sets of) interactions with the surface.
- the mean number of collisions that a molecule will undergo during interaction with the column surface per unit length.
- the average time the molecule spends adsorbed on the surface.

By knowing the time spent in the column and the half-life of the radioisotope, we can arrive at a prediction of the yield of the compound. When the residence time of the compound in the column is prolonged by interaction with the surface to a time significantly greater than the half-life of the radioisotope, a large fraction of the atoms will decay in the column and will not be detected in the detection system, and the observed chemical yield will be low. When the compound does not strongly interact with the column surface, the residence time will be short- on the order of a tenth of a second or less- most of the isotopes will reach the detection system before decaying, and the observed yield will be higher.

2.1.1 Displacement along the column between interactions

A molecule will normally travel along the column by means of a large number of collisions with the wall of the column in which the molecule adsorbs and desorbs practically without moving (these will be discussed further in the next section). Between collisions with the column, the molecule will rarely leave the environment of the column wall because of the short mean free path length and randomness of direction of travel, and the probability is high that the molecule will strike the surface of the column again before moving any significant length along the column. However, with each mean free path there is a small chance that the path of the molecule will take it further away from the surface of the column and then the molecule will diffuse along the column without significant interaction with the column.

This process is modeled for laminar flow in a cylindrical column as shown in Figure 2-1(a), and the approximation used for computer simulation is shown in

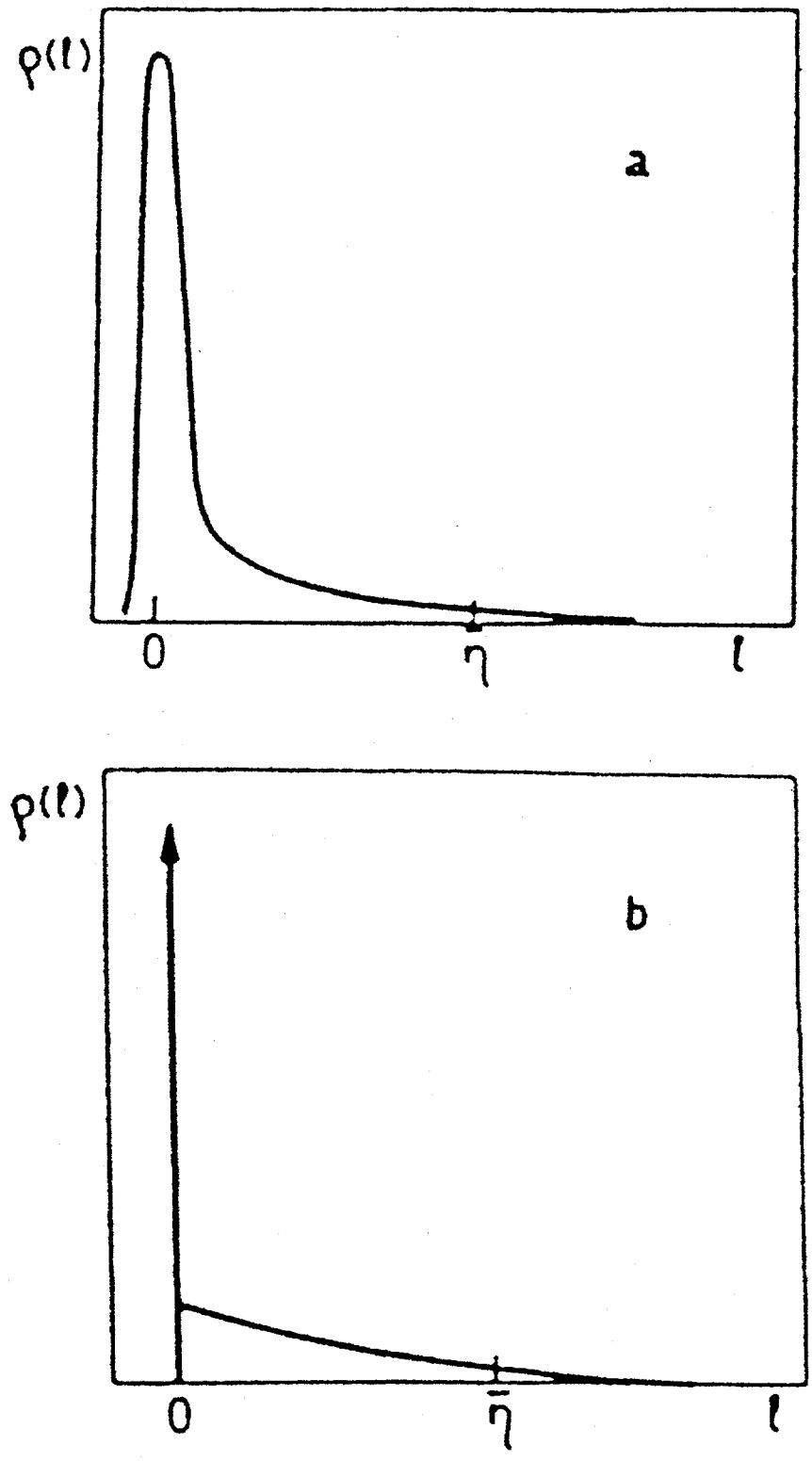

Figure 2-1: Graph of the probability density distributions for displacements l: (a) character of the real distribution. (b) the accepted approximation. From [Zvara 85].

Figure 2-1(b). The approximation is given by a delta function representing the near-unity chance of an insignificant jump length with the addition of an exponential tail representing the small chance for the molecule to move away from the column wall. The probability ρ of a jump of displacement *l* is given by:

$$\rho(l) = (1-a)\delta(l) + (a/\bar{\eta}) \cdot \exp(-l/\bar{\eta}) \tag{3}$$

where

$$\bar{\eta} = \frac{11Q}{48\pi D} \tag{4}$$

$$a = 1/\nu_1 \bar{\eta} \tag{5}$$

Q is the true volume flow and D is the diffusion coefficient given by:

$$D = D_{298} \cdot \left(\frac{T}{T_{298}}\right)^{1.75} \tag{6}$$

D_{298} is the diffusion coefficient. It is derived from Gilliland's equation and is a function of pressure, molecular volume, and molecular mass. Note that using the above expressions $\bar{\eta}$ can be simplified to $\bar{\eta} \approx 1/\sqrt{T}$.

2.1.2 Mean number of collisions per unit length.

According to the kinetic theory of gasses the mean number of collisions , ν_l, that a molecule will undergo with the column surface per unit length of the cylindrical tube when the gas has the true volume flow rate Q along the surface is given by:

$$\nu_l = \frac{r}{Q} \cdot \sqrt{\frac{2\pi RT}{M}} \tag{7}$$

where r is the radius of the column, Q is the true volume flow rate, M is the molecular mass, R is the gas constant, and T the temperature.

2.1.3 Residence time based on adsorption

A molecule spends some random time in the adsorbed state which depends on its adsorption enthalpy, the temperature of the column, and the period of oscillations of the molecule perpendicular to the surface. The mean retention time is given by:

$$\bar{\tau}_a = \tau_0 \cdot \exp(-\Delta H_a / RT) \tag{8}$$

Where τ_0 is the period of oscillations of the molecule perpendicular to the column surface, ΔH_a the adsorption enthalpy, R the gas constant and T the temperature. The probability distribution for τ_a is given by:

$$\rho(\tau_a) = (1/\bar{\tau}_a) \cdot \exp(-\tau_a / \bar{\tau}_a) \tag{9}$$

2.1.4 The Monte Carlo simulation code

Figure 2-2 shows a flow diagram for the computer program; the listing for the code for the Monte Carlo program is given in Appendix 1. The following variables have thus been used to model the behavior of the molecule as it moves along the column: adsorption enthalpy, ΔH_a; true volume flow rate, Q; period of oscillation, τ_0; molecular mass, M; and half-life, $t_{1/2}$.

The number N of molecules to be simulated is also entered into the program, but does not affect the Monte Carlo simulation of the molecule as it moves down the column.

The following constants are used in the program (these are specified for HEVI, though they may be easily changed to accommodate use of the program for instruments such as OLGA III): temperature of the column at 1-cm intervals,T; radius of the column, r; and pressure, p.

The variables and constants listed above contribute to the calculation of the values for the semi-random quantities: mean jump length, $\bar{\eta}$; mean residence time in the adsorbed state, $\bar{\tau}_a$; and mean number of collisions, ν_l.

The program models this process by allowing the compound to proceed through a large number of random interactions based on the above characteristics, checking after each interaction to ascertain if the isotope has decayed. A large number (2,000-10,000) of compound molecules are tested and a yield for the compound at that particular temperature is derived. The yield is calculated for temperatures from 50° C to 650° C in 50° C steps, with the actual temperature profile for HEVI entered into the program for each of these steps. The program is reiterated, varying the adsorption enthalpy until a best fit to the data is obtained.

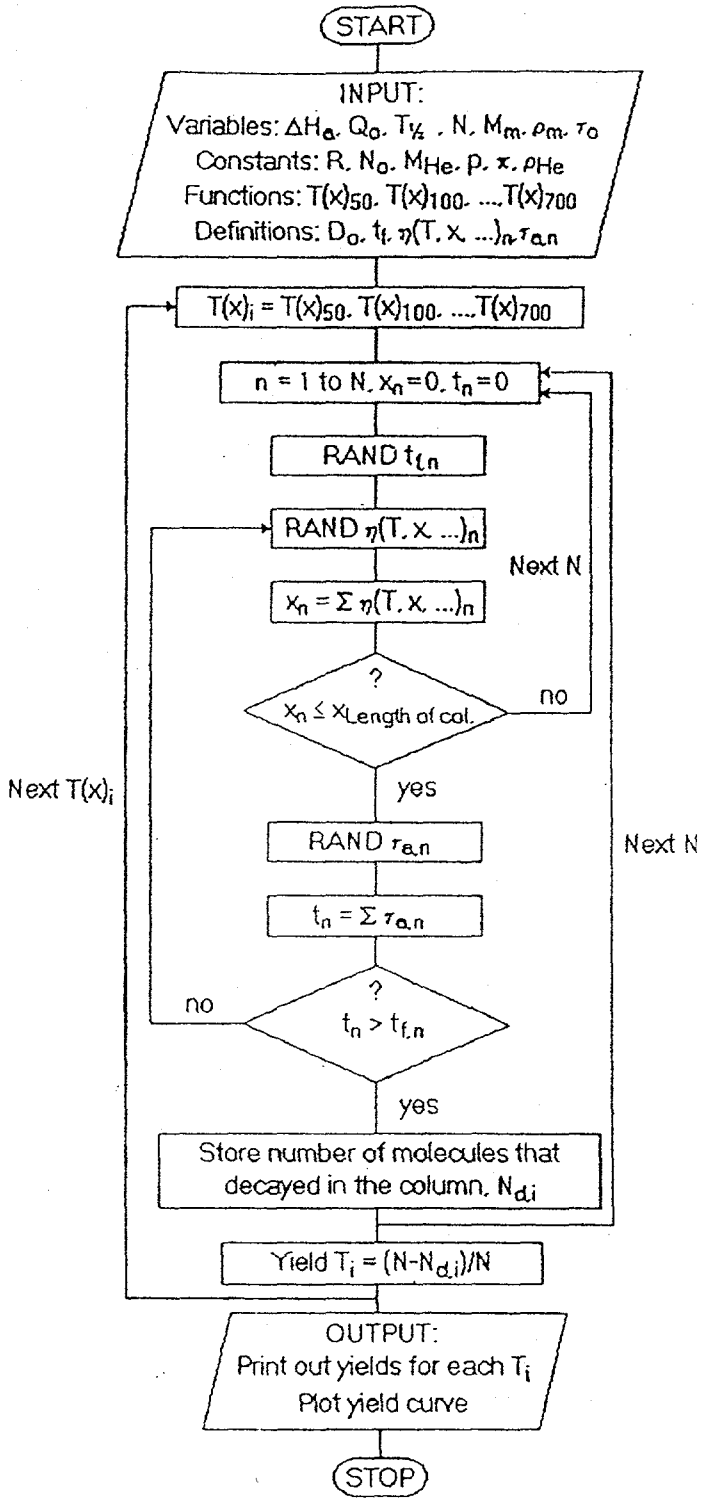

Figure 2-2: Computer program flow chart. Reproduced from [Zvara 85].

2.1.5 Estimation of the error in determination of adsorption enthalpies.

The weighted least-squares method used to fit the Monte Carlo simulation yields to the data results in some error in adsorption enthalpy values based on the errors associated with the experimental points. Additionally, the Monte Carlo program has no provision for entering values which have some uncertainty associated with them. Only exact values may be used as inputs, yet four of the variables used to calculate adsorption enthalpy have some uncertainty associated with them, either due to the limitations of HEVI or due to our lack of knowledge of the properties of the compounds studied.

The *true volume flow rate* through the column is assumed to be unvarying, while during the normal operation of HEVI fluctuations averaging 10% of the measured flow are not unusual. The *density* of the compound at standard temperature and pressure (STP) conditions is also required by the program to calculate adsorption enthalpy. Though the densities of the homologs are in general known, the densities of the transactinide-halides are unknown. The *half-lives* of the transactinide isotopes, though measured during the on-line experiments, have a statistical standard deviation associated with them (e.g. 74^{+7}_{-6} for ^{261}Rf). Finally, the *period of oscillation* perpendicular to the surface is assumed to be 1×10^{-12} s^{-1} for all compounds.

2.1.5.1 Error resulting from error in experimental data

Figure 2-3 shows the data for $^{261}RfBr_4$ (see also Section 5.2.2), along with the adsorption enthalpy curves –77 kJ/mol, –82 kJ/mol, –87 kJ/mol, –92 kJ/mol, and –97 kJ/mol, where none of the program-dependent variables were allowed to vary. The values used for this original simulation match the values used for data analysis of

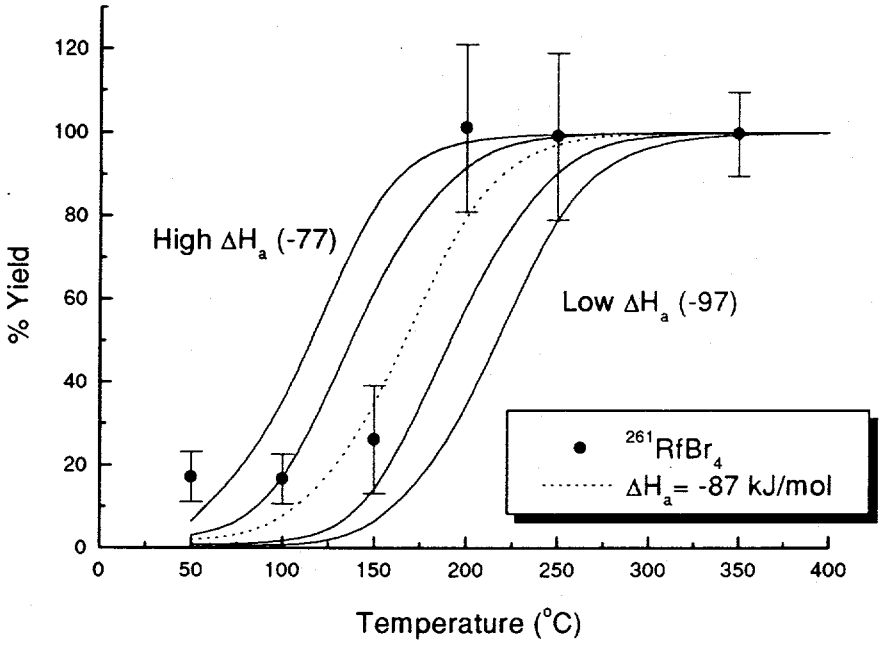

Figure 2-3: Adsorption enthalpy curves for $^{261}RfBr_4$. The volatility temperature of $RfBr_4$ is the temperature at which the chemical yield is 50% of maximum (here, where each curve reaches 50% yield).

$^{261}RfBr_4$ in Section 5.2.2, and are: Half-life, 74s; molecular weight, 581 amu; density, 5 g/cm^3; flow rate of He, 30 torr l/s; and period of oscillation, 1e-12 s^{-1}. For this simulation 2,000 atoms were used.

It can be seen that even a variation in adsorption enthalpy on the order of 5 kJ/mol results in a large expected change in the volatility temperature of the compound; approximately 20° C. Volatility data collected using HEVI, even data with relatively large error bars, such as is the case with ^{261}Rf, provides a highly sensitive reading of the adsorption enthalpy, and in the absence of other errors we expect a weighted least-squares fit of the data to the adsorption enthalpy curves to provide adsorption enthalpy values with errors no greater than ±(1-2) kJ/mol. This error is in many cases smaller and can in some cases be effectively zero, meaning that a significant change in the quality of the fit to the data is observed in even a change of ±1 kJ/mol, which is the smallest interval simulated.

Figures 2-4 through 2-7 show the changes in the expected adsorption enthalpy curve based on changes in flow rates, densities of the compounds, and half-life of the radioisotope when only that single variable is allowed to change. For these simulations, the values of the other variables were kept constant at the expected values for $^{261}RfBr_4$ given above, except that all of the adsorption enthalpy curves shown are for a value of –90 kJ/mol.

2.1.5.2 True volume flow rate

Figure 2-4 shows the change in the volatility temperature expected with changes in the true volume flow rate for $RfBr_4$. Adsorption enthalpy can be seen to vary

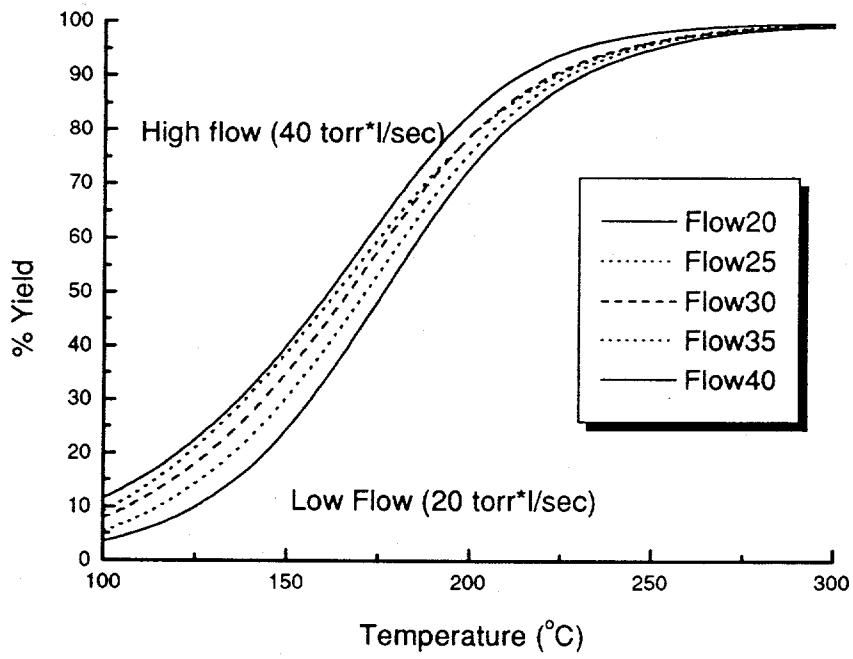

Figure 2-4: Monte Carlo curves for the same adsorption enthalpy value when the flow rate is changed.

approximately linearly with flow rate over a wide range in flow rate values, with a change in the flow of 5 l/min causing an error in the calculated adsorption enthalpy of approximately 2 kJ/mol. HEVI typically runs at flow rates between 2-3 l/min (25-38 torr l/s). These rates can change for different experiments due to slight changes in the density and mass of the quartz wool plug and the He pressure placed on the target.

Variations in the flow rate during an experiment are on the order of 10% of the actual flow rate or less, so that an error margin of less than 1 kJ/mol can be expected based on typical variations (3-4 torr*l/s) in the true mass flow rate.

2.1.5.3 Density of the compound

The density of the studied compound at standard temperature and pressure (STP) is a required input for the Monte Carlo program to give a prediction of adsorption enthalpy. These values are well known (within 0.01 g/cm^3) for almost all cases of the homolog compounds, but not for transactinide compounds. Any estimation of a compound's density will thus necessarily include some uncertainty.

Density values for compounds with known densities were taken from the Handbook of Chemistry and Physics, 77th ed. [Lide 96]; density values for the transactinides were based on the values of their homologs. For reference, the values given in [Lide 96] for group 4 and 5 bromides (in g/cm^3) are: $HfBr_4$; 4.90, $TaBr_5$; 4.99, $NbBr_5$; 4.36. The density of $^{261}RfBr_4$ used for estimation of adsorption enthalpy was 5 g/cm^3.

Figure 2-5 shows the change in expected volatility temperature with a change in the density for the same adsorption enthalpy value. An order of magnitude change in the

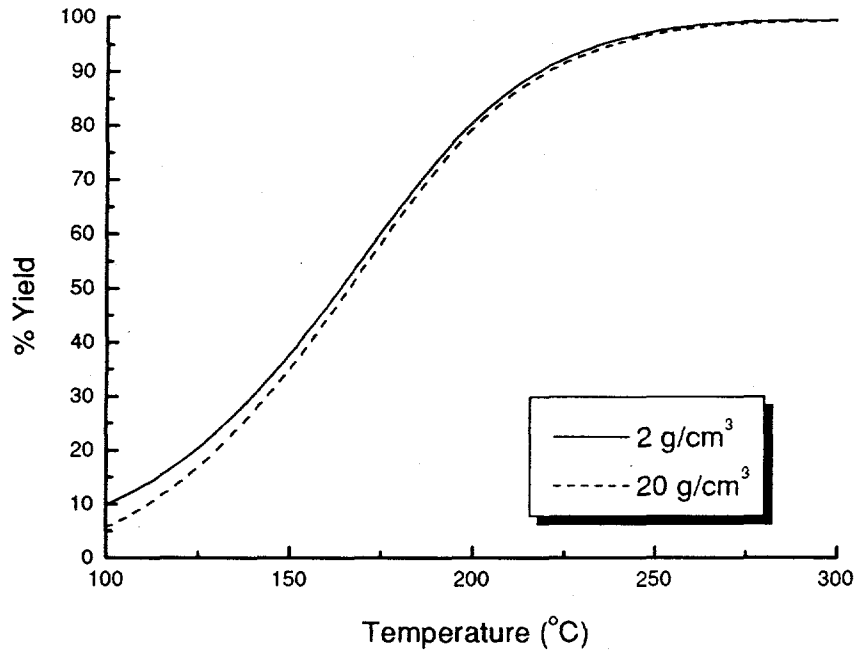

Figure 2-5: Change in volatility temperature as a function of change in expected density. The density value used for $^{261}RfBr_4$ was 5 g/cm^3.

expected density results in only a small change in volatility temperature (5° C or less). The curve representing 5 gm/cm3 has been omitted for clarity; were it included, it would lie between the two curves shown. The expected change in adsorption enthalpy resulting from error in density is less than 1 kJ/mol for any value of density within an order of magnitude of the reported densities of the group 4 and 5 homologs.

2.1.5.4 Half-life

Though the half-lives of the group 4, 5, and 6 homolog elements are well known, the half-lives of the transactinides are still being studied. Data from the experiments in this work and others still provide a significant contribution to the best estimates of the values for the half-lives of the transactinides, so that the error in the observed half-life of ^{261}Rf during this experiment contributes directly to the error in adsorption enthalpy.

The half-life of ^{261}Rf was measured in this work to be 74^{+7}_{-6} seconds (see Section 5.2.2). Figure 2-6 shows the change in volatility temperature with a change in half-life of ±7 seconds from the measured value of 74 seconds. The change in half-life from the lower limit of error to the upper limit of uncertainty results in approximately a 5° C change in volatility temperature. Based on these observations the error in measured half-life can be expected to contribute and error of ±0.5 kJ/mol to the total estimated error assigned to the calculated adsorption enthalpy value.

The errors associated with the half-lives of the isotopes of the lighter elements are generally only 1-2 % and add less than 0.5 kJ/mol to the total estimated error. Values for the half-lives of the lighter elements were taken from [Firestone 96], and were verified during the experimental procedures by decay analysis of a single sample for elements

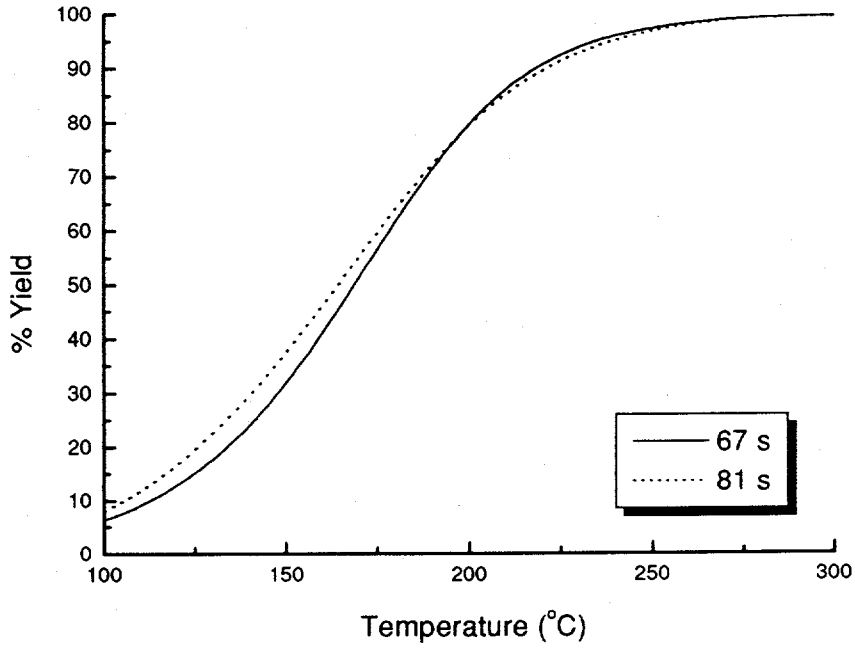

Figure 2-6: Expected change in volatility temperature with a 10% change in the half-life for $^{261}RfBr_4$.

with relatively long half-lives (>2 min).

2.1.5.5 Period of oscillation

The period of oscillation (perpendicular to the surface) is assumed to be $1x10^{-12}$ s^{-1} for all compounds, based on typical vibrational frequencies of particle-surface bonds [Atkins 86] for single molecules. Actual vibrational frequencies for the compounds studied here have not been measured for HEVI. For purposes of the estimation of error in adsorption enthalpy, values for the period of oscillation are assumed to be between double the stated frequency and half the stated frequency (100% error).

Figure 2-7 shows the change in expected volatility temperature assuming periods of oscillation of $0.5x10^{-12}$ s^{-1} and $2x10^{-12}$ s^{-1}, with the curve for 1x10-12 s^{-1} added as a reference. This change in the period of oscillation results in a change of approximately 10-15°C in volatility temperature. A corresponding error in adsorption enthalpy of approximately 4 kJ/mol is expected for all compounds.

2.1.5.6 Summation of error

The errors expected from the above sources were calculated separately for each isotope in each experiment and summed to give a total expected error in adsorption enthalpy values. Though these values may differ from isotope to isotope, some general conclusions can be made. By far the largest contributions to the error in reported adsorption enthalpy come from the error in the experimental data and the error associated with the period of oscillation. Combined, these two factors will give an average error of

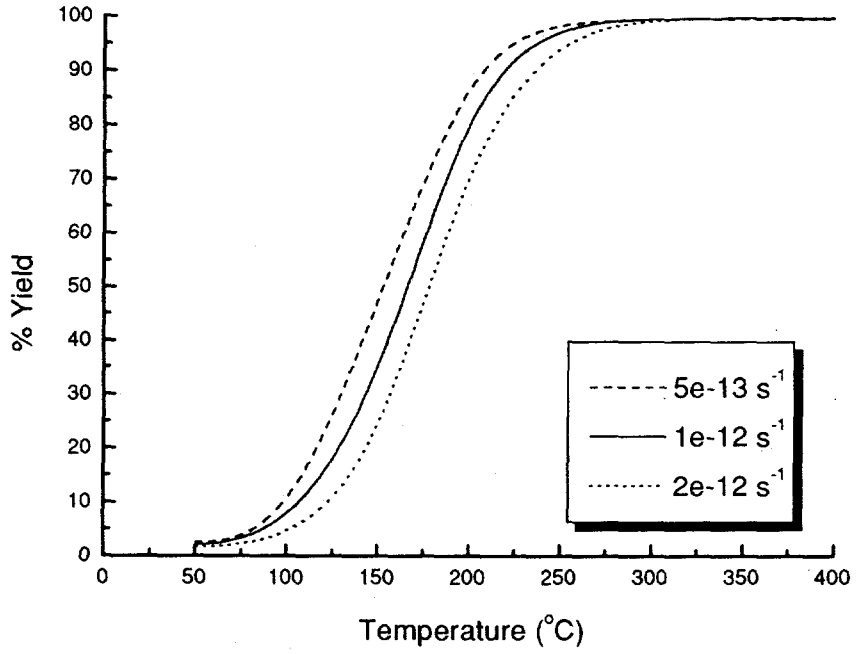

Figure 2-7: Expected change in volatility temperature of $^{261}RfBr_4$ with a change in the period of oscillation.

±(5-7) kJ/mol, depending on the precision of the data. Variation in the average flow rate throughout an experiment contributes error only in cases where the fluctuation in flow is large (> 10%), and the error contributed will be at most ±(1-2) kJ/mol. Adsorption enthalpy is largely independent of the density of the compound within the range of 1 order of magnitude around the densities of the homolog compounds, and is not expected to contribute any significant error. Finally, the error in half-life contributes ±0.5 kJ/mol to the error in adsorption enthalpy value for ^{261}Rf, but is expected to contribute < 0.5 kJ/mol uncertainty in the cases of the isotopes of lighter group 4, 5, and 6 elements.

2.2 Thermodynamic Predictions of Volatility.

Data for the thermodynamic properties of macroscopic quantities of the compounds studied in HEVI have been used to predict the volatility and to confirm assignments of the chemical structure observed. The data used are derived from the following equations [Knacke 91].

Macroscopically, volatility is based on the vapor pressure equilibrium of a vapor over a solid surface composed of the same compound. This equilibrium is dependent on the standard enthalpy ΔH and entropy ΔS of vaporization for the compound in the gas state (for compound *i*):

$$\ln P_i = -\frac{\Delta H_i}{RT} + \frac{\Delta S}{R} \tag{10}$$

Where R is the gas constant, T is the temperature, and where the standard enthalpy of vaporization ΔH_i is known to vary with T. Usually this variation is regular and is given by the heat capacity:

$$\frac{d\Delta H_i}{dT} = \Delta C_i(T) \tag{11}$$

With the assumption of a constant ΔC_i (constant change in heat capacity for compound *i*) between two temperatures T_1 and T_2, we can integrate equation 10 and combine with equation 11 to get an equation with the standard form:

$$\ln P_i = \frac{a}{T} + b \ln T + c \tag{12}$$

This is sometimes simplified even further by omitting the central term, resulting in:

$$\ln P_i = \frac{a'}{T} + c' \tag{13}$$

Numerous reference books exist which tabulate thermodynamic quantities for inorganic compounds. Rather than presenting a graph of vapor pressure vs. temperature they usually report the terms a, b, and c (or a' and c') shown in equations 12 and 13 above. Note that values of a and a', and c and c' are not necessarily equal; the same character has been used here to show the connection between terms rather than any equivalent numerical value.

Results with HEVI and OLGA II have shown empirically that the macroscopic measure of vapor pressure can be used as an accurate gauge of volatilities in the on-line gas phase chromatography experiments [Türler 96a, b]. Despite the fact that the solid surface in the gas chromatography experiments is assumed to be quartz or an inorganic salt [Kadkhodayan 93] instead of being composed of the volatile compound, differences in temperature at a particular pressure for different compounds are equal to the differences in Volatility Temperature in the on-line experiments. Figures 2-8, 2-9, and 2-10 show the vapor pressure curves for various group 4, 5, and 6 halides and oxyhalides, based on data given in [Canterford 68, Knacke 91] and on theoretical predictions from [Pershina 92b].

Vapor pressures for some transactinide halides have also been calculated based on the energy of intermolecular interactions of the molecules in the gas phase. The intermolecular interactions are based on the polarizabilities of the interacting molecules, which can be calculated using MCDF methods. Using the Dirac-Slater Discrete Variational (DS-DVM) Method (discussed below in Section 2.3) V. Pershina has calculated the temperature dependence of the vapor pressure for $HaBr_5$ (shown in Figure 2-9):

> "As a result, a much higher pressure (i.e. higher volatility) of $HaBr_5$ in comparison with $TaBr_5$ was predicted. By analogy, a higher vapor pressure was proposed for $RfCl_4$ than that of $HfCl_4$." [Pershina 97]

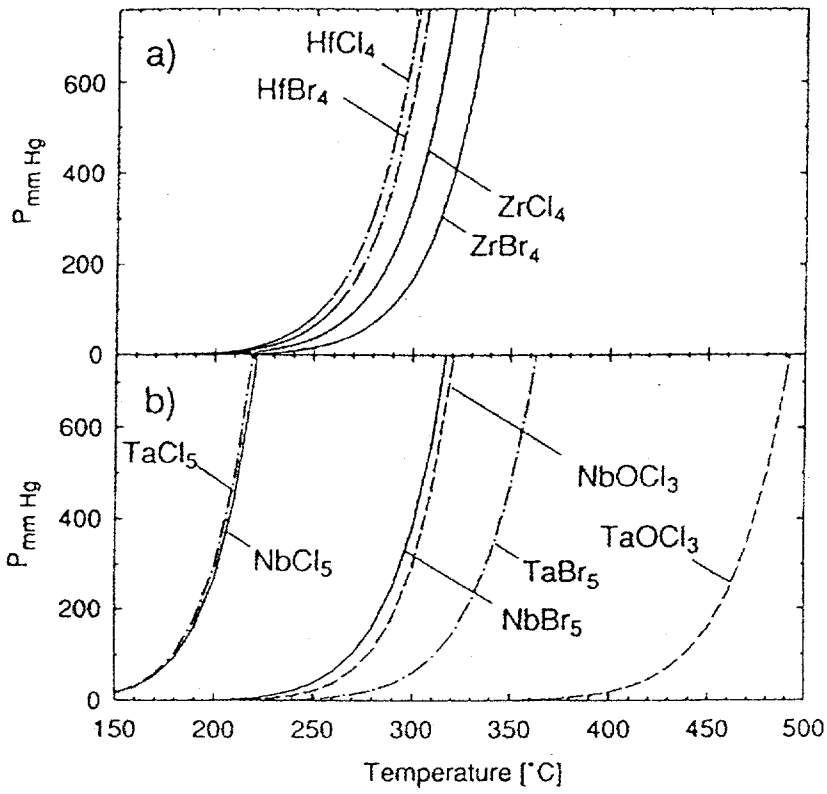

Figure 2-8: Vapor pressure curves for some group 4 and 5 halides and oxyhalides. Reproduced from [Pershina 94b].

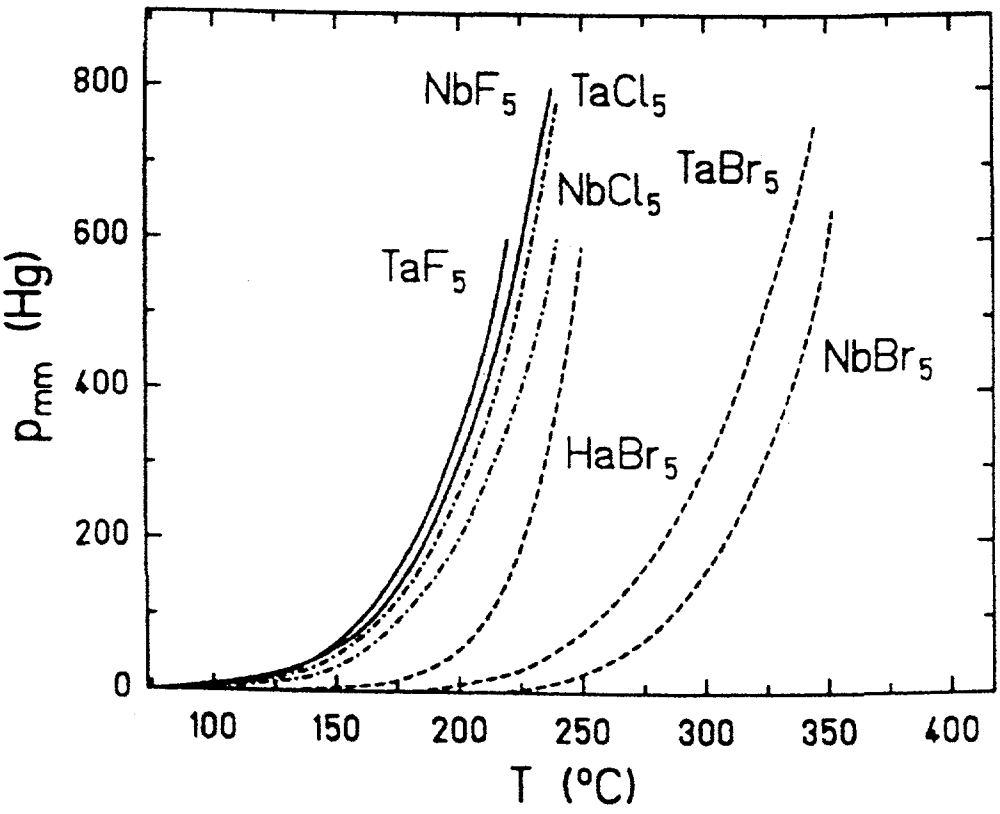

Figure 2-9: Vapor pressure curves for the group 5 halides. Reproduced from [Pershina 97].

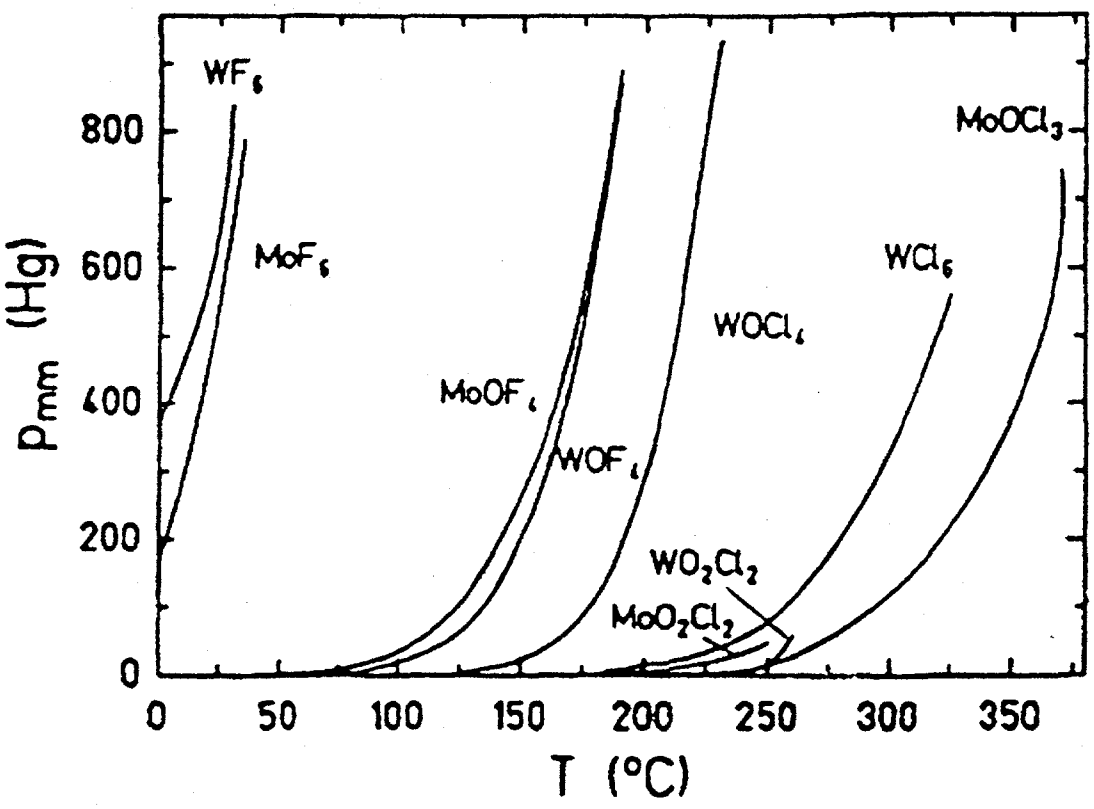

Figure 2-10: Vapor pressure curves for the group 6 halides and oxyhalides. Reproduced from [Pershina 95].

2.3 Relativistic Predictions and Calculation

Relativistic effects are calculated via a variety of methods. Malli [Malli 83, 92, 96] performs *ab initio* calculations to build up the atomic orbitals by adding electrons successively until the neutral atom is reached. The basis of the method used by V. Pershina *et al.* [Pershina 92a] is the Dirac-Slater Discrete Variational Method (DS-DVM), which can be found in [Rosen 75]. It is a fully relativistic, self-consistent method for calculating molecular orbitals and orbital energies based on MCDF theory. Details of this method are given in [Rosen 74, 75, 78, Ellis 84, Freeman 85, Meyer 88, 89]. V Pershina has specifically attempted to predict the volatilities of the group 4, 5, and 6 transactinide halide compounds based on relativistic calculations of molecular orbitals and energies.

It is not our purpose here to describe this method in detail. However, it will be useful to discuss some of the major steps used to move from a relativistic picture of electronic orbitals around a single atom to the predictions of chemical properties, such as volatility, of inorganic compounds.

For all relativistic calculations the starting point is the Dirac wave equation for a single electron in a potential V(r):

$$h\psi = (c\alpha \bullet p + \beta mc^2 + eV(r))\psi = E\psi \qquad (14)$$

where p is the momentum operator p= $-ih\nabla$, α and β are velocity operators, and the potential V is defined as the sum of the Coulomb and exchange potentials:

$$V(r) = V_c(r)+V_x(r) \qquad (15)$$

There are various methods used to calculate the exchange potential. All of the *Local Density Functional* (LDF) methods, of which the DS-DVM is one, calculate exchange

potential based on local electron density. The *Slater local exchange approximation* used in these calculations treats the exchange potential at point r as a function of the electron density at that point.

$$V_x(r) = -3C(3\rho(r)/8\pi)^{1/3} \tag{16}$$

where C is the termed the exchange constant. The value used for C may vary between values of 2/3 and 1 for different methods, with larger values resulting in more tightly bound orbitals [Rosen 75]. Rosen and Ellis further note:

> "In the X_α method as suggested by Slater and co-workers,[20] C is chosen so that the statistical total energy of separated atoms agrees with the Hartree-Fock result....the choice of potential $V(r) = V_c(r)+V_x(r)$ serves to define the Dirac-Slater model." [Rosen 75]

Reference 20 in this case refers to reference [Löwden 72] of this work.

2.3.1 Atomic wave functions

Since the atoms to be treated are not limited to those containing a single electron, multi-electron systems must be represented. This is commonly done by constructing a single determinant built up from one-electron orbitals:

$$\Psi = |\psi(1)\psi(2)\ldots\psi(n)| \tag{16}$$

This is termed the Slater Determinant [Rosen 75, Pyykkö 79].

Solutions for atomic wave functions can be calculated by several different methods and are used to construct a basis set for symmetry orbitals. *Extended* basis sets

are usually used in the real calculations, and are derived by superimposing a spherical potential well upon a self-consistent atomic potential. This method has already been used to construct basis sets for non-relativistic calculations as noted by Rosen and Ellis:

> "This procedure is identical to that used in recent nonrelativistic calculations[10] where the eigenfunctions are named Single Site Orbitals (SSO's). The potential in which the SSO's for atom v have been calculated is given by the following form:
>
> $$V_{SSO}^{v}(r) = \begin{cases} V_a^v(r) - V_s^v & \text{for } r < R_s^v \\ 0 & \text{for } r > R_s^v \end{cases}$$
>
> where $V_a^v(r)$ represents the atomic potential, $V_s^v(r)$ the potential well depth, and R_s^v the well radius. Generation of basis sets in a similar way has also been used by Newman and Taylor,[23] in atomic nonrelativistic configuration interaction calculations." [Rosen 75]

Where references 10 and 23 refer in this work to references [Averill 73, Newman 72] respectively.

2.3.2 Molecular orbitals and the Dirac-Slater Discrete Variational Method

From the basis sets calculated above, molecular orbitals are calculated as a linear combination of atomic orbitals, substituting the relativistic Dirac equations for atomic orbitals for the usual nonrelativistic ones but using methods which are directly analogous. The results of these calculations are four-component molecular wave functions, which can then be used to create molecular symmetry orbitals.

Because of the spin-orbit coupling which results from relativistic effects, these four-component wave functions must be treated using double groups rather than the simpler single groups used in nonrelativistic calculations:

> "The two small components [of the four component wave function], which are necessary for calculations involving electromagnetic field interactions, are often later omitted from the molecular wave functions. Because the electrons are subject to spin-orbit coupling, the calculated orbitals are bases for representations of the less-familiar double groups, which can sometimes complicate interpretations of computational results." [Pepper 91]

Double groups have previously been used by Bethe [Bethe 29] and others to calculate the effects of crystal-field splitting, and details on the use of such groups can be found in a variety of texts such as [Wigner 59] and [Tinkham 64].

2.3.3 Use of covalency and overlap potentials to predict volatility

Pershina and Fricke [Pershina 96a] have used Mulliken population analysis [Mulliken 55] to interpret the molecular orbitals and energies given by the DS-DVM in terms of ionic and covalent bonding contributions.

> "As a measure of the covalent bonding, the overlap population (OP) parameter will be used in this paper. The partial OP between orbitals j and k on centers r and s is expressed as follows
>
> $$OP(j_r,k_s)=\sum_i OP(i:j_r,k_s)=\sum_i 2N(i)c_{ij_r}c_{ik_r}S_{j_rk_s} \qquad (1)$$
>
> Here c_{ij} are MO coefficients, S_{ij} is an overlap integral between orbitals j and k, and N(i) is the number of electrons on molecular orbit i. The total overlap population is
>
> $$OP=\sum_{j_rk_r} OP(j_r,k_s) \qquad (2)$$
>
> The OP parameter was shown[13] to be a direct counterpart of the covalent bonding energy." [Pershina 95]

Reference 13 in the quoted text refers to [Mulliken 55].

Table 2-1 shows the results of calculations of the charges on atoms (Q_m) and total overlap populations (OP) for the chlorides of the highest oxidation states of the group 4, 5, and 6 elements (bromides were not printed) as reported by V. Pershina in [Pershina 97].

A small effective charge and large overlap population correlate with a more covalently bound molecule, which, in turn, is expected to correlate with a higher volatility. The results of these calculations are summarized by Pershina as follows:

> "A large series of the DS-DVM calculations[52-64] has enabled the establishment of a more universal character for the dependence "OP(covalency)-volatility." Thus, assuming that in a group, analogous compounds have similar structures in the solid state and in the gas phase, the following has been established: (a) higher values of OP(tot) for the 5d halides compared to the 4d ones correspond to their higher volatilities; (b) higher values of OP for the group 5 halides compared to the group 4 halides correspond to their higher volatility; (c) smaller OP data for oxyhalides compared to the pure halides correspond to their lower volatility; (d) much lower OP data for the halides of the d elements are in line with their low volatility.
>
> Thus, the higher values for the OP(tot) of the transactinide halides compared to the lighter analogs would be a reason to think their volatility should be higher." [Pershina 93a]

References 52-64 are listed here as [Pershina 92a, b, c, 93, 94 a-e, 95, 96b, and Ionova 92].

A comparison of Pershina's predictions with the experimental data given in this work will be explicitly discussed in Section 5.3. However, it will be useful to share some general trends now, based on the collected results of gas chromatography experiments with HEVI and OLGA II and III. For group 4, where we have the clearest understanding of chemical form, we do not find that the 5d element Hf is more volatile than the 4d element Zr. We do, however, find that the 6d element Rf is more volatile than the 5d element Hf. We do find that the volatilities of the group 5 elements are higher

Table 2-1: Effective charges (Q_m) on the metal ion and overlap populations (OP) for the group 4, 5, and 6 chlorides			
	MCl_4	MCl_4	MCl_4
Qm	Zr 1.18	Nb 0.93	Mo 0.79
	Hf 1.04	Ta 0.95	W 0.74
	Rf 1.07	Ha 0.81	Sg 0.59
OP (M-Cl)	Zr 0.48	Nb 0.41	Mo 0.36
	Hf 0.55	Ta 0.50	W 0.46
	Rf 0.57	Ha 0.52	Sg 0.45

than the group 4 elements, and we also find that the oxyhalides show a much lower volatility than the pure halides. Pershina's predictions based on overlap populations, therefore, match very well with the experimental data in all cases with the exception that they predict the 5d pure halide Hf to be more volatile than the 4d pure halide Zr.

3. Instrumentation

3.1 The Heavy Element Volatility Instrument (HEVI)

The Heavy Element Volatility Instrument was developed in 1990 by B. Kadkhodayan as an on-line instrument to separate volatile group 4, 5, and 6 halides from non-volatile reaction products, and to study the gas phase properties of the transactinide elements. Figure 3-1 shows a schematic of HEVI. A gas jet consisting of a He carrier gas containing salt aerosols is used to sweep out a target chamber containing short-lived nuclear reaction products, which collect on the aerosol particles and are transported to the beginning of the chromatography column. There they collect on a plug of quartz wool which is kept at 900° C. The high temperature of this section of the column vaporizes the aerosol particles leaving the reaction products on the quartz wool plug. A second gas stream consisting of an oxidizing halogenating agent is introduced into the column, which reacts with the elements on the quartz wool to produce halide species, and in some cases oxyhalides, of the reaction products. At 900° C these species are highly volatile and enter the remaining isothermal section of the chromatography column, which is kept at a lower temperature, between 50° and 650° C during each experiment. Because the isotopes studied are short-lived, if their halogenated compound is nonvolatile at the temperature of the column it will remain for a relatively long time on the column's surface compared to the half-life of the isotope, and it will undergo significant decay while on the column. If the compound is volatile at the temperature of the column, it will quickly pass through and enter the recluster chamber on the downstream end of the column, where the gas stream is cooled via adiabatic expansion and where the compound

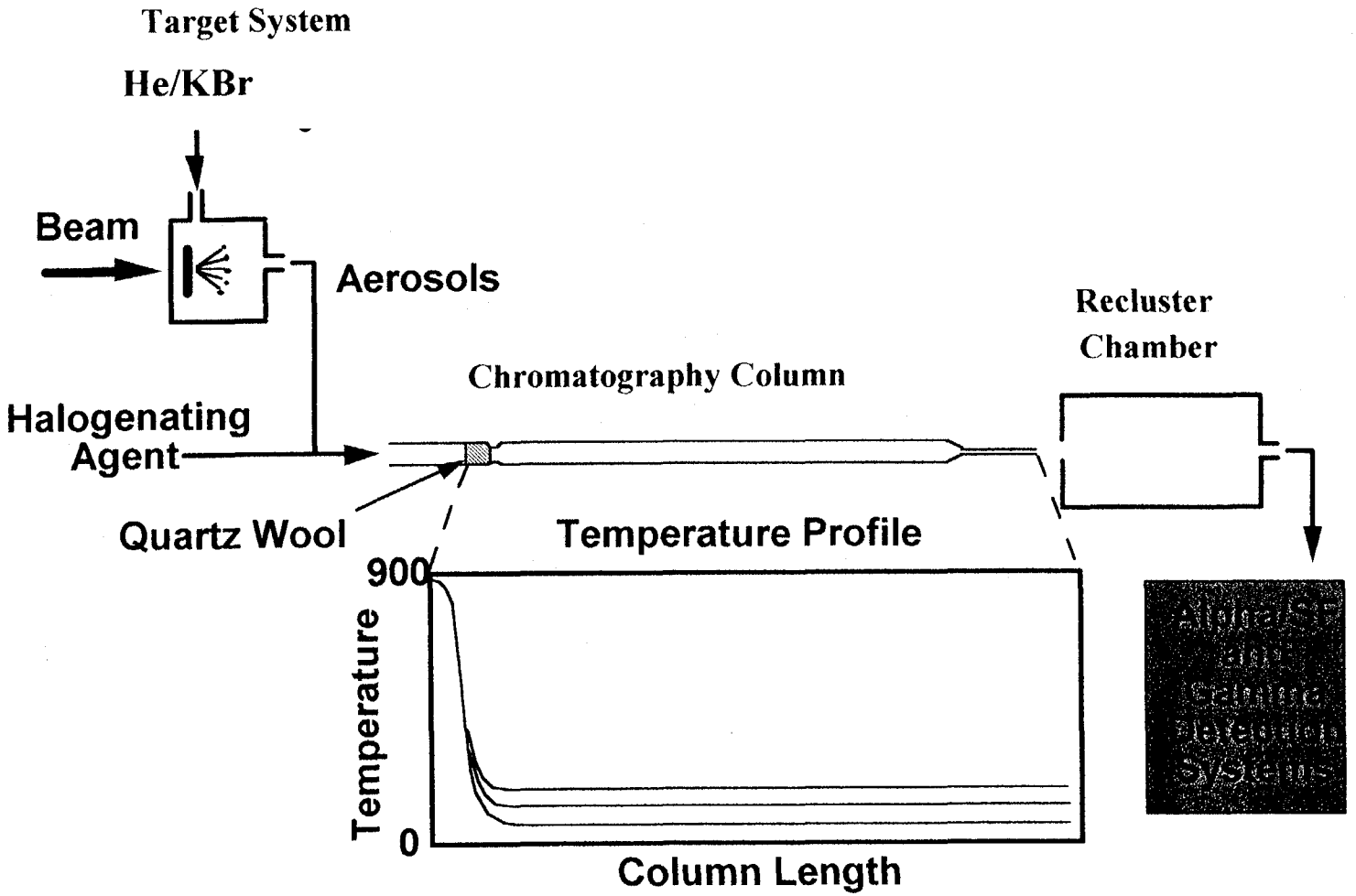

Figure 3-1: Schematic of the Heavy Element Volatility Instrument (HEVI).

is reattached to aerosol particles. It will then be transported via gas jet to a collection/detection site such as the MG rotating wheel system [D Hoffman 81] or a glass fiber filter, and counted using α-, SF-, or γ- spectroscopy. The volatility of the halide can be determined by varying the temperature of the isothermal section of the column and measuring the radiochemical yield as a function of temperature.

Internally, HEVI consists of a quartz chromatography tube enclosed in a series of graphite and ceramic cylinders within an inconel jacket, all of which is surrounded by 4 split-shell ovens. A heat sink consisting of a copper jacket cooled by an interior water circulation system is used to isolate the hot (900°) first section of the column from the isothermal section. The cylindrical inserts and the separate ovens are used to control the temperature of the column and to keep it isothermal. The inlet of the column includes an attachment which allows for the introduction and mixing of two separate gas streams at a temperature of 900° C while the temperature of the remaining length of the column can be varied throughout the experiment.

The exact specifications for the individual parts of the HEVI apparatus can be found in [Kadkhodayan 92]. The general experimental procedures for the initial gas chromatography studies are given in [Kadkhodayan 93, Section 2]. These procedures were followed in the current experiments in order to duplicate the experimental conditions of his experiments allowing a direct comparison of the results of this work with Kadkhodayan's previous work. Section 3.5 of this document describes the changes made to the HEVI apparatus and procedures from those used by Kadkhodayan.

3.2 The On-Line Gas Apparatus III (OLGA III)

Since HEVI was developed, OLGA II has been replaced with OLGA III [Eichler 94]. OLGA III utilizes an all-quartz design, which eliminates contact of the reactive gases with metal and avoids the possibility of corrosion and corrosive byproducts. The column length was increased to 1.9 m by forming it into a corkscrew shape around a quartz rod, so that the whole column may sit in a single heating oven. This allows the temperature of the column to be controlled to a theoretical accuracy of ±0.5° C or better, but the actual temperature profile inside the quartz tube has not been directly measured for the exact shape and size of this column. Initial results with OLGA III match the previous results from OLGA II. OLGA III can reach temperatures up to 450° C. The combination of longer column length and greater temperature control produces greater precision in the observed volatility profiles. The recluster chamber has also been improved. The volume has been greatly reduced and the flow of carrier gas now meets the outflow from the chromatographic column head on so that turbulent mixing of the two gas streams is used to cool the flow from the column. Recluster times in OLGA III have been observed to be only a few seconds. A schematic of OLGA III, along with the results of a typical experiment, are shown in figure 3-2 [Eichler 94].In collaboration with A. Türler, H. Gäggeler, and others, Olga III was used as part of this research to study the volatility of $^{262,263}HaCl_5$ and $^{262,263}HaOCl_3$.

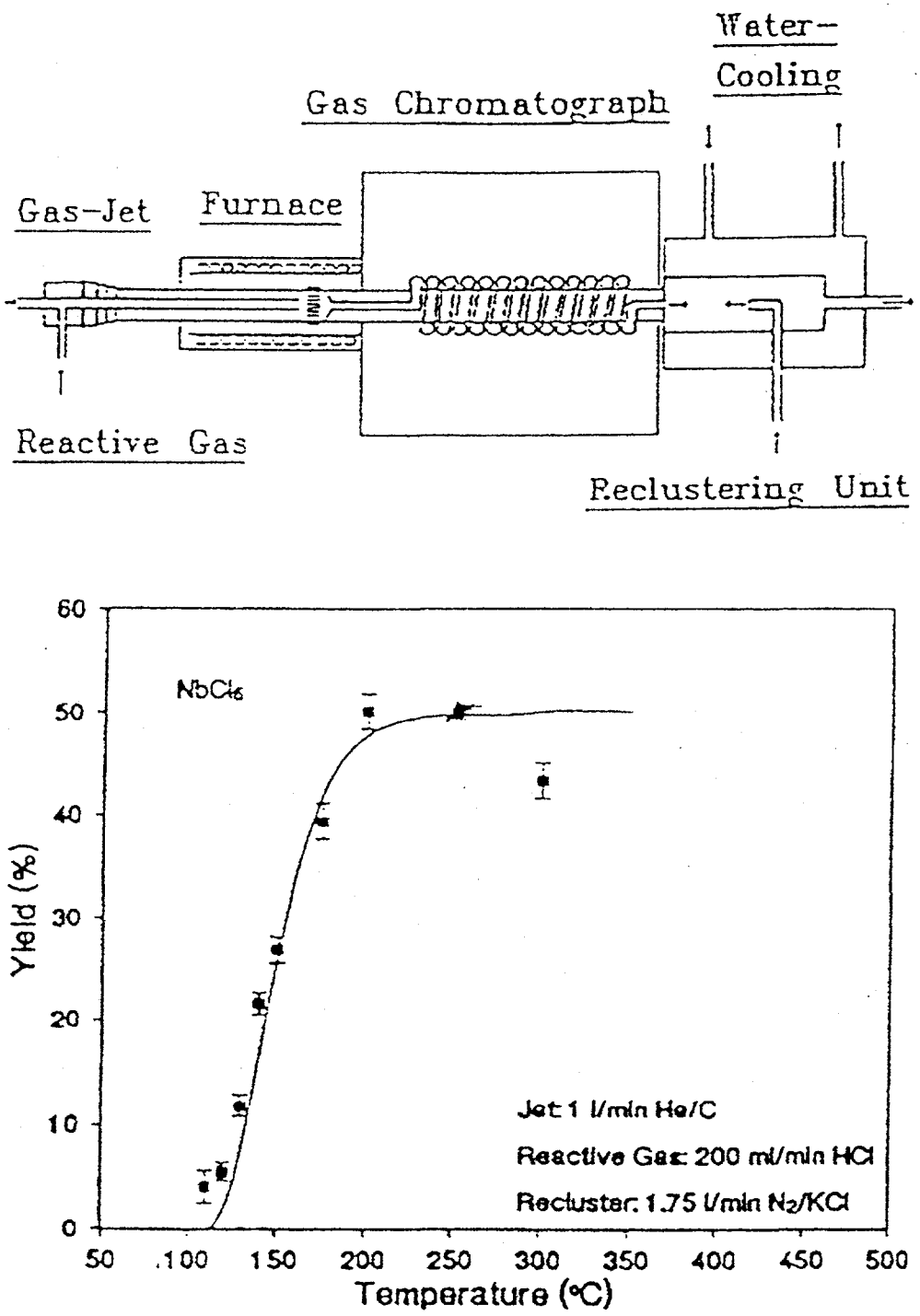

Figure 3-2. Top; a schematic of OLGA III. Bottom; results of an experiment with OLGA III for $^{99g}NbCl_5$. The curve shown is a Monte Carlo fit to the data representing an adsorption enthalpy of –80 kJ/mol.

4. Experimental Procedures

Two separate types of experimental procedures were used during the course of this research. The first consisted of on-line experiments performed using short-lived radionuclides produced via compound nucleus reactions at the Lawrence Berkeley National Laboratory (LBNL) 88-inch cyclotron. Section 4.1 gives the procedures, targets, nuclear reactions, and detection systems used in the on-line studies.

The second procedure consisted of off-line experiments where the isotopes studied were the recoil products ^{221}Fr and ^{213}Bi ($t_{1/2}$ = 4.8 min, and 45.6 min, respectively). Details for the off-line studies can be found in Section 4.2.

4.1 On-Line (Cyclotron) Procedures

In the on-line experimental procedures, the radioisotope to be studied is produced via a compound nucleus reaction of a charged beam and a target within a target chamber. The nuclear reaction products recoil out of the target material, attach to KBr aerosols in a flowing He carrier gas, and are then carried to the experimental apparatus and from there to either an α- or γ-detection system. All of the targets except for the ^{nat}Cu and mixed Ho/Tb/Cs-bromide targets consisted of the target material electroplated onto a backing of 4.75 or 2.38 mg/cm^2 Be foil. The ^{nat}Cu target consisted of a copper foil mounted behind a HAVAR backing foil. The mixed Ho/Tb/Cs-bromide target consisted of $HoBr_3$, $TbBr_3$, and CsBr deposited onto a Be backing foil using resistance heating followed by vapor deposition.

4.1.1 Target System and Gas Transport System

A schematic of the target system is shown in Figure 4-1. The beam from the cyclotron passes through a thin (1.8 mg/cm^2) HAVAR window used to separate the target system from accelerator vacuum, and then through the Be target backing before interacting with the target material. N_2 gas is used to cool the target and target backing. The reaction products recoil out of the target as ionized particles and attach to the KBr aerosols carried through the chamber with He gas. This gas enters the chamber through 6-mm polyethylene tubing and exits the chamber through a 3-mm Teflon capillary. A water-cooled copper beam stop is mounted at the end of the target chamber for cooling. Gas flow through the whole system is maintained by a vacuum pump positioned after HEVI.

The He gas transport method employed here has been used extensively in on-line chemical studies because of its ability to transport reaction products over long distances in short periods of time with a consistently high yield [Nai-Qi 89, MacFarlane 98, Herrmann 82, Kadkhodayan 93a, Trautmann 75, Schaedel 88, Mazumdar 80]. In the current studies, KBr was used as the aerosol both in the initial transport of the activity and as the recluster aerosol to transport the activity from HEVI to the detector apparatus. Previous gas chromatography experiments with HEVI used KCl and MoO_3 as aerosol materials. Both of these materials were rejected for the current studies due to the possibilities of forming mixed halides such as $RfCl_xBr_{4-x}$, and oxyhalides such as MoO_2Cl_2 or MoO_2Br_2.

The single exception was the experiment to study the chloride compounds of ^{262,263}Ha, in which KCl was used as both the carrier aerosol and the recluster aerosol.

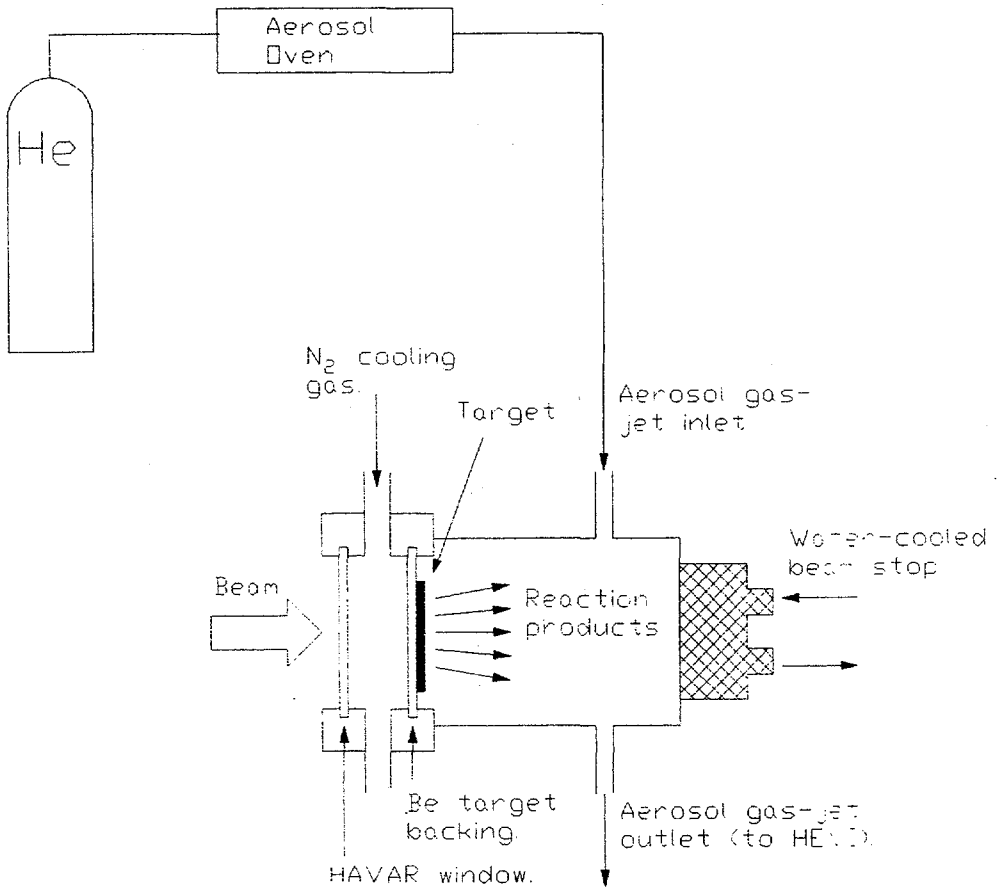

Figure 4-1: Target chamber used for on-line experiments at the LBNL 88-inch Cyclotron.

Previous studies [Kadkhodayan 93a] have shown that the optimal temperature for the release of aerosol particles of these salts is 620° to 640° centigrade, and that the transport time for this system was on the order of 1 second.

In all cases a small amount (10-20 grams) of either KBr or KCl was placed in a quartz tube oven kept at a temperature of 640° C. Pressurized He was connected to the oven through 6-mm polyethylene tubing, which was then also used to transport the aerosols to either the target chamber or the recoil chamber. The initial 3 meters after the quartz oven was arranged in 30-cm loops and functioned as a presorter to separate out the larger salt clusters so that the aerosol particles used in the transport of activity were of a uniform size. The target material attached to the aerosol particles was then swept up through a 3-mm teflon capillary and transported to the beginning of our experimental apparatus. The total transport length from the target to the HEVI system was 5 meters and the observed transport yield varied between 60-80% for the listed experiments.

4.1.2 Target Preparation

4.1.2.1 Rare Earth and Actinide Targets

All of the rare earth and actinide targets used in these experiments were produced by high voltage molecular plating from an isopropanol solution onto 6-mm diameter Be disks of 2.38 mg/cm^2 thickness [Aumann 74, Evans 72, Müllen 75].

A known amount of the rare earth target material, in metallic or oxide form, is first converted into a nitrate salt ($X(NO_3)_y$, usually $X(NO_3)_3$) where X is the desired target isotope, by dissolving it in a solution of nitric acid and then evaporating to

dryness. This procedure is repeated to ensure the material is fully converted to the nitrate form and the remaining salt from the last step is dissolved in isopropanol.

An aliquot of this solution, containing enough of the target material to produce a layer of the desired thickness is placed in the plating cell (Figure 4-2), with the Be backing foil at the base of the cell acting as the cathode and a wire within the solution acting as the anode. Approximately 500 V is applied across the solution at a current of 0.6 mA for 20-30 minutes for each deposition of the hydrated oxide on the Be foil.

After the isopropanol solution remaining in the cell is removed, the target is removed and placed in a quartz tube in a split-shell furnace and heated to 500° centigrade to convert it to the more stable oxide form. After cooling, the target layer thickness is determined (see individual descriptions below). The yield of the plating process approached 100% in the cases of the europium, gadolinium, and samarium, but was not as consistent for californium and berkelium.

This process is then repeated using the same target as the cathode until the desired target thickness is reached.

^{nat}Eu target

A target of 1000 $\mu g/cm^2$ $^{nat}Eu_2O_3$ was prepared via the same procedure outlined above. The europium was purchased as europium oxide powder from K & K Laboratories, Inc. and dissolved in a solution of 3 M HNO_3. This solution was evaporated to dryness and the process was repeated twice more to ensure that the europium was converted to the nitrate form. The remaining salt was dissolved in isopropanol to produce a stock solution of known concentration from which aliquots were

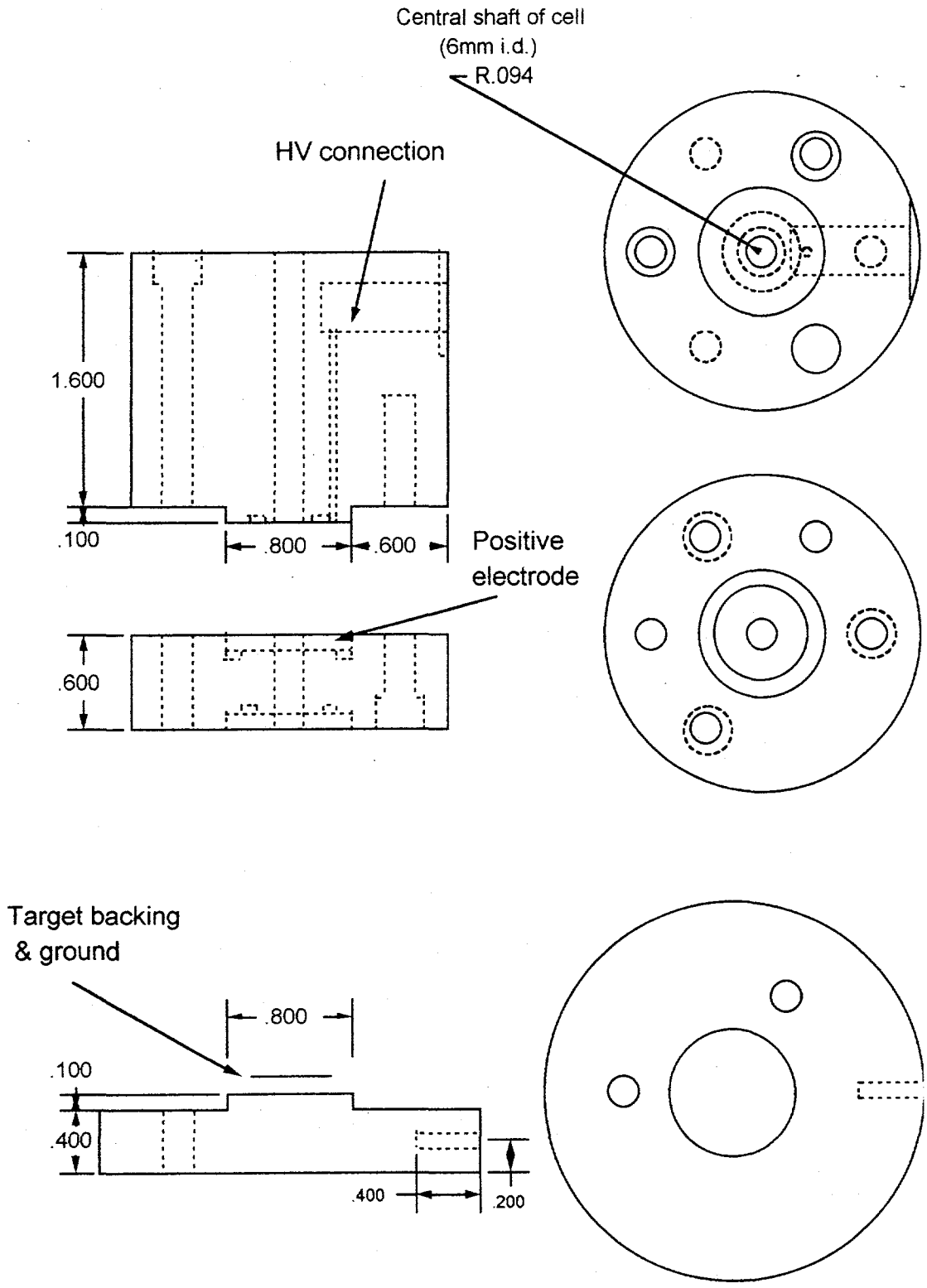

Figure 4-2: Plating Cell used for target production. All measurements are given in cm.

taken for the plating procedure. The target was produced in four approximately equal layers of 200-300 $\mu g/cm^2$ each. No tracer was added; the mass of each layer was determined gravimetrically using a Mettler M5 microbalance which was capable of determining weight to within 0.01 ± 0.005 mg.

Mixed ^{nat}Eu and ^{147}Sm target

A mixed target consisting of 151 $\mu g/cm^2$ $^{nat}Eu_2O_3$ and 214 $\mu g/cm^2$ $^{147}Sm_2O_3$ was prepared by B. Kadkhodayan using the same procedure outlined above. The europium was purchased as europium oxide powder from K & K Laboratories, Inc. and the ^{147}Sm was purchased in isotopically pure form from Oak Ridge National Laboratory. In separate procedures, both were dissolved in solutions of 3 M HNO_3. These solutions were evaporated to dryness and the process was repeated several times to ensure full conversion to the nitrate forms. The remaining salts were then dissolved in separate solutions of a known quantity of clean isopropanol. A known tracer of ^{241}Am was added to the Sm solution and a tracer of ^{248}Cm was added to the Eu solution, in order to determine the yields and hence the target thicknesses. Known amounts of both solutions were added to the plating cell simultaneously and the target was plated as described above. After each plating, the target was dried and counted using alpha spectroscopy with a Si(Au) solid state surface barrier detector. This process was repeated several times before the final target thickness was reached.

^{248}Cm target

A target consisting of 810 μg/cm^2 $^{248}Cm_2O_3$ was prepared by K. Gregorich. The curium was purified prior to electroplating. The Cm_2O_3 is dissolved in 0.2 M HNO_3. This is then extracted into 0.5 M di-2-ethylhexylorthophosphoric acid (HDEHP) in heptane [Horowitz 69], which separates the Cm^{3+} from any 2+ impurities such as Pb^{2+}. The organic phase is washed with 0.2 M nitric acid. The Cm^{3+} is then back extracted with 10 M HNO_3, leaving any 4+ impurities such as Pb^{4+} in the organic phase. The aqueous phase is washed with heptane to remove any traces of HDEHP. The pure Cm is dissolved in 10 M HNO_3 is then heated to dryness, redissolved in HNO_3, heated to dryness again, and then dissolved in a known amount of clean isopropanol for plating. An aliquot of this solution containing enough Cm to produce a layer of approximately 100 μg/cm^2 thickness of the Cm_2O_3 was added to pure isopropanol in the cell and plated. After each plating, the target was dried and the α-activity assayed with a Si(Au) solid state surface barrier detector. This process was repeated until the final target thickness of 810 μg/cm^2 $^{248}Cm_2O_3$ was reached.

^{249}Bk target

A target of 790 μg/cm^2 ^{249}Bk was produced by K. Gregorich for the $^{249}Bk(^{18}O^{5+}$, 4-5n) ^{262,263}Ha experiments. ^{249}Bk has a half-life of 320 days and produces ^{249}Cf via β^- decay. ^{249}Cf has a half-life of 351 years and so builds up with time in the $^{249}Bk_2O_3$. Both Cf and Bk behave similarly in the experimental conditions used for the target deposition so that it was necessary to separate the Cf daughter from the Bk before producing the target. Additionally, the presence of impurities such as lead made purifying the Bk

necessary. The berkelium with the californium daughter was dissolved in 10 M HNO_3 and was oxidized by $KBrO_3$ to the (IV) oxidation state. The 4+ species will extract into 0.5 M di-2-ethylhexylorthophosphoric acid (HDEHP) in heptane, while the 3+ species will not. The organic phase was washed with 10 M HNO_3 containing $KbrO_3$ to improve the separation between the 4+ species and any remaining 3+ species in solution. The Bk^{4+} was then shaken with 0.2 M nitric acid containing a small amount of H_2O_2 to reduce the Bk^{4+} to Bk^{3+}, which will still remain in the organic phase while Pb^{2+} will extract into the aqueous phase. The Bk^{3+} is then finally back extracted into 10 M HNO_3 containing H_2O_2 and washed twice with heptane to remove traces of HDEHP.

The resulting HNO_3 solution is heated to dryness and the remaining $Bk(NO_3)_3$ salt was dissolved in a known amount of clean isopropanol solution. An aliquot of this solution containing enough Bk to produce a target layer of approximately 100 $\mu g/cm^2$ thickness Bk_2O_3 was added to the plating cell with isopropanol and electroplated as before. After each layer the target was baked at 350° for 30 minutes to convert it to the oxide and then assayed via α-spectroscopy to determine its thickness. The electroplating process was repeated until the desired target thickness of 790 $\mu g/cm^2$ was reached.

4.1.2.2 Lanthanide and Transition Metal targets

Mixed ^{165}Ho, ^{159}Tb, and $^{133}CsBr$ target

A target composed of 100 $\mu g/cm^2$ ^{165}Ho as $HoBr_3$, 100 $\mu g/cm^2$ ^{159}Tb as $TbBr_3$, and 100 $\mu g/cm^2$ ^{133}Cs as CsBr was prepared by MicroMatter, Inc. (Deer Park, Wa.). The target was prepared in vacuum by resistance heating of the target material and its

subsequent vapor deposition on the backing. The Be backing used for this target was 4.70 mg/cm^2, twice as thick as normal, on the request of MicroMatter.

Further examples of this method of target preparation can be found in [Trigg 97].

^{nat}Cu Target

A target of ^{nat}Cu was used for the reaction ^{nat}Cu(^{28}Si, pxn) ^{88,89}Mo. A 1.14 mg/cm^2 Cu foil from the Braun-Knecht-Weimann Co. (San Francisco) was cut and mounted behind a HAVAR backing. The backing was included in order to maintain the integrity of the vacuum within the beam line.

4.1.3 Production of Isotopes for On-Line Studies

The details of the nuclear reactions used to produce isotopes for all of the on-line experiments are given in Table 4-1, below. Examples of γ- spectra for each of the homolog producing reactions shown in Table 4-1 are given at the end of this chapter, with the spectroscopic lines used for the identification of the product isotopes identified along with the other major products of the reactions. A spectrum of a yield check (described in section 1-2) is included, as is a spectrum of the second count of a collection for those experiments for which a long-lived (≥ 5 min.) isotope was studied. Alpha spectra for the ^{248}Cm(^{18}O^{5+}, 5n)^{261}Rf and ^{249}Bk(^{18}O^{5+}, 4-5n)^{262,263}Ha reactions are shown in section 5 of this document.

Table 4-1: Production Reactions for the on-line experiments performed with HEVI							
Target		*Beam*		*Products*			
Isotope(s)	Thickness ($\mu g/cm^2$)	Projectile and Ionization state	Energy[1] (MeV)	Reaction Channel	Isotope(s) observed	σ (mb)[2]	Half-life
$^{nat}Eu_2O_3$	860 ^{nat}Eu	$^{19}F^{5+}$	116, 94	5n	^{165}Hf, ^{167}Hf	262, 377	1.7 min, 2.0 min
$^{147}Sm_2O_3$, $^{nat}Eu_2O_3$	214 ^{147}Sm, 151 ^{nat}Eu	$^{20}Ne^{6+}$	140, 122	4-6n	^{162}Hf, ^{166}Ta, ^{167}Ta	≈100-500	38sec, 34 sec, 1.4 min
$^{159}TbBr_3$, $^{165}HoBr_3$, $^{133}CsBr$	100 $^{159}TbBr_3$, 100 $^{165}HoBr_3$, 100 $^{133}CsBr$	^{14}N	96, 85	3-5n 3-5n, pxn	^{167}Hf, $^{172,174}W$, ^{141}Sm, ^{88}Nb	≈300-500[3]	2.0 min, 6.6 min (^{172}W), 10.2 min, 14 min
$^{nat}Gd_2O_3$	500 ^{nat}Gd	$^{20}Ne^{6+}$	144, 91	5n	$^{170-173}W$	≈50-200	2.4 min-7.0 min
^{nat}Cu	1140	$^{28}Si^{6+}$	143, 86	pxn, 2pxn, 3pxn	$^{88,89}Mo$, ^{88}Nb ^{85}Zr	≈100-500	8.0 min, 2.0 min, 14.4 min, 7.9 min
$^{248}Cm_2O_3$	800 ^{248}Cm	$^{18}O^{5+}$	117, 99	5n	^{261}Rf	5 nb	74 sec[4]
$^{249}Bk_2O_3$	790 ^{249}Bk	$^{18}O^{5+}$	119, 99	5n, 4n	$^{262,263}Ha$	6 nb	35 sec

[1]Energies shown are the energy of the beam in the laboratory frame out of the 88-inch Cyclotron, followed by the energy of the beam as it interacts with the target, after passing through the target backing

[2]Unless otherwise noted, the cross-sections shown were calculated using the PACE 2 [REF] code.

[3]Calculated using the SPIT code [Alonso 73].

[4]measured half-life; this document (see section 4).

4.1.4 Detection Systems

Two different detection systems were used during the on-line experiments. An intrinsic germanium detector was used for gamma spectroscopy during the experiments with the light group 4, 5, and 6 transactinide homologs. The Merry-Go-Around (MG) alpha detection system [D Hoffman 80] was used for the detection of ^{261}Rf and ^{262,263}Ha..

4.1.4.1 The Gamma Detection System

The gamma detection system consisted of a teflon collection site in front of an EG&G Ortec intrinsic germanium γ-ray detector. Data collection was performed using the ORTEC Ace 4-K system with a PC and consisted of a 4096 channel sum spectrum for each 5- or 10-minute collection.

Activity enters the collection site via the aerosol gas-jet transport system and is collected on a glass fiber filter, while the helium gas passes through. This collection site sits directly in front of the face of the detector and counting of the sample takes place as the activity is collected on the glass fiber filter. This filter is replaced after each collection. The resulting gamma spectra are analyzed using the SAMPO code [Routti 69], which was used for peak fitting, energy and efficiency calibration as well as deconvolution of multiple peaks. The calculation of yield was based on the most intense photopeak of each isotope seen in the spectrum, and was corrected for variations in the beam current, and dead time of the ADC. The dead time was 10-12% for the 5-min yield check collections and 17-20% for the 10-min yield check collections. Dead times for the gas chromatography collections were significantly lower, typically 2-5%. When possible, other photopeaks of the same isotope were also analysed. Figures 4-6 through

4-10 show example spectra from both yield check and gas chromatography collections for all experiments in which γ-ray spectroscopy was used.

4.1.4.2 The Merry-Go-Around (MG) detection system

The MG rotating wheel system was used for the collection and detection of the transactinides ^{261}Rf and ^{262,263}Ha and their daughters. A capillary transports the activity-containing aerosols from the target chamber to the MG system where they are deposited on thin (40 ± 10 $\mu g/cm^2$) polypropylene foils, arranged around the periphery of a 51-cm diameter wheel holding a total of 80 such foils.

This wheel rotates (steps) between 6 pairs of Passivated Ion Implanted Planar Silicon (PIPS) detectors, each pair arranged with one detector above and one detector below the wheel, allowing a solid angle detection efficiency of approximately 60% for α decay. The entire apparatus is kept under vacuum, and the He gas stream is evacuated through a chemically inert vacuum pump and then to the scrubber. The stepping rate of the wheel is varied depending on the half-life of the isotope under study. For the ^{261}Rf experiment, the wheel was stepped at 1-min intervals and for the ^{262,263}Ha experiment, 30-s intervals were used. Each wheel is replaced with a new wheel containing clean foils after two complete rotations in order to minimize the buildup of long-lived activities and the aerosol clustering material.

The Realtime Data Acquisition System (RAGS) [D Hoffman 80, Leres 87] was used to record the data. Signals from the α- and SF- events are amplified and digitized using an ORTEC AE811 analog to digital converter (ADC). Each event is then stored with the time of event, detector identity, and channel number. Yield analysis for the ^{261}Rf

was then corrected for variations in the beam current throughout the run as well as the presence of α events within the expected energy range which were due to the presence of reaction products of Pb impurities in the target (mainly Po).

4.2 Off-line Studies

4.2.1 ^{221}Fr and ^{213}Bi

Off-line studies of the decay daughters from ^{229}Th (Figure 4-3) were performed using several recoil sources, all of which were produced in the same way and which replaced the target system in HEVI. Both the 4.8-min ^{221}Fr and 45.6-min ^{213}Bi decay daughters were studied in the HEVI system. The recoil source was used in two separate off-line studies; one to measure the volatility of the ^{221}FrBr and $^{213}BiBr_3$, and a second where the yield of FrBr at temperatures below the measured volatility was used to study an observed high yield of both volatile and non-volatile species at low temperatures, seen previously [Kadkhadayan 93a].

Metal foils (2.54 cm diameter) were suspended over a ^{229}Th source in a He atmosphere for a period ranging of 6-8 hours. A 300 V potential between the foil and source was used to increase the recoil and collection efficiency of the ^{229}Th decay products on the foil, which include ^{225}Ra, ^{225}Ac, ^{221}Fr, ^{217}At, ^{213}Bi, ^{213}Po, ^{209}Pb, and ^{209}Bi. The entire decay scheme is shown in figure 4-3.

The activity of the collection foil was first measured using a PIPS detector and then mounted in the recoil chamber shown in figure 4-4. This chamber consisted of a glass tube 2 inches in diameter and 8 inches in length attached at either end to female brass LRL fittings. Each of the connecting male end fittings consisted of an LRL (Lawrence Radiation Laboratory)-to- Swage compression fitting for ¼-inch tubing, and contained a hollow metal post which would extend 2-3 inches into the glass tube when attached. Each tine had holes in the far end to allow the gas jet to flow through the end pieces.

The foil with the $^{225}Ra/^{225}Ac$ recoil activity deposited on the surface was attached to one of the posts with the active surface facing away from the face of the post. A current of a few mA, ranging from 50-100 V was run across the tines with the tine on which the recoil source was attached acting as the anode. The positively charged recoil daughters from the ^{225}Ac- ^{221}Fr and its decay daughters– recoil off the foil, attach to the KBr aerosols, and are transported via the gas jet to HEVI.

4.2.2 Modifications to the Operation of HEVI

The operation principles of HEVI were the same as with the on-line system (see Figure 3-1), with the following modifications:

1) The He-KBr aerosol gas jet, which was used to transport the reaction products in the on-line experiments from the target chamber was attached to the recoil chamber shown in Figure 4-4.

2) The aerosol gas flow, with the recoil products attached, was directed into HEVI through a 3-mm teflon capillary identical to the capillary used to transport the target recoil products from the target chamber to HEVI.

3) The flow rate for the transport He was regulated to 2 l/min, which is the same flow rate used in the on-line gas chromatography experiments.

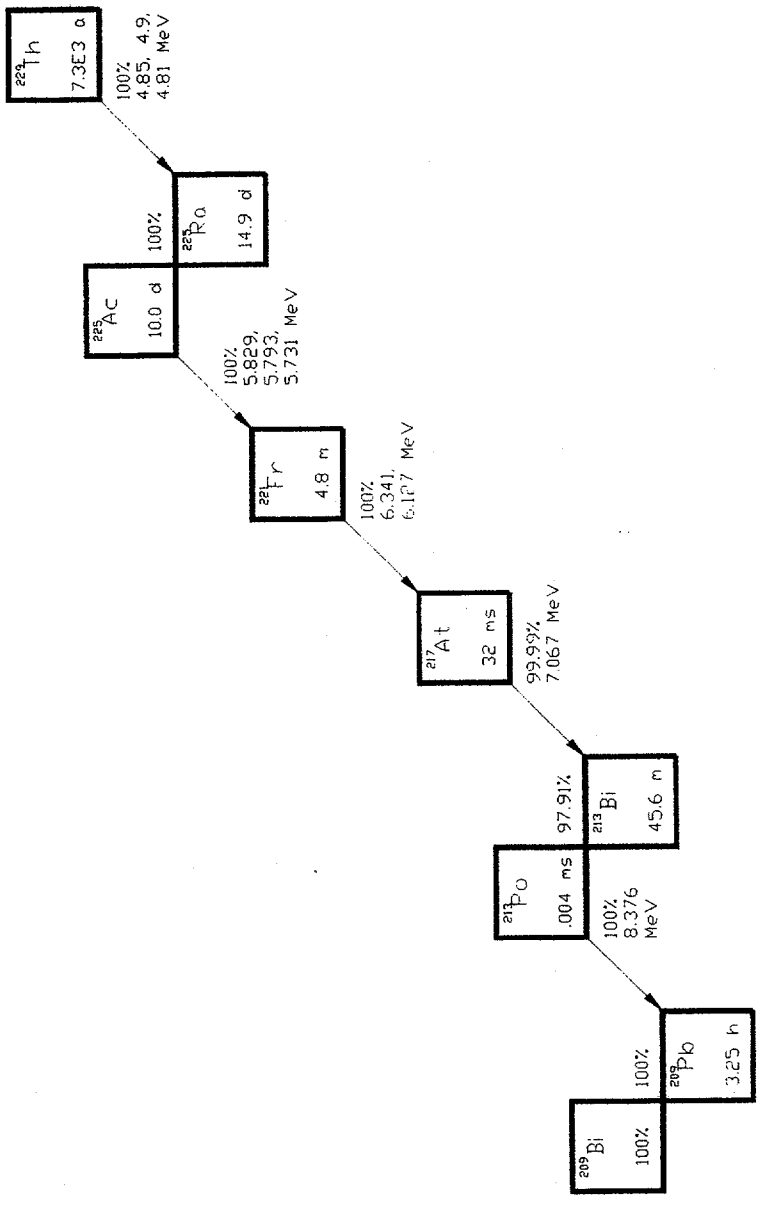

Figure 4-3: Decay chain of ^{229}Th

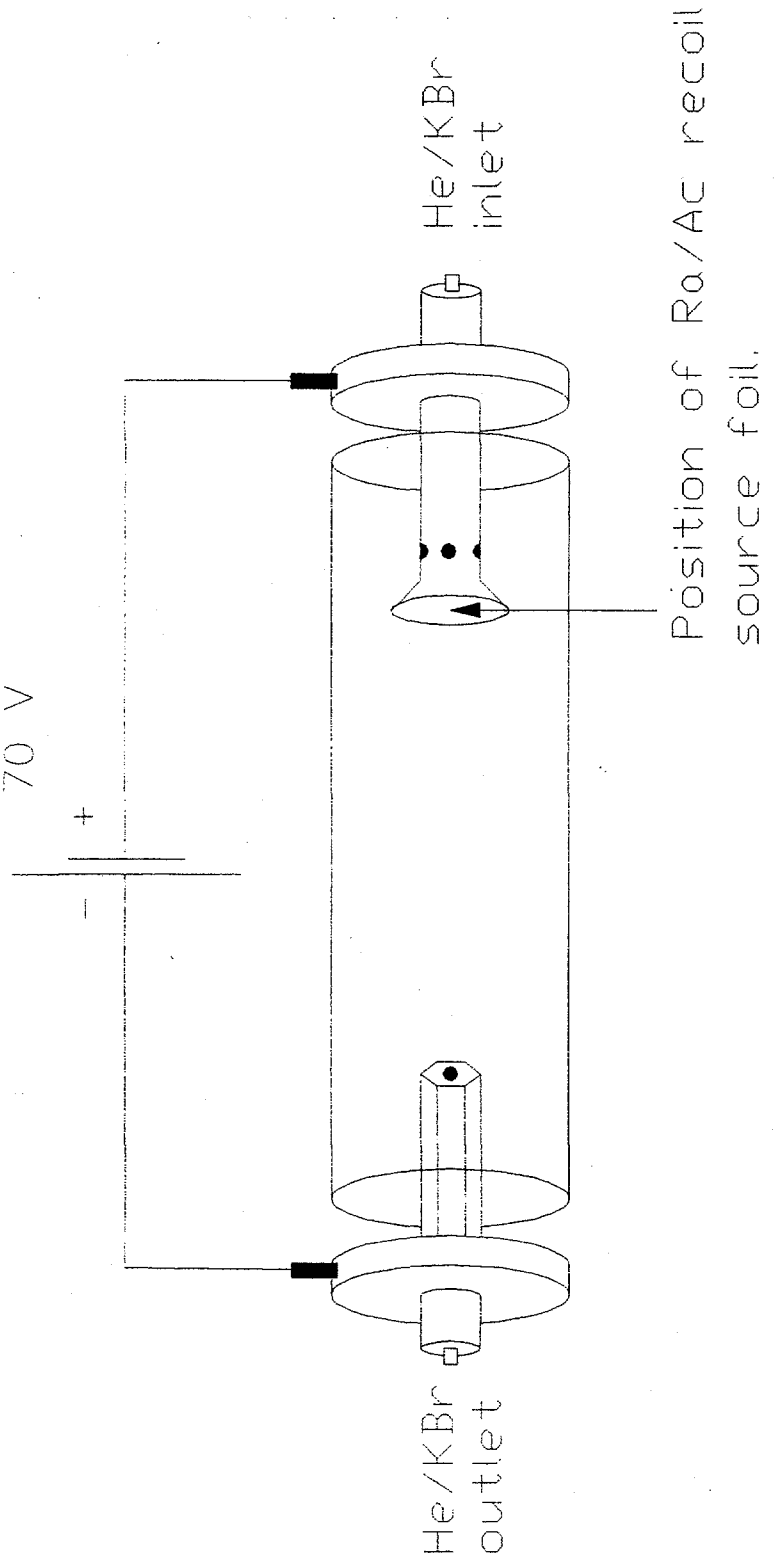

Figure 4-4: Recoil Chamber.

4.2.3 Off-line Experimental Procedures

Before the recoil source was used for off-line chromatography experiments the recoil yield as a function of applied voltage was studied. Activity from the recoil source was collected on a Gelman Sciences 25-mm glass fiber filter for 5 minutes and then counted. The total alpha activity between 6.0 MeV and 9.0 MeV was used to measure yield, and the results are shown in Figure 4-5. For the remaining experiments an applied potential of 75 V was used.

For the off-line studies, the yield at each temperature was measured by first performing a 5-minute yield check, which bypassed the chromatography column and was directly collected on the filter, followed by two 5-minute gas chromatography collections and a final 5-minute yield check. Two 5-minute background counts of the detectors with no sample present were performed between each temperature to monitor any build-up of activity on the detector surface in the region studied.

4.2.4 Off-line detection and data analysis

For the off-line studies of the recoil products of the $^{221}Ra/^{221}Ac$ source a single PIPS detector was used, coupled with the ORTEC Ace 4-K system described in Section 4.1.4.1. The aerosol gas-jet containing the activity was passed through the teflon collection site (also described in section 4.1.4.1) and the activity collected on a glass fiber filter. After a 5-minute collection the filter was removed and placed on the PIPS detector where it was counted for an average of 5 minutes, and a clean filter placed in the collection sited for the collection of the new sample. At each temperature a yield check measurement was followed by two separate gas chromatography measurements and

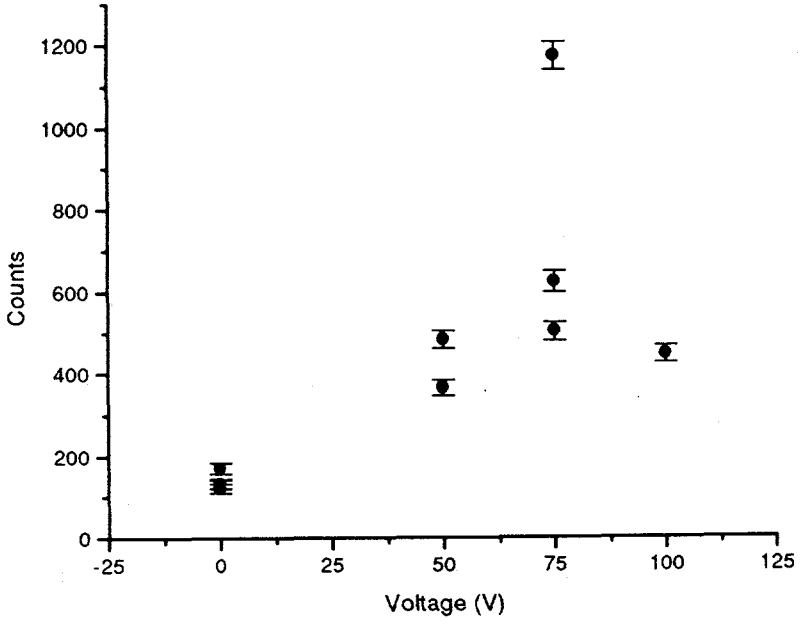

Figure 4-5: Total measured activity as a function of the voltage applied across the recoil chamber.

then a final yield check. The system was recalibrated using a $^{212}Bi/^{212}Po$ source every 4 hours and a 5-minute background count was taken at each temperature. Data analysis consisted of integration of the gross counts for each peak, corrected for background counts in the detector, count times, and shifts in the energy calibration.

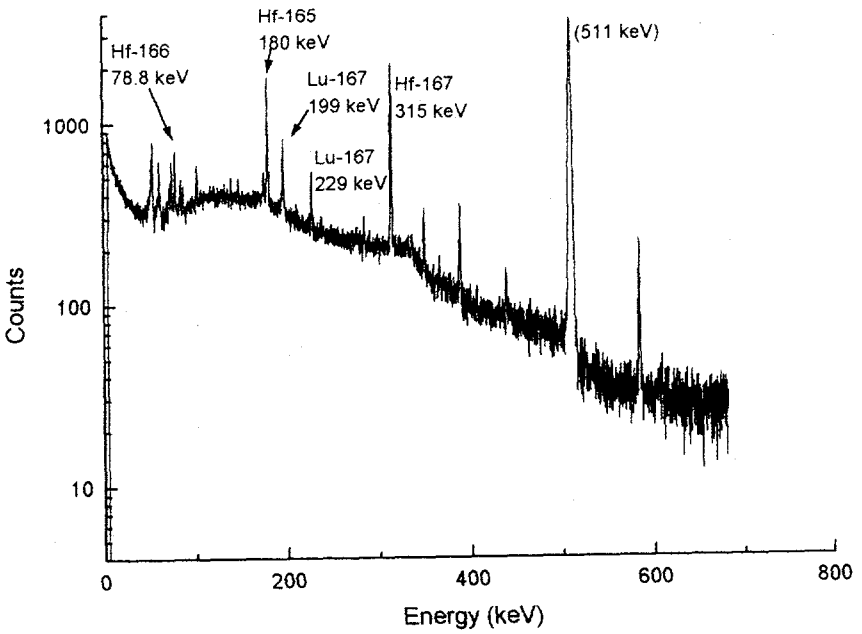

Figure 4-6 (a): γ-Spectrum of Yield Check collection for the $^{nat}Eu(^{19}F^{5+}, xn)\ ^{165,166}Hf$ reaction.

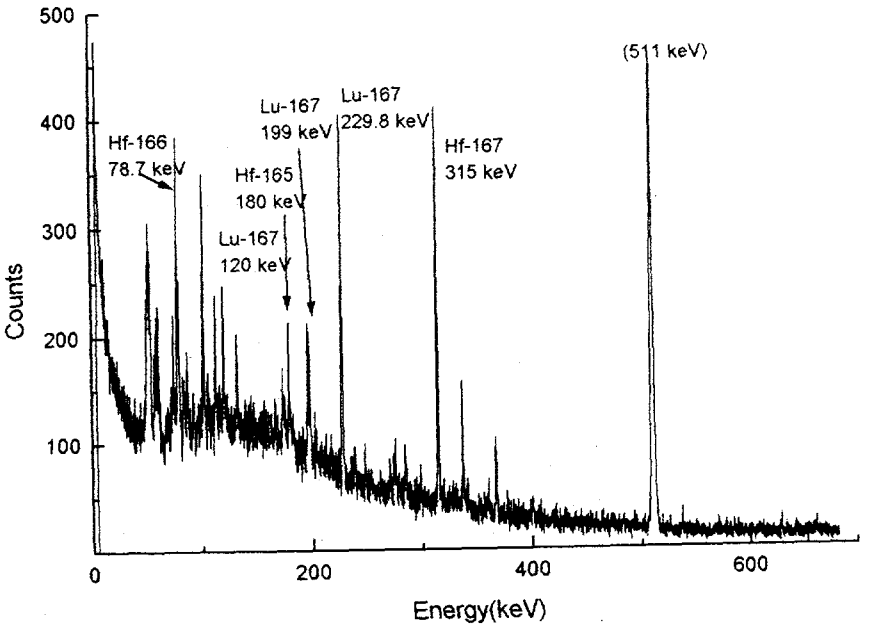

Figure 4-6 (b): γ-Spectrum of Gas Chromatography collection for the $^{nat}Eu(^{19}F^{5+}, xn)\ ^{165,166}Hf$ reaction. Temp.= 500° C.

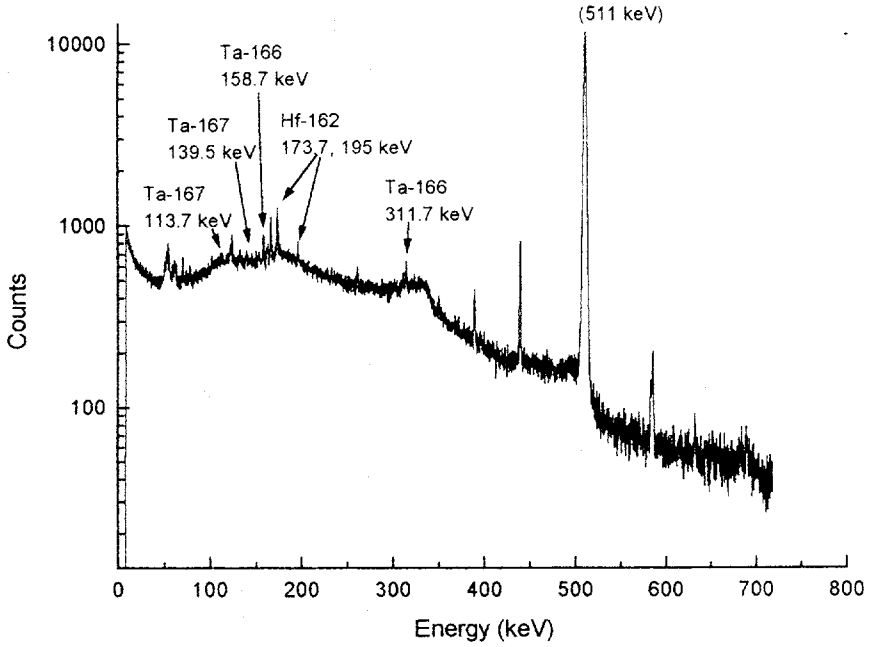

Figure 4-7 (a): γ-Spectrum of Yield Check collection for the $^{147}Sm/^{nat}Eu(^{20}Ne^{6+}, xn)\ ^{162}Hf,\ ^{166,167}Ta$ reaction.

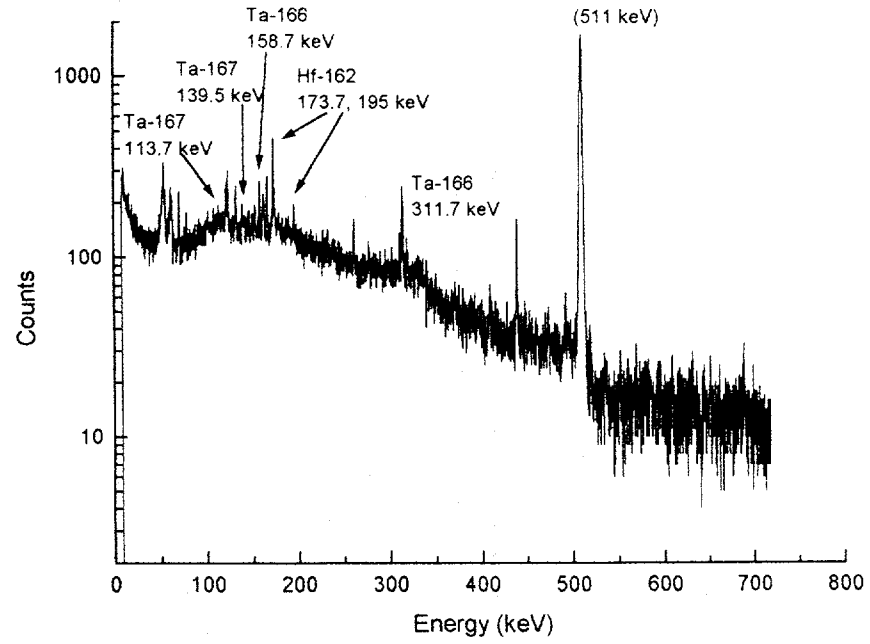

Figure 4-7 (b): γ-Spectrum of Gas Chromatography collection for the $^{147}Sm/^{nat}Eu(^{20}Ne^{6+}, xn)\ ^{162}Hf,\ ^{166,167}Ta$ reaction. Temp.= 500° C.

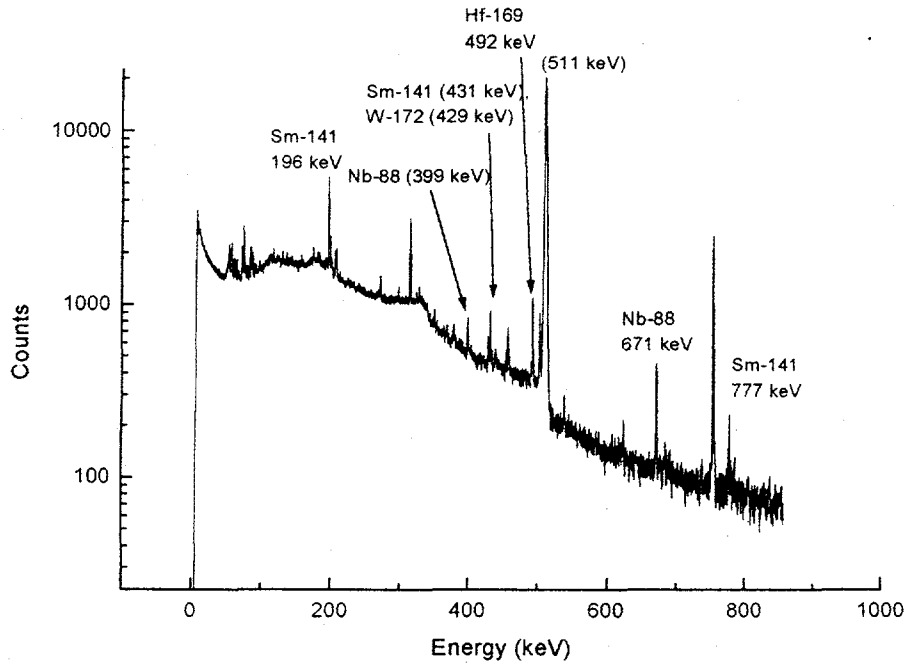

Figure 4-8(a): γ-Spectrum of Yield Check collection for the $^{165}Ho/^{159}Tb/^{133}Cs(^{14}N^{5+}, xn)$ $^{167,168}Hf$, ^{88}Nb, ^{141}Sm, $^{172,174}W$ reaction.

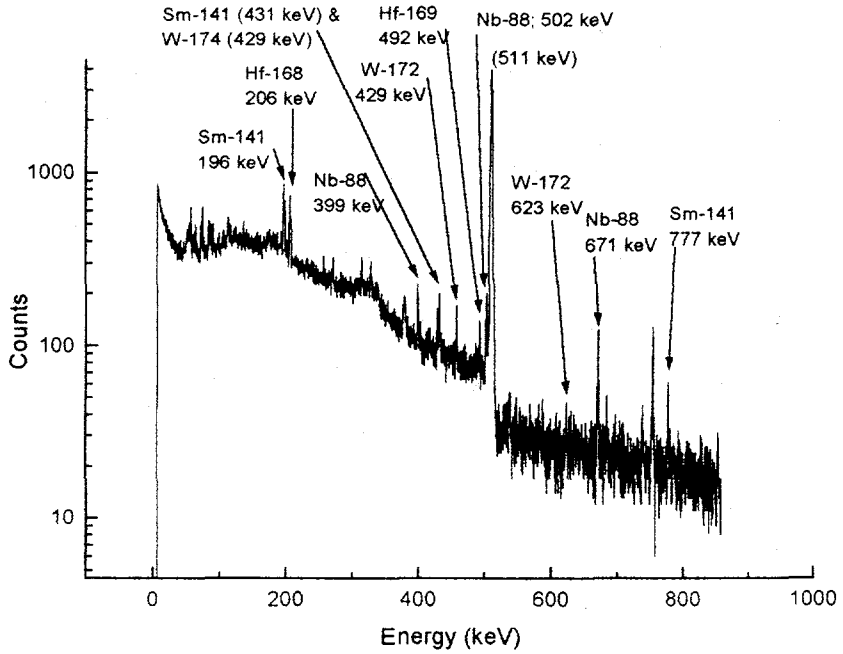

Figure 4-8 (b): γ-Spectrum of Gas Chromatography collection for the $^{165}Ho/^{159}Tb/^{133}Cs(^{14}N^{5+}, xn)$ $^{167,168}Hf$, ^{88}Nb, ^{141}Sm, $^{172,174}W$ reaction. Temp.= 500° C.

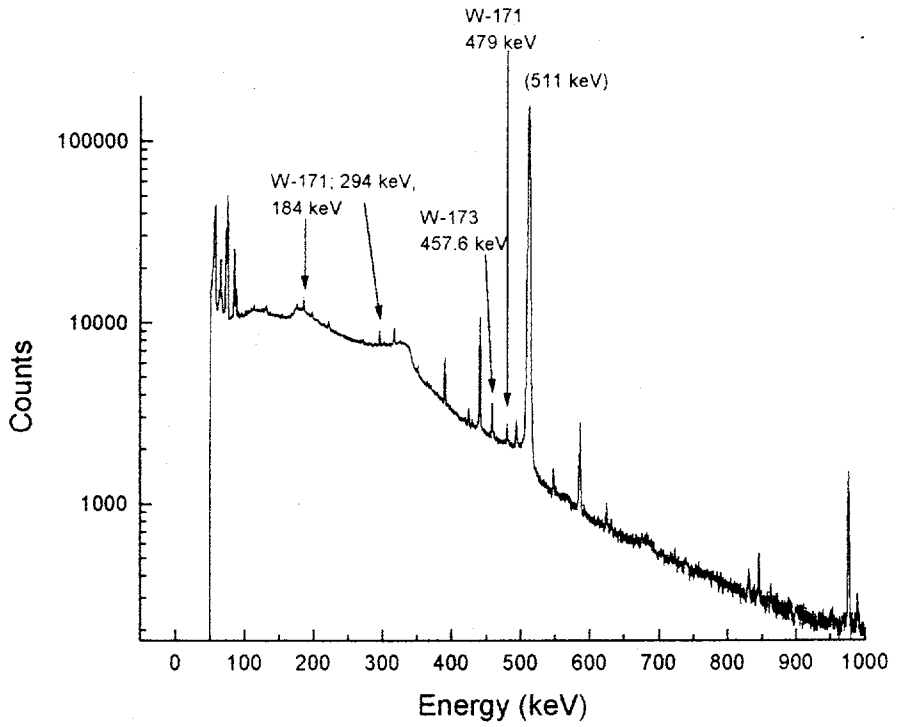

Figure 4-9(a): γ-Spectrum of Yield Check collection for the $^{nat}Gd(^{20}Ne^{6+}, xn)\ ^{162}Hf,\ ^{166,167}Ta$ reaction.

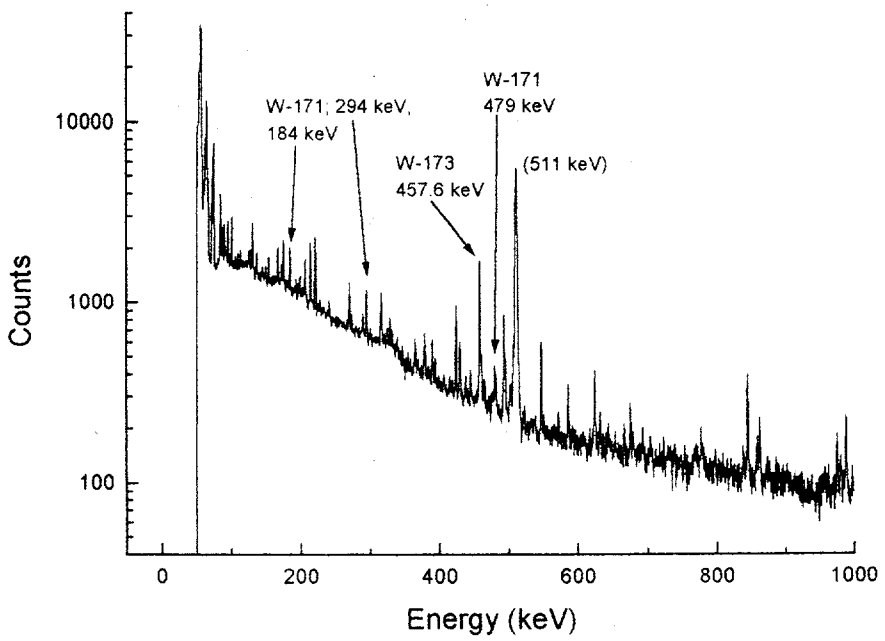

Figure 4-9(b): γ-Spectrum of second count for the collection shown above in (a).

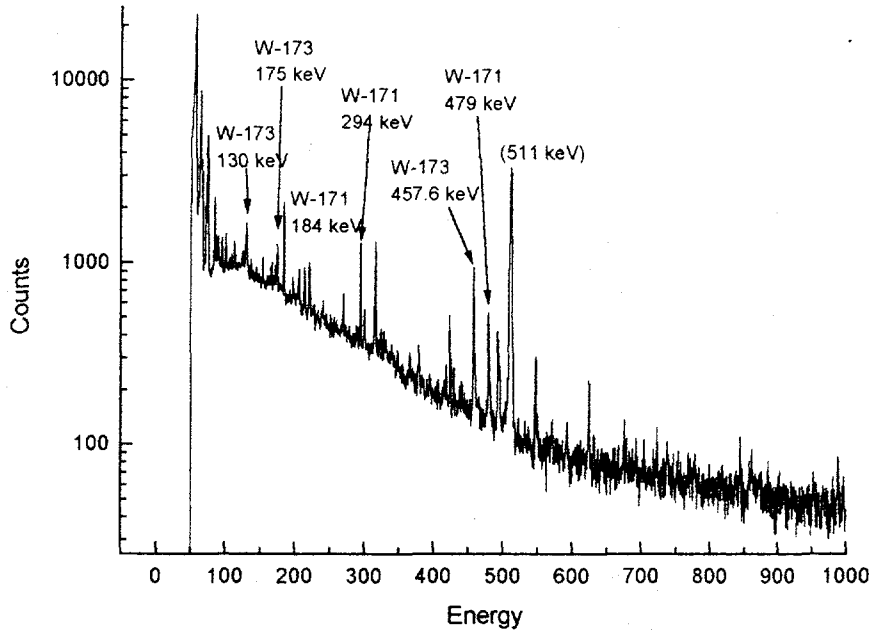

Figure 4-9(c): γ-Spectrum of Gas Chromatography collection for the $^{nat}Gd(^{20}Ne^{6+}, xn)\ ^{162}Hf,\ ^{166,167}Ta$ reaction. Temp.= 500° C

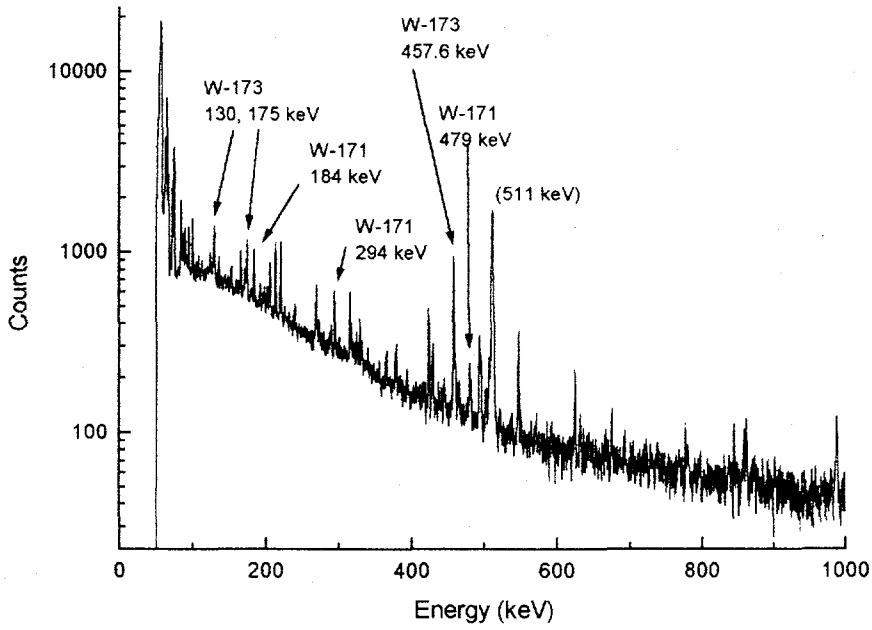

Figure 4-9(d): γ-Spectrum of second count for the collection shown above in (c).

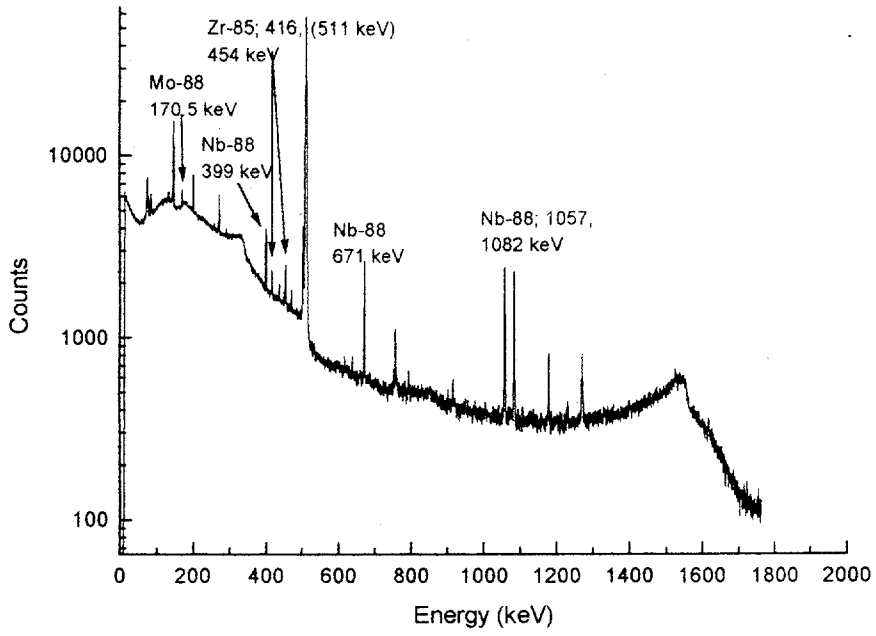

Figure 4-10(a): γ-Spectrum of Yield Check collection for the $^{nat}Cu(^{28}Si^{6+}, pxn)^{88,89}Mo, ^{88}Nb, ^{85}Zr$ reaction.

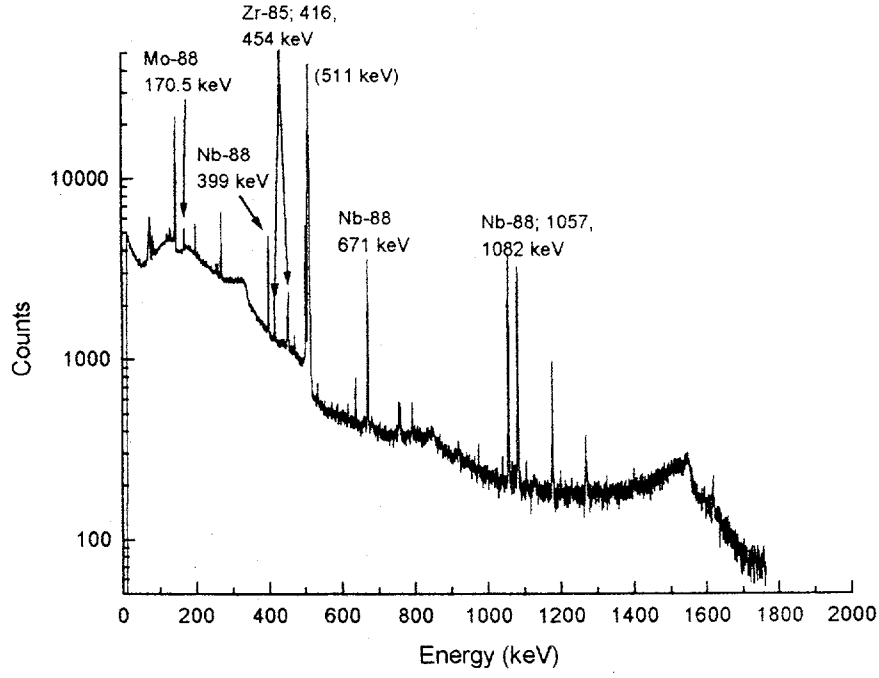

Figure 4-10(b): γ-Spectrum of second count for the collection shown above in (a).

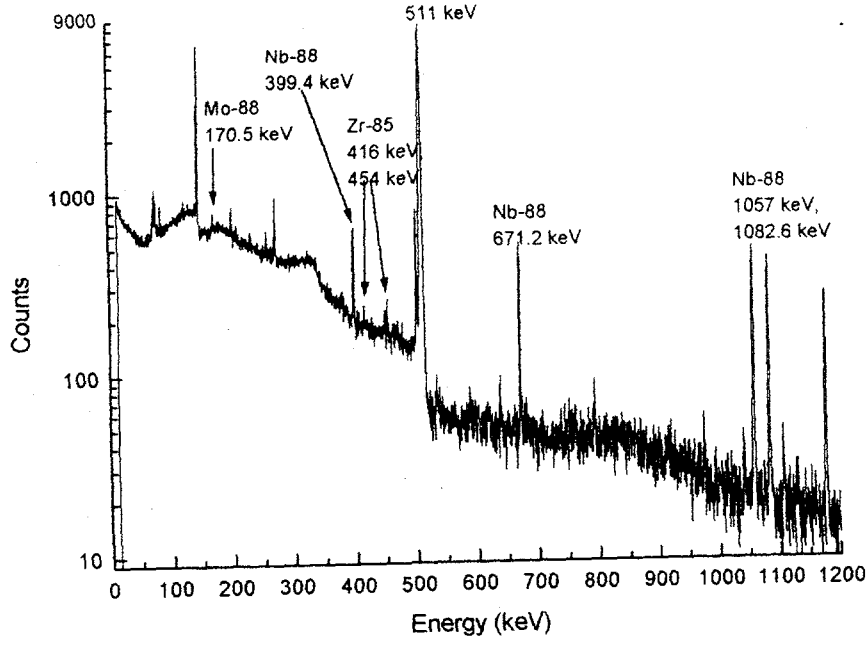

Figure 4-10(c): γ-Spectrum of Gas Chromatography collection for the $^{nat}Cu(^{28}Si^{6+}, pxn)^{88,89}Mo$, ^{88}Nb, ^{85}Zr reaction. Temp.= 500° C

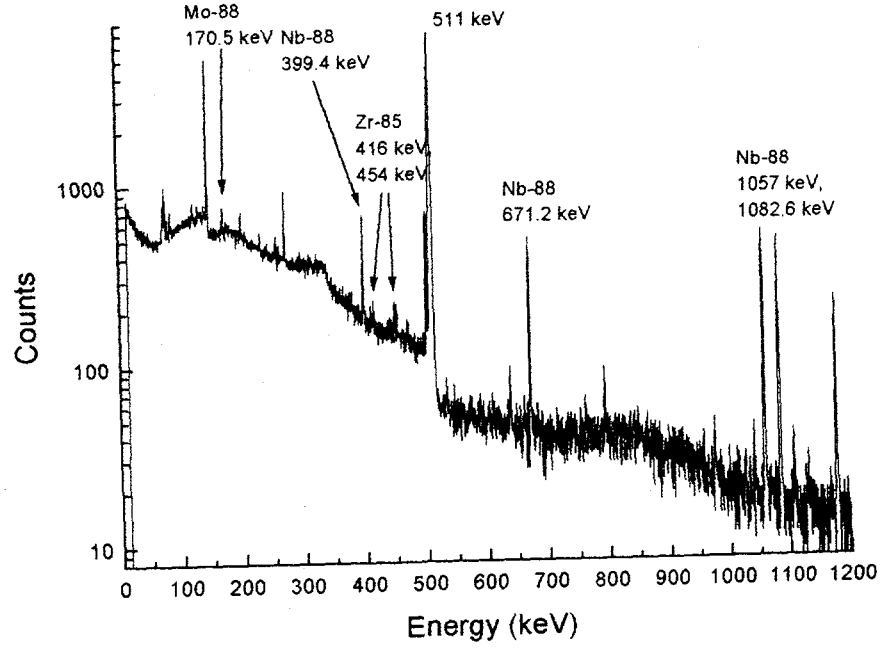

Figure 4-10(d): γ-Spectrum of second count for the collection shown above in (c).

5. Results

The presence of low temperature yields in HEVI noted in [Kadkhodayan 93] has been studied in order to determine whether this effect is a function of the volatility of the species or of some non-volatile transport method. These results are shown in Section 5.1. The volatilities of the bromides of Fr, Bi, Zr, Hf, Rf, Nb, Ta, and W, and the chloride of Ha have been measured, and the results are presented in Section 5.2. For each compound the *Volatility Temperature*, defined as the temperature at which the yield observed through the column is equal to 50% of the maximum chemical yield through HEVI, is reported. Adsorption enthalpies for these compounds have been calculated using a Monte Carlo simulation program to fit the data to an expected volatility curve. Preliminary results are presented for Mo-bromides.

All results are shown in graphs of % yield vs. temperature. The Monte Carlo simulation curve for the best fit to the data is also shown. From the best fit, the adsorption enthalpy ΔH_a, is obtained.

The error bars shown for all experimental points represent statistical one-σ uncertainties based on the measured peak areas. Where no error bars are presented, the error in the measured yield is smaller than the plotted point.

Except for the ^{262,263}Ha chloride experiment, all experimental results shown used HBr as the brominating agent and KBr as both the gas jet aerosol and recluster aerosol material.

5.1 Off-line Studies

High yields at low temperatures were seen for a variety of compounds both in these studies as well as in previous studies using HEVI [Kadkhodayan 93, 96]. During some of the same experiments, a high yield of radioisotopes expected to form nonvolatile compounds, such as ^{94}Sr, have been simultaneously observed at low temperatures (50° C to ≈200° C), indicating that some mechanism other than gas phase chromatography is responsible for the yield of activity through the column at these temperatures. Kadkhodayan noted a correlation between this effect and the presence of hydrogen in the system, and further hypothesized the formation of water aerosols in the presence of oxygen within the column as a possible transportation method.

This effect was studied directly by varying the amount of quartz wool in the column and observing the low temperature yield using FrBr. Figures 5-1 and 5-2 show the relative yield curves for the 4.8-min ^{221}FrBr. The experiment was run three times; first with with no HBr added to the gas flow and with the quartz wool plug normally used to stop the aerosol clusters from passing through the column removed. In the second run, a quartz wool plug of 0.025 g was used and 150 ml/min of HBr was added to the gas flow. These are the same conditions under which previous on-line experiments with HEVI had been conducted. In the third run, twice the standard amount of quartz wool (0.051 g total) was used, and again 150 ml/min HBr was added to the gas flow. In the latter two cases, the density of the quartz wool packing was held approximately constant.

These preliminary results show that the effect decreases significantly with a larger amount of quartz wool (0.051 g) versus the "standard" amount of quartz wool (0.025 g) or no quartz wool at all. Also, the addition or absence of the brominating agent HBr did

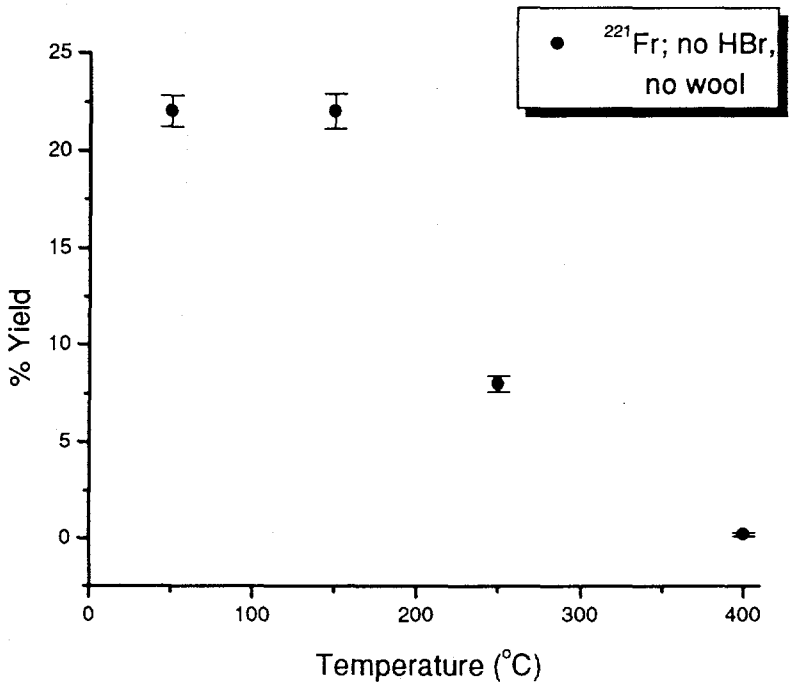

Figure 5-1: Yield of ^{221}FrBr between 0° and 400° C with no quartz wool and no HBr flow.

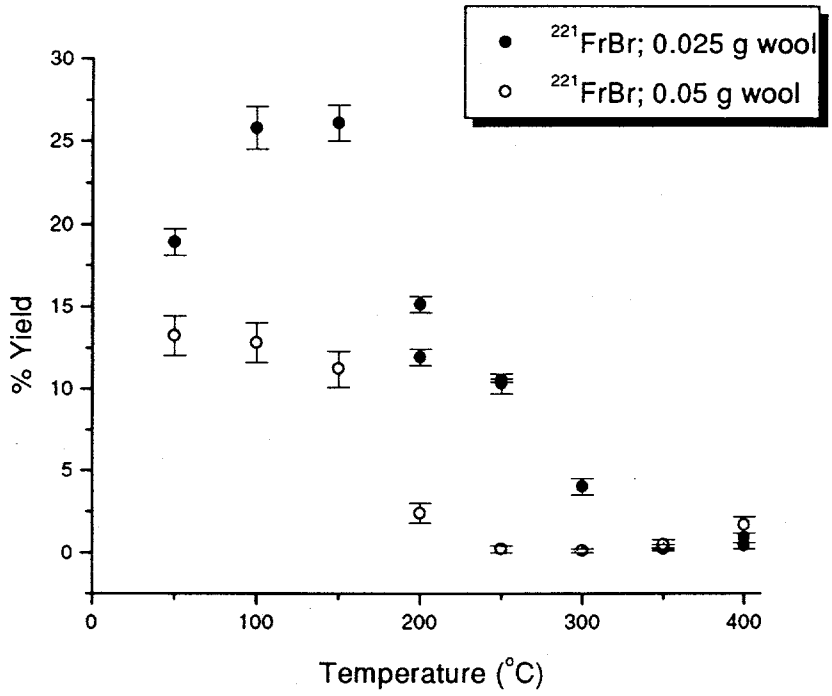

Figure 5-2: Yield of the 4.8-min ^{221}FrBr between 0° and 400° C, with 150 ml/min HBr flow and a variable mass of quartz wool.

not seem to change the yield at low temperatures.

These results are consistent with the theory that the yield is not caused by the volatility of the compounds studied or of other halogen compounds which may be volatile at low temperatures, but rather by some mass transport method that is independent of the volatility of the chemical form of the activity. With smaller amounts of quartz wool, some gas jet aerosols pass through the plug and high temperature section without being destroyed, leading to high yields of all compounds at the lower temperatures regardless of their volatility. With higher temperatures, both the length of the high temperature section and the average temperature of the quartz wool is effectively increased leading to a more complete destruction of the aerosol particles, and with larger amounts of quartz wool in use, the filtering action of the quartz wool becomes more efficient. It is also worth noting that the effects observed in the on-line experiments with HEVI in this work often vanish at 250°. This temperature corresponds with the removal of the heat sink from between the high temperature oven and the first chromatography column oven, which leads to a less sudden drop in temperature between these two ovens (See Kadkhodayan 93 for a detailed drawing of the temperature profiles of HEVI).

5.2 Volatility Temperatures and Adsorption Enthalpies

5.2.1 Fr, Bi Bromides

During the off-line experiments to study the non-volatile yield of FrBr at low temperatures, the volatilities of 4.8-min ^{221}FrBr and 45.6-min $^{213}BiBr_3$ were also studied. The results are shown in Figures 5-3 and 5-4, respectively.

The best estimate of the volatility temperature of FrBr from the results is ≥550° C. It is difficult to assign a volatility temperature to it due to the extremely low volatility of the compound. No constant yield above the volatility temperature was observed as the volatility temperature of FrBr approached the maximum temperature attainable in HEVI. Assuming the yield continues to rise or remains at 18%, the adsorption enthalpy of ^{221}FrBr is calculated to be ≤ (more negative than) –160 kJ/mol.

The relatively long half-life of the ^{213}Bi in comparison to the collection time, counting time, and the time between different temperatures (approximately 40 minutes) results in an unusually high volatility temperature of 260°C. At high temperatures, undecayed activity remaining in the column from previous gas chromatography experiments continues to pass from HEVI into the detection site giving an erroneously high yield. The high yield at higher temperatures leads to observation of a volatility temperature which is also too high and a Monte Carlo calculation of adsorption enthalpy which fits the higher volatility temperature. Based on the results of this experiment, the adsorption enthalpy for $^{213}BiBr_3$ is calculated to be –125 kJ/mol, which is significantly lower than the –84 kJ/mol calculated for $^{211}BiBr_3$ (see Figure 5-11). These results are not unexpected and serve as a warning about using HEVI for the study of isotopes with longer half-lives.

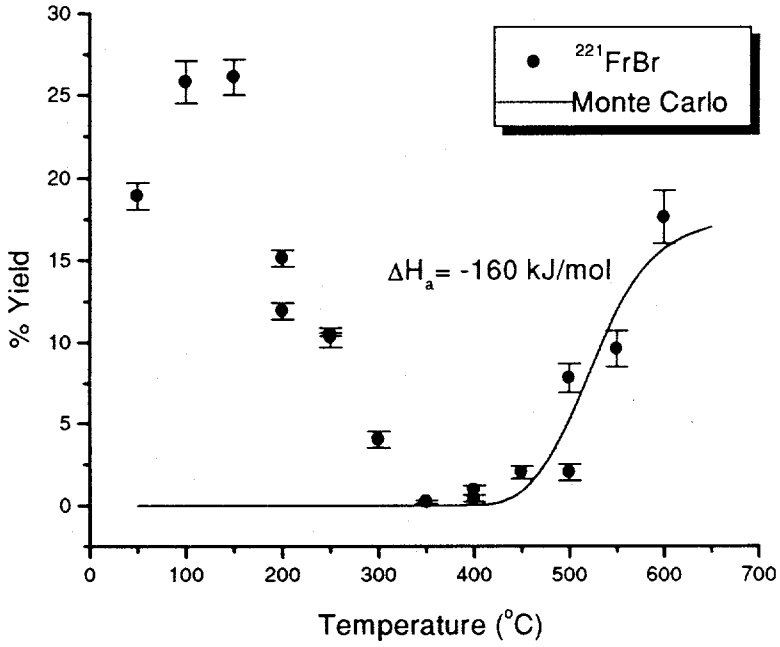

Figure 5-3: Volatility and calculated adsorption enthalpy curve from the Monte Carlo program for ^{221}FrBr. Volatility data are taken from the run using 0.025 g of quartz wool.

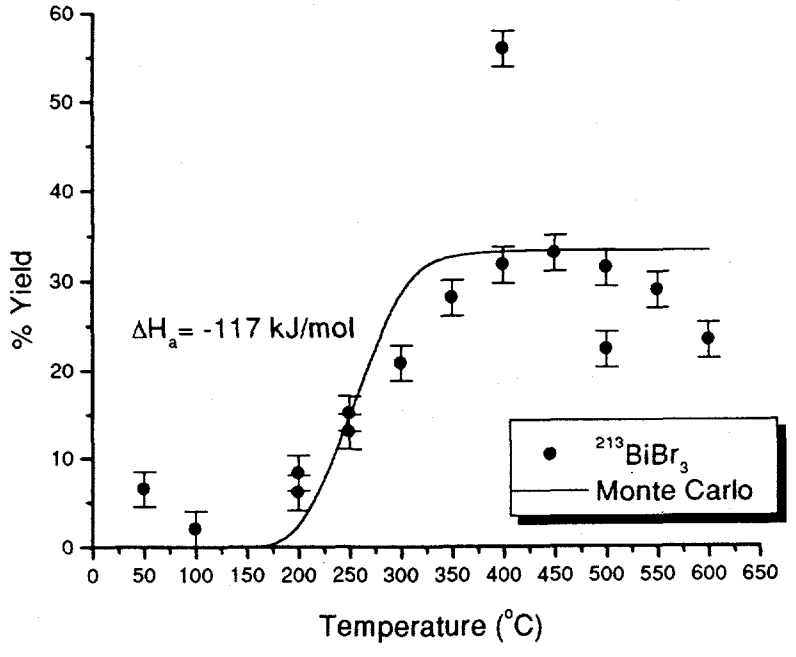

Figure 5-4: Volatility and calculated adsorption enthalpy curve from the Monte Carlo program for $^{213}BiBr_3$. Volatility data are taken from the off-line experiment, using 0.025 g of quartz wool.

5.2.2 Group 4 Bromides

Zirconium

Figure 5-5 shows the relative yield curve for 7.9-min $^{85}ZrBr_4$ from the reaction $^{nat}Cu(^{28}Si, 3p3n)^{85}Zr$. From these data, a volatility temperature of 250° C is obtained for $^{85}ZrBr_4$, giving a calculated adsorption enthalpy of -108 kJ/mol, somewhat less than the results for $^{98}ZrBr_4$ of -91±6 kJ/mol reported by Kadkhodayan [Kadkhodayan 93]. Kadkhodayan reported his results as preliminary, showing low yields at all temperatures (<20%), and had used MoO_3 as his aerosol material.

Our current volatility measurement for $^{85}ZrBr_4$ agrees with results of similar experiments performed with OLGA III [Türler 95a] on $ZrCl_4$. Türler et. al report volatility temperatures for ^{99}Zr with different chlorinating agents to be between 250° C and 400° C. The lowest volatility temperatures of $ZrCl_4$ are observed with the chlorinating agent HCl, which is analogous to the brominating agent HBr used in these experiments. Pershina's calculations [Pershina 96a] also predict that $ZrBr_4$ should be less volatile than $ZrCl_4$. Her estimates of volatility based on overlap potentials and the effective charge on the central atom predict that Rf should be more volatile than either Zr or Hf, a result that we see here (see also Section 5.3.1).

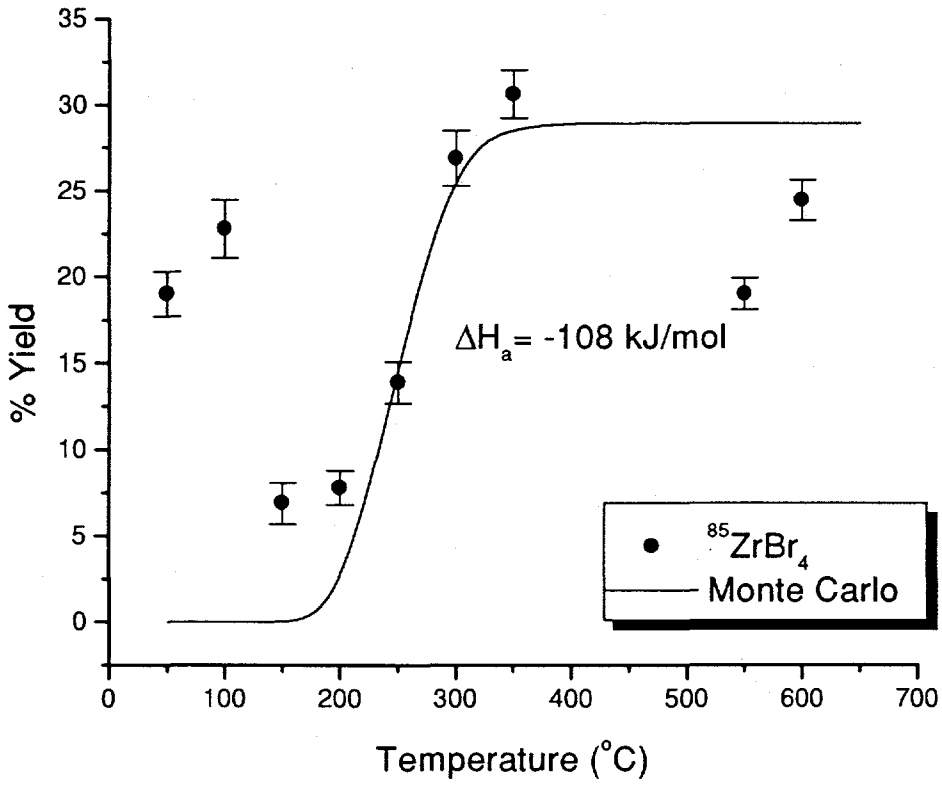

Figure 5-5: Volatility and calculated adsorption enthalpy curve from the Monte Carlo program for $^{85}ZrBr_4$, from the reaction $^{nat}Cu(^{28}Si, 3p3n)^{85}Zr$. Data are taken from the second count of each collection.

Hafnium

In order to study the volatility of $HfBr_4$, 1.26-min ^{165}Hf and 2.0-min ^{167}Hf were both produced in the reaction $^{nat}Eu(^{19}F^{5+}, xn)^{165-167}Hf$, and the results are shown in Figure 5-6. The observed volatility temperature for both $^{165}HfBr_4$ and $^{167}HfBr_4$ was 300° C, and the calculated adsorption enthalpy for $HfBr_4$ based on these results was –113 kJ/mol for both isotopes.

^{165}Hf was also produced in a separate experiment via the reaction $^{159}Tb(^{14}N, 6n)^{167}Hf$, and the results of this experiment are shown in Figue 5-7. Due to time constraints no data were taken above 350° in this experiment, so it is difficult to assign an upper boundary to the chemical yield or exact values for either volatility temperature or adsorption enthalpy. A lower limit for the volatility temperature and an upper limit to the adsorption enthalpy can be assigned on the assumption that the yield at 350° C would have been the maximum chemical yield. The volatility temperature was observed to be ≥320° C, and the calculated limit for adsorption enthalpy is ≤ -117 kJ/mol.

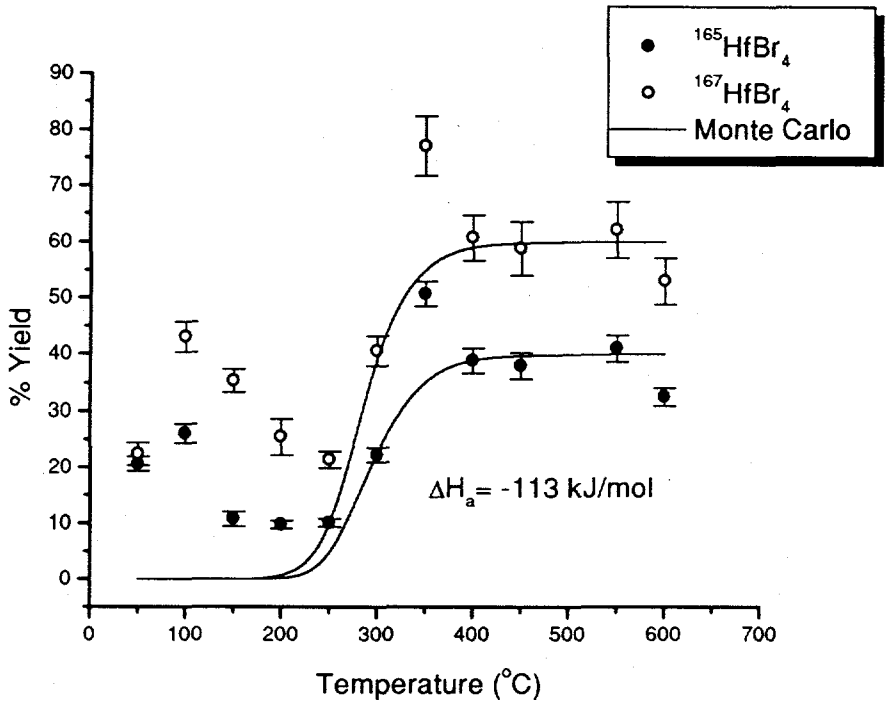

Figure 5-6: Volatility and calculated adsorption enthalpy curves for $^{165,167}HfBr_4$ from the reaction $^{nat}Eu(^{19}F^{5+}, xn)^{165\text{-}167}Hf$.

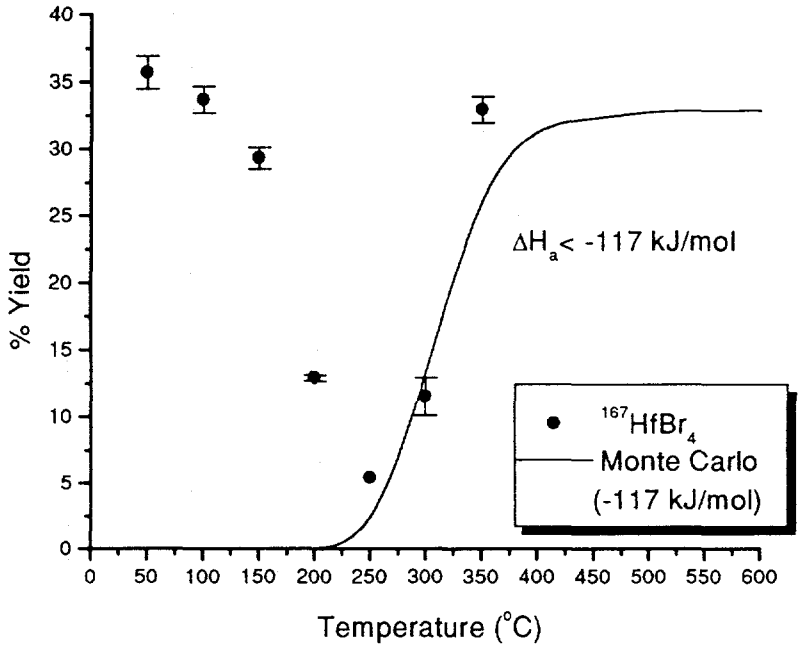

Figure 5-7: Volatility and calculated adsorption enthalpy curve for $^{167}HfBr_4$ from the reaction $^{159}Tb(^{14}N, 6n)^{167}Hf$. Monte Carlo curve is based on best fit to the data assuming a maximum chemical yield of 32.9%, which was the highest yield seen for this isotope. No measurements above 350 °C were made.

Rutherfordium and Bismuth

^{261}Rf was produced in the reaction ^{248}Cm(^{18}O, 5n)^{261}Rf and a new half-life of 74^{+7}_{-6} s measured. This result is in excellent agreement with the previously measured value of 78^{+11}_{-6} s from [Kadkhodayan 96]. Both values are expected to be better values that the previous value of 65±10 seconds measured by Ghiorso et. al [Ghiorso 70] due to the ability of HEVI to separate out nonvolatile interfering activities prior to counting. Based on this experiment and the previous experiment of Kadkhodayan we calculate a weighted average value for the half-life of 75.5±6.6 seconds. Our recommended best value is 75±7 s.

A decay curve for the region around 8.3 MeV is shown in Figure 5-8. Figure 5-9 shows the summed α-spectra of gas chromatography collections for the first 3 minutes of counting for the region between 6.0 and 10.0 MeV. Also shown is the region between 7.5 MeV and 9.0 MeV with an enlarged scale for the gas phase cromatography collection at 350° C.

The yield dependence vs. temperature is shown in Figure 5-10. The volatility temperature of $^{261}RfBr_4$ was determined to be 175° C, and a corresponding adsorption enthalpy of -87±5 kJ/mol was calculated.

The 2.14-min ^{211}Bi was produced in the same experiment as ^{261}Rf, from transfer reactions with Pb impurities in the ^{248}Cm target. The volatility and adsorption enthalpy of $^{211}BiBr_3$ was studied concurrently with that of $^{261}RfBr_4$. The yield of $BiBr_3$ as a function of temperature is shown in Figure 5-11. Based on these graphical results the volatility temperature of $^{211}BiBr_3$ was observed to be 175° C and a corresponding

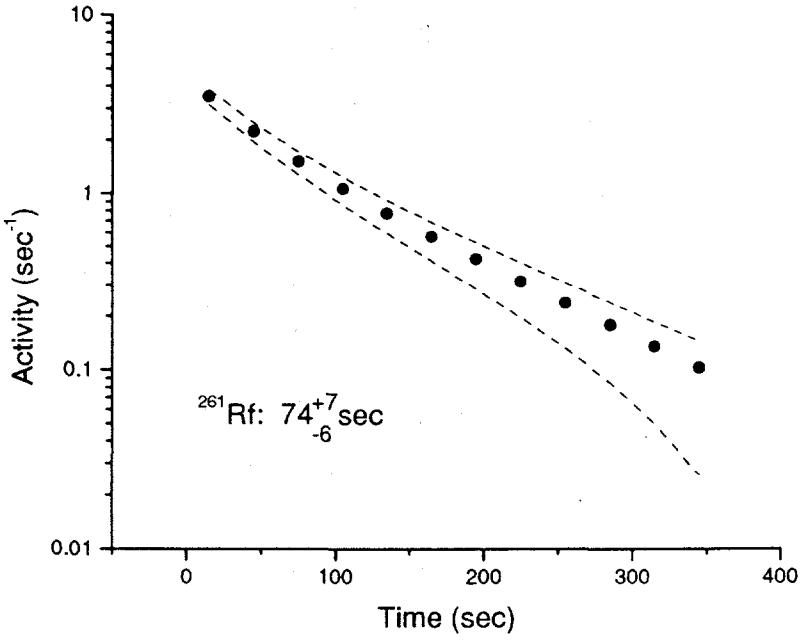

Figure 5-8: Growth (^{261}Rf) and decay (^{257}No) with a single interfering component (^{211}Po^{m}) fit around 8.3 MeV. The half-lives of Po and No and the initial activity of Po are fixed and all other components are allowed to vary. A maximum likelihood decay (MLDS) [Gregorich 91] fit has been used. The upper and lower limits shown represent a confidence level of 68%.

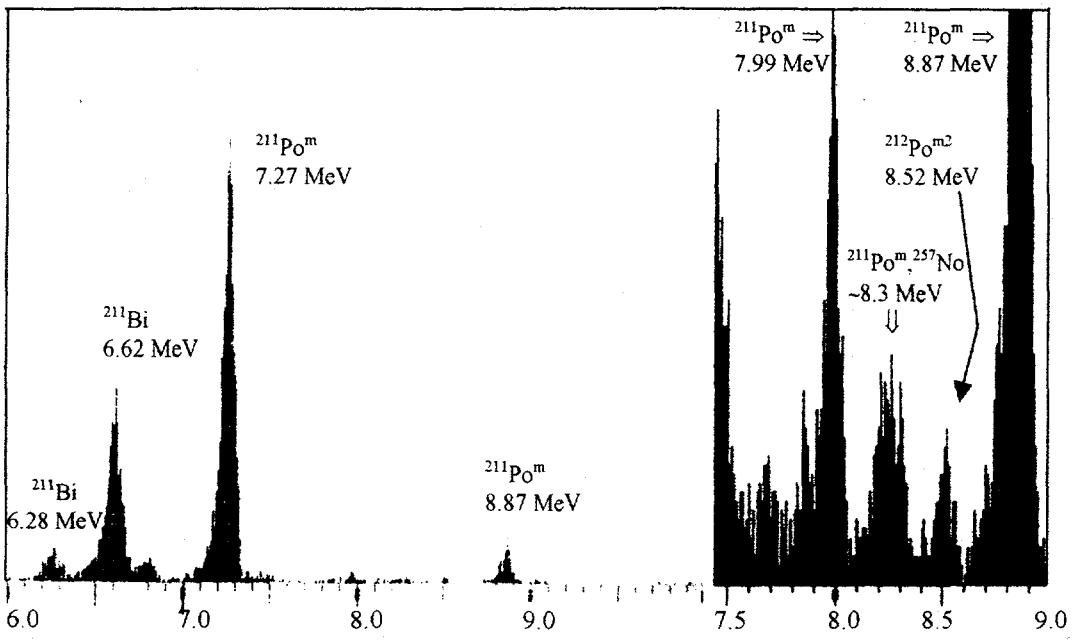

Figure 5-9: α-spectra from Gas Chromatography collections from the $^{248}Cm(^{18}O^{5+},5n)$ ^{261}Rf reaction, for the first 3 minutes of counting. Left- 6.0 MeV to 10 MeV region for data taken at 350° C. Right- 7.5 MeV to 9 MeV for summed α-spectra from all temperatures, with increased vertical scale.

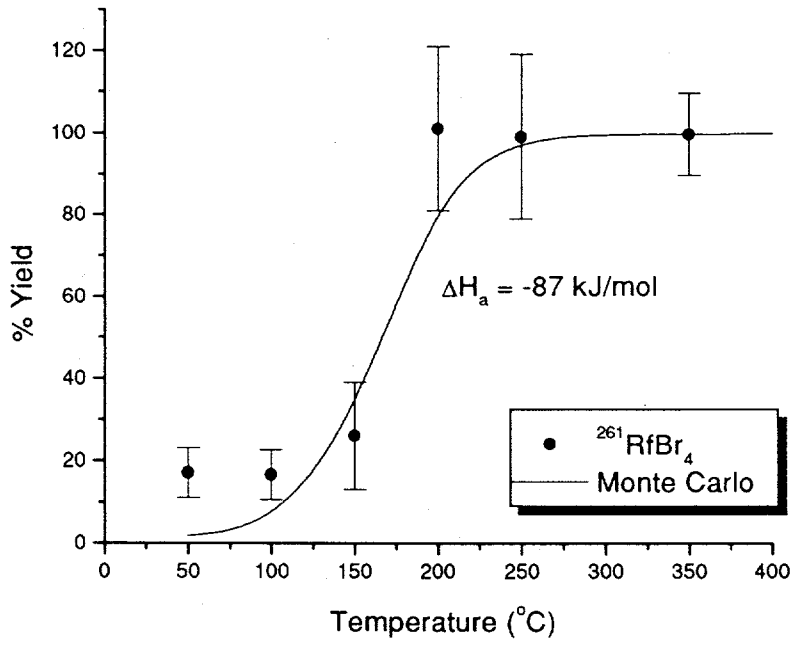

Figure 5-10: Volatility and calculated adsorption enthalpy curve for $^{261}RfBr_4$ from the reaction $^{248}Cm(^{18}O, 5n)^{261}Rf$.

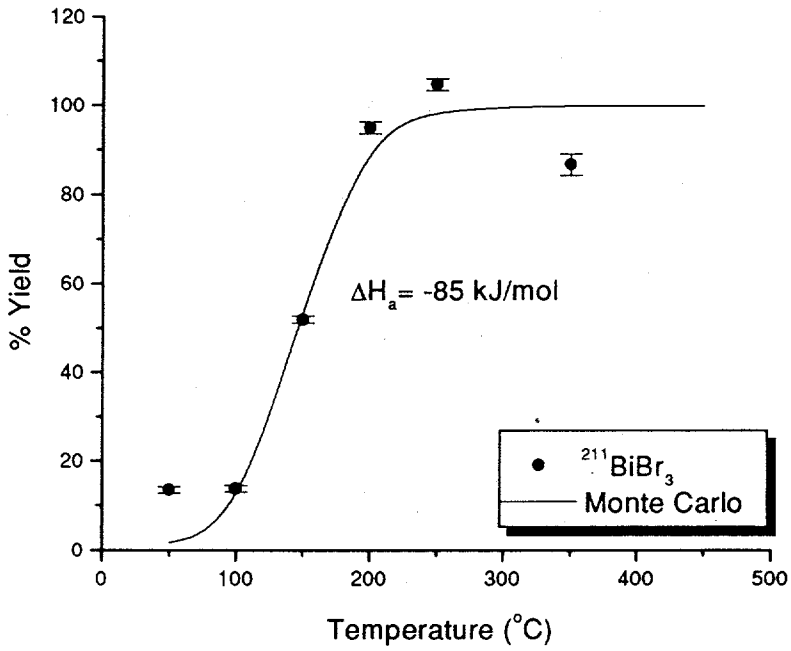

Figure 5-11: Volatility and calculated adsorption enthalpy curve for $^{211}BiBr_3$, produced from impurities in the target in the reaction $^{248}Cm(^{18}O, xn)\ ^{261}Rf$.

adsorption enthalpy of -85±5 kJ/mol was calculated.

5.2.3 Group 5 Bromides and Chlorides

Niobium

The bromides of Nb were studied with 2.6-min $^{87}Nb^{m}$ produced in the reaction $^{nat}Cu(^{28}Si, \alpha xn)\,^{87}Nb^{m}$, and 14.4-min $^{88}Nb^{m}$ produced in the reaction $^{nat}Br(^{14}N, pxn)\,^{87}Nb^{m}$ with a mixed $^{165}HoBr_3/^{159}TbBr_3/^{133}CsBr$ target.

From the data shown in Figure 5-12, the volatility temperature for $^{87}Nb^{m}Br_5$ was found to be between 170° C and 250° C. The best fit of the Monte Carlo simulation to the data yields a calculated adsorption enthalpy of -86 kJ/mol, which corresponds to the highest estimates for volatility temperature.

During the experiment with the mixed target (producing $^{88}Nb^{m}$), the high-yield-at-low-temperature effect (discussed in section 5.1) was evaluated at temperatures up to 250° C by observing the yield of the nonvolatile $^{141}SmBr_3$. Determination of the volatility temperature and adsorption enthalpy for $^{87}Nb^{m}Br_5$ was accomplished by the subtracting the yield of the ^{141}Sm from the yield of $^{87}Nb^{m}$ after taking into account the differences in half-life. Figure 5-13(a) shows the yield of $^{87}Nb^{m}Br_5$ observed in the experiment; Figure 5-13(b) shows the corrected yield after subtraction of the yield of $^{141}SmBr_3$.

From the data shown in Figure 5-13(b), the volatility temperature for $^{88m}NbBr_5$ was found to be 200° C, and the calculated adsorption enthalpy based on these results yields a value of -103 kJ/mol. These results are shown in Figures 5-12, 5-13(a) and (b).

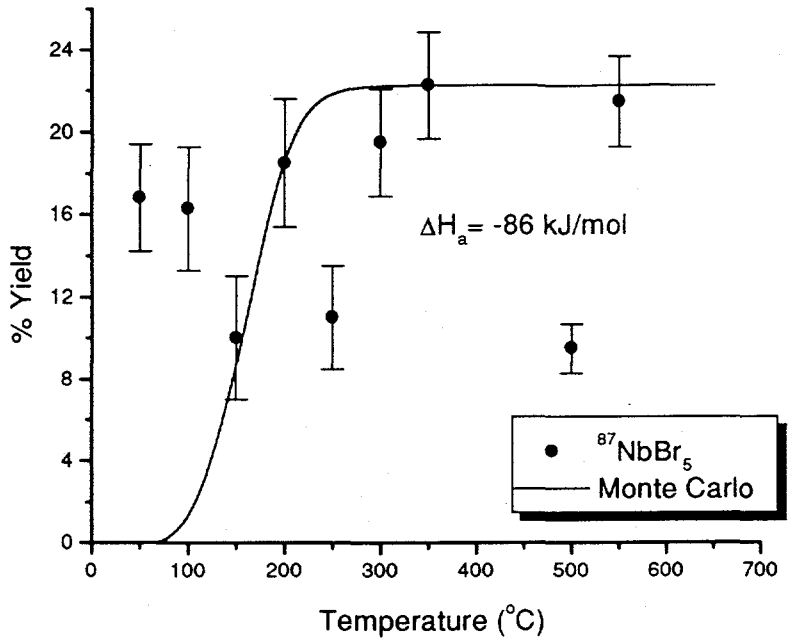

Figure 5-12: Volatility and calculated adsorption enthalpy curves for $^{87m}NbBr_5$. From the reaction $^{nat}Cu(^{28}Si, \alpha xn)^{87m}Nb$.

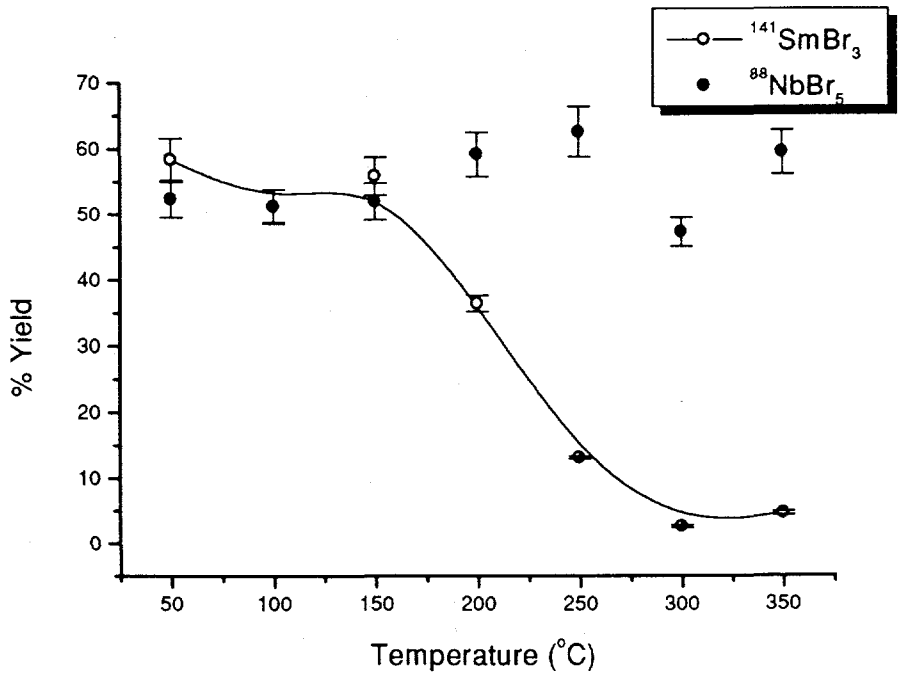

Figure 5-13(a): Observed yield as a function of temperature for $^{88}NbBr_5$ and $^{141}SmBr_3$. From the reaction $^{nat}Br(^{14}N, pxn)^{88}Nb$.

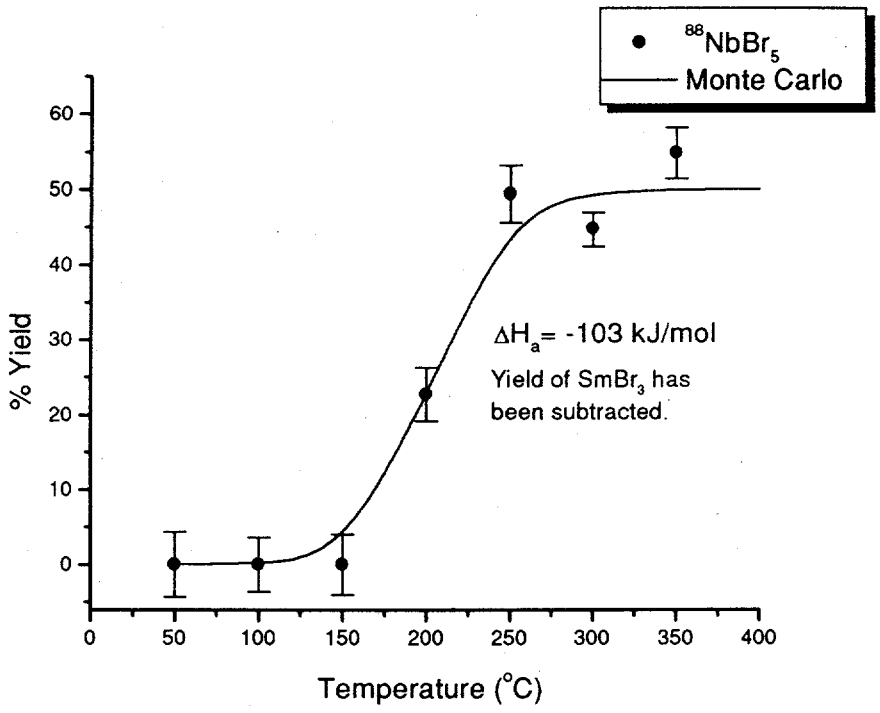

Figure 5-13(b): Volatility and calculated adsorption enthalpy curves for $^{88}NbBr_5$.after subtracting the yield of $^{141}SmBr_3$. From the reaction $^{nat}Br(^{14}N, pxn)^{88}Nb$.

Tantalum

For studies of the Ta bromides, 34-sec ^{166}Ta was produced in the reaction ^{nat}Eu(^{20}Ne^{6+}, xn)$^{166-167}$Ta. Figure 5-14 shows that the yields of the bromide species as a function of temperature are very low, with the observed species becoming volatile at approximaely 550° C.

The observed species is probably $^{166}TaOBr_3$, based on the following reasons. First, B. Kadkhodayan observed that the Ta-chlorides studied in HEVI also showed an unusually low volatility and assigned the molecular form $TaOCl_3$ to this species based on his experiments [Kadkhodayan 92]. Second, Gäggeler *et al.* observed Ta-bromide species with a measured volatility temperature of 200° C in OLGA II, when the brominating agent used was HBr saturated with BBr_3, a very strong brominating agent [Gäggeler 92] (see also Figure 5-23) and this volatile species was believed to be $TaBr_5$. Finally, the low volatility observed for the bromide compound more closely resembles the expected volatility temperature of $TaOCl_3$ (500° C) rather than the volatility temperature of $TaCl_5$ (200° C) expected based on the reported equilibrium vapor pressure over the solid [Knacke 91] for the chlorides. Our results also are not consistent with the expected volatility temperature of $TaBr_5$ of 400° C, based on the same data [Knacke 91].

The volatility temperature observed from our data is probably at least 525° C. The calculated adsorption enthalpy of $^{166}TaOBr_3$ based on the data is -153 kJ/mol.

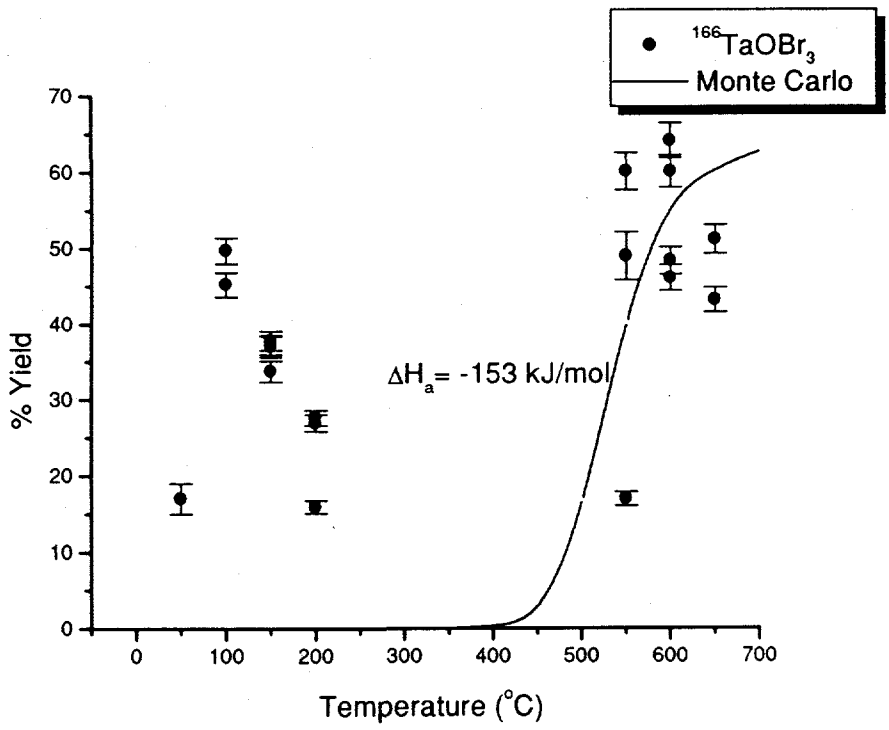

Figure 5-14: Volatility and calculated adsorption enthalpy curves for $^{166}TaOBr_3$. From the reaction $^{nat}Eu(^{20}Ne^{6+}, xn)^{166\text{-}167}Ta$.

Hahnium

The 34-sec ^{262}Ha was produced via the ^{249}Bk($^{18}O^{5+}$, 5n) ^{262,263}Ha reaction and studied at the 88-Inch Cyclotron. In collaboration with the Swiss experimental Group of H. Gäggeler and A. Türler, OLGA III coupled with the MG detection system was used for this experiment. Figure 5-15 shows the combined α-spectra from all chemistry runs (8245 samples) for detector pairs 1-5 (0-150 seconds). 27 α-α pairs were observed with energies between 8.40 and 8.75 MeV and identified as ^{262}Ha-^{258}Lr pairs, giving half-life values of $22.0^{+4.3}_{-3.5}$ seconds for ^{262}Ha and $6.8^{+2.2}_{-1.5}$ seconds for ^{258}Lr. 45 SF events attributed to ^{263}Ha were also observed and a half-life of $21.0^{+4.9}_{-4.5}$ seconds was determined, consistent with the half-life previously determined to be 27^{+10}_{-7} seconds [Kratz 92]. However, no ^{263}Ha-^{259}Lr α-α correlations were observed to confirm the assignment. ^{263}Ha decays via emission of an 8.355 MeV α with a branching ratio of 43%, and via SF with a branching ratio of 57%.

Figure 5-16 shows the combined yield of all ^{262,263}Ha events as a function of the temperature of the column. Separate analysis of the α events attributed to ^{262}Ha and the SF events attrributed to ^{263}Ha yielded the same behavior [Türler 96b] for both. The data have been interpreted by Gäggeler *et al.* as showing the presence of two chloride species; one volatile at temperatures ≤ 200°C and the other volatile at temperatures > 300° C, with the more volatile species being observed in a ratio of 1:3 to the less volatile compound [Türler 96a]. These species have been assigned the molecular forms $HaCl_5$ and $HaOCl_3$, respectively, based on the similarity with Nb-chloride species and theory. Adsorption

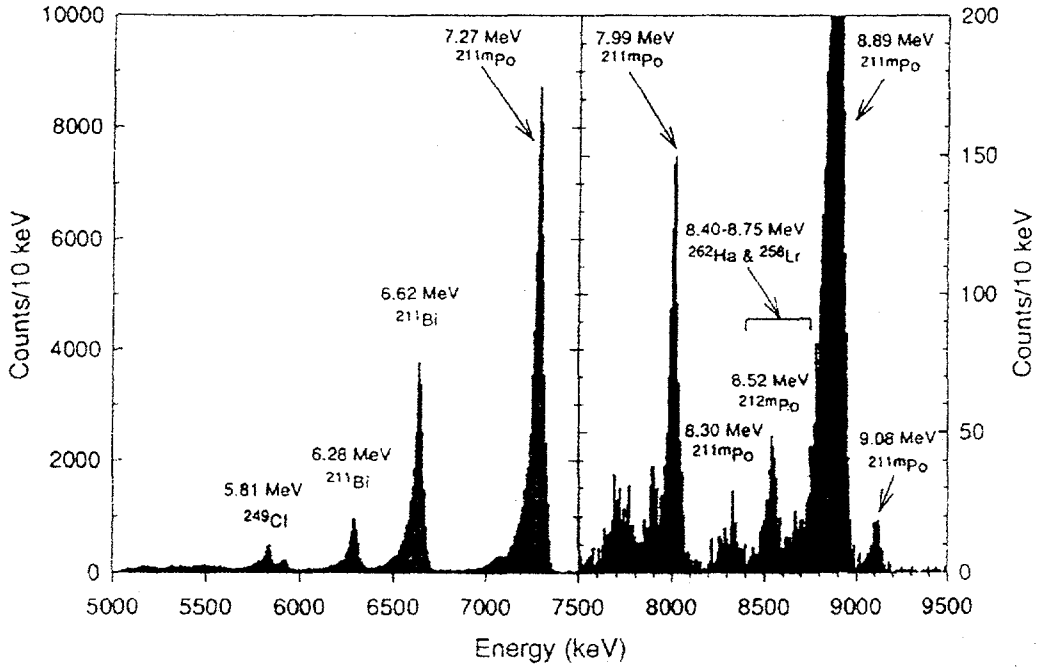

Figure 5-15: Sum of α-spectra of Gas Chromatography collections for detector pairs 1-5 (0-150 sec.) for the $^{249}Bk(^{18}O^{5+},5n)\ ^{262,263}Ha$ reaction. The vertical scale above 7.5 MeV was expanded. From [Türler 96b]

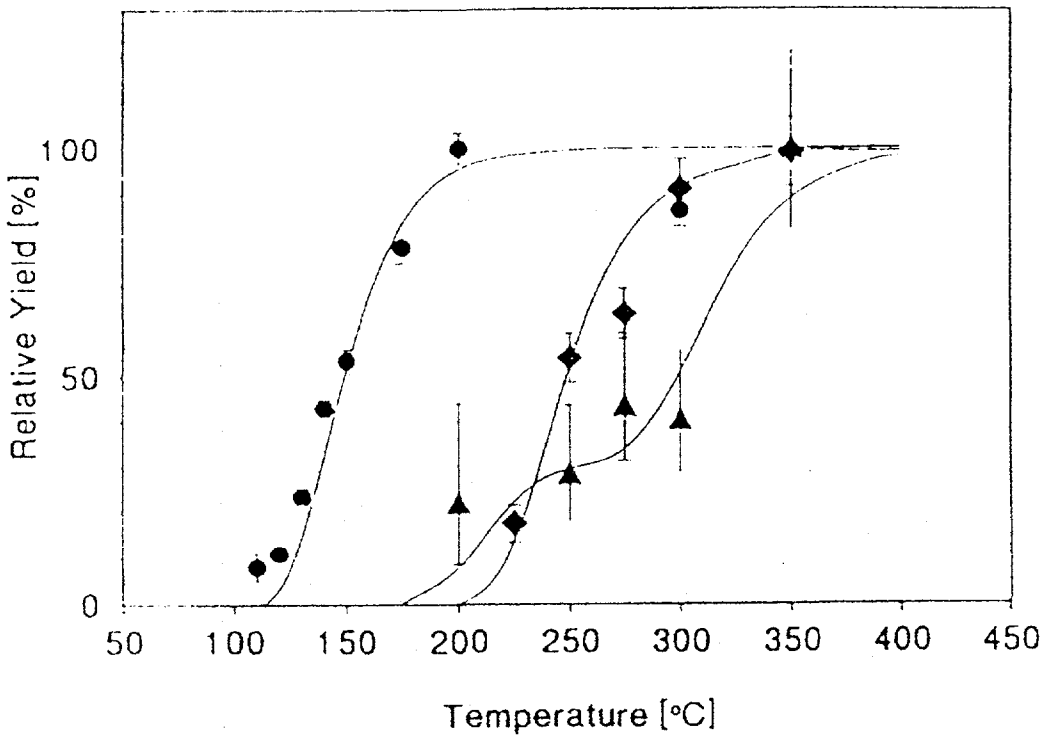

Figure 5-16: Yield of Ha-chloride species as a function of temperature (shown as the black triangles). Also shown are the species $NbCl_5$ (circles) and $NbOCl_3$ (diamonds) for comparison. Yield of Ha is interpreted as two separate species; $HaCl_5$ (volatile at approximately 200° C) and $HaOCl_3$ (volatile at approximately 300° C). Reproduced from [Turler 96a]. Note that there is a data point for Ha at 350° C with a relative yield of 100%, hidden by a $NbOCl_3$ point at the same position.

enthalpies for these species were calculated to be ≤ -97 kJ/mol for $HaCl_5$ and –117 kJ/mol for $HaOCl_3$. Both the fission and the α-α correlation data show a high yield at 350° C, which in comparison to the low yields observed at temperatures between 200° C and 300° C supports the conclusion that there are in fact two different Ha species being formed. However, it is unfortunate that OLGA III is limited to temperatures of approximately 350° C and lower, as proof of a low-volatile compound at high (> 300° C) temperatures could be more conclusively argued with multiple high-temperature data points.

The absolute chemical yield could not be determined for this experiment due to the difficulty of identifying Ha events above background in yield check measurements.

5.2.4 Group 6 Bromides

Molybdenum

The observed yield as a function of temperature for the 8.0-min. ^{88}Mo-bromides is shown in Figure 5-17. These preliminary results are from the reaction ^{nat}Cu(^{28}Si, pxn)^{88}Mo. A comparison of the ^{88}Mo results with the results given above for $^{87}NbBr_5$ (from the same experiment) shows that a very high yield for both is observed at 200° C.

Vapor pressure curves measured for macroscopic quantities of Mo-chloride and Mo-oxychloride compounds show MoO_2Cl_2 becomes volatile at 100°-150° C and $MoOCl_4$ at 200°-250° C [Knacke 91, Türler 95b]. Türler *et. al* observed the MoO_2Cl_2 with OLGA 3; however, in that experiment the halogenating gas stream was composed of

300ml/min O_2 saturated with $SOCl_2$, heavily favoring the formation of the dioxydichloride over the formation of the oxytetrachloride or pure chlorides.

We expect the volatilities of the bromide compounds to be slightly lower than those of the corresponding chloride compounds; our results could support the formation of either MoO_2Br_2 or $MoOBr_4$ based on the observed yields. No attempt has been made to assign a molecular form or adsorption enthalpy value from the observed ^{88}Mo yield. The volatility temperature is estimated to be between 200° and 350° C.

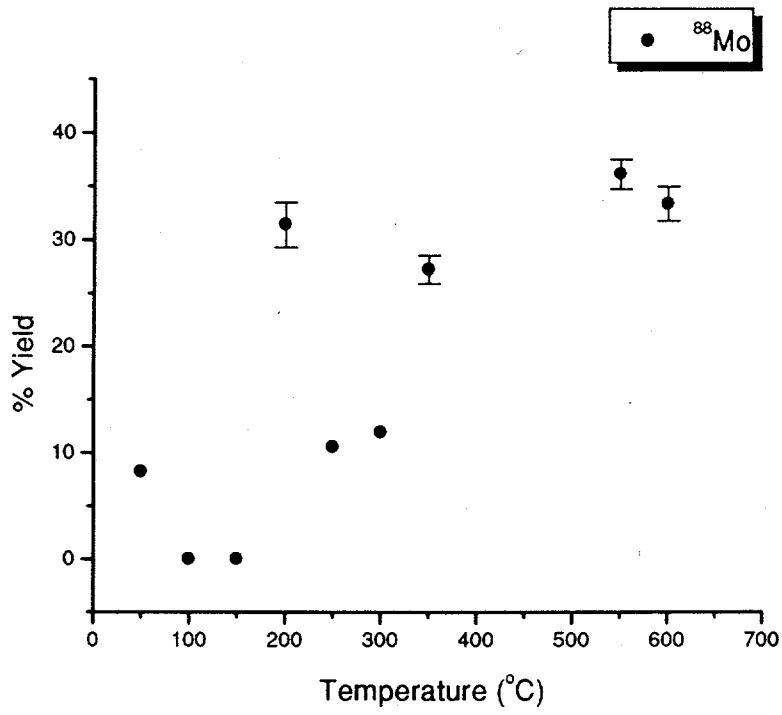

Figure 5-17: Yield of ^{88}Mo-bromides as a function of temperature. From the reaction ^{nat}Cu(^{28}Si, pxn)^{88}Mo.

Tungsten

The 2.4-min ^{171}W and the 6.6-min ^{172}W were produced via the reactions $^{nat}Gd(^{20}Ne,xn)^{168-173}W$ and $^{165}Ho(^{14}N, 7n)^{172}W$. The results are shown in Figures 5-18 and 5-19.

Results from the experiment with ^{171}W (Figure 5-18) show a volatility temperature ≥140° C. Due to time constraints in the experiment no data were taken above 250° C, which makes it difficult to assign an adsorption enthalpy value to the data. A calculated adsorption enthalpy of –77 kJ/mol for $^{171}WBr_6$ is obtained by assuming the maximum chemical yield is 62%, the same as the yield observed at 200° C and 250° C. We feel that this value should be interpreted as a lower limit; higher yields at higher temperatures would result in lower estimates of volatility temperature and lower (more negative) estimates in adsorption enthalpy.

$^{172}WBr_6$ (Figure 5-19) shows a volatility temperature of 175° C, with a calculated adsorption enthalpy for this compound of –92 kJ/mol. The yield for $^{172}WBr_6$ had to be corrected for a large non-volatile yield at low temperatures obtained from the yield of $^{141}SmBr_3$; Figure 5-20 shows the uncorrected yield of $^{172}WBr_6$ (see also the discussion under "Nb Bromides" in this section).

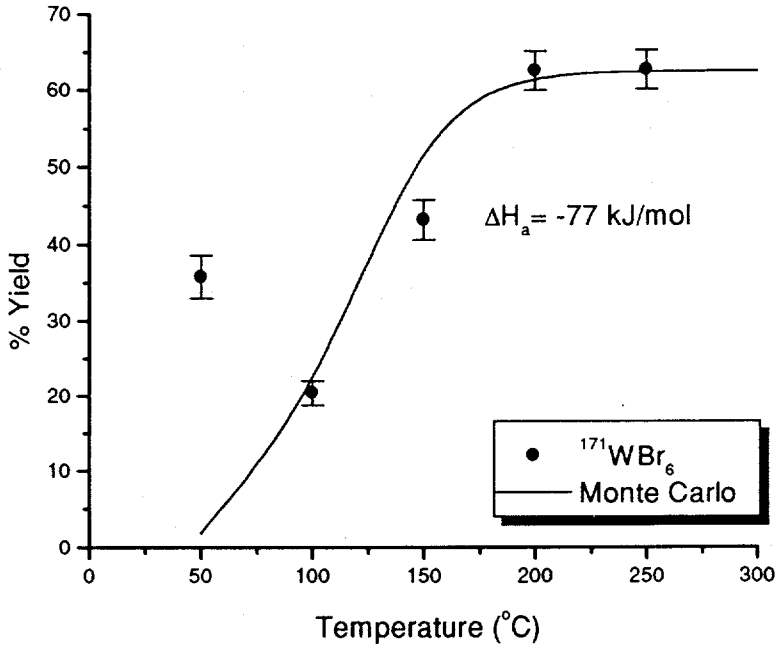

Figure 5-18: Yields of $^{171}WBr_6$ as a function of temperature. From the reaction $^{nat}Gd(^{20}Ne, xn)^{168\text{-}173}W$.

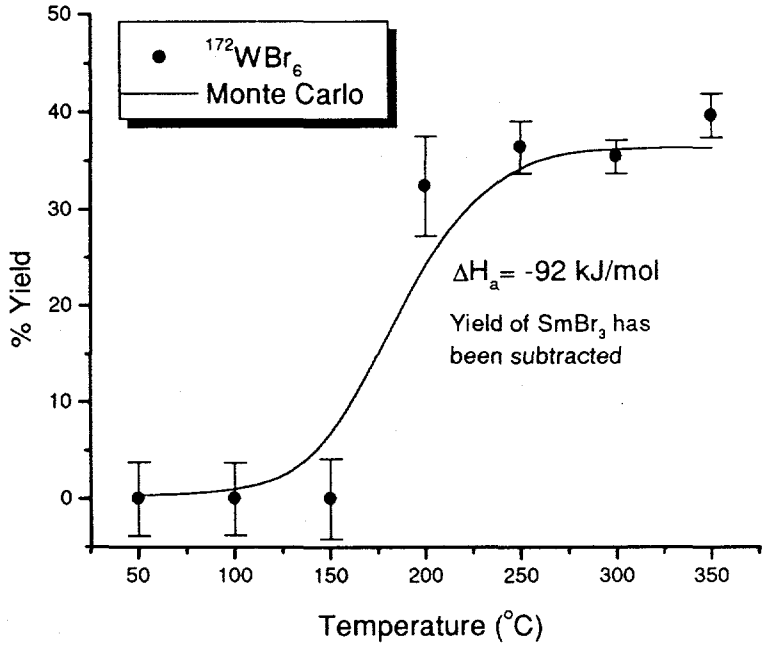

Figure 5-19: Corrected volatility and calculated adsorption enthalpy curve for $^{172}WBr_6$. From the reaction $^{165}Ho(^{14}N, 7n)^{172}W$.

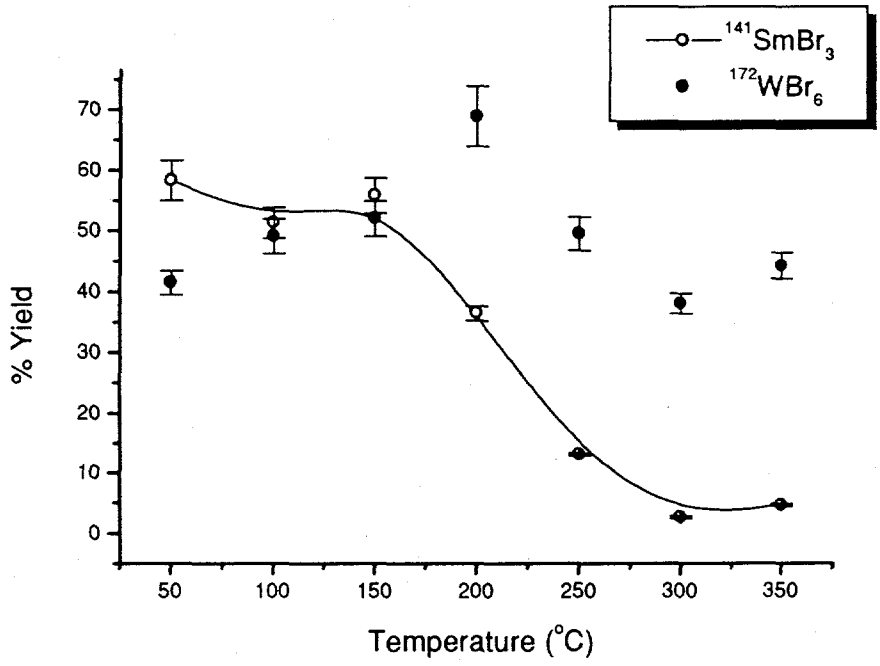

Figure 5-20: Observed yield as a function of temperature for $^{172}WBr_6$ and $^{141}SmBr_3$. From the reaction $^{165}Ho(^{14}N, 7n)^{172}W$.

5.3 Discussion

5.3.1 Group 4 Results

In this study, the lighter group 4 compound ($ZrBr_4$) was found to be more volatile and have a larger adsorption enthalpy than $HfBr_4$. Were this trend to continue down the group, $RfBr_4$ would be expected to be less volatile than $HfBr_4$. The reverse has been observed (see Table 5-1), and the volatility for the group 4 bromides has been established to decrease in the order: $RfBr_4 \geq ZrBr_4 > HfBr_4$.

Volatilities observed for $RfBr_4$ and $HfBr_4$ with HEVI are similar to the results of the OLGA II experiments, shown in Figure 5-21, within error. The volatilities observed in OLGA II were at 200°-250° C for $RfBr_4$, with large errors, and 300°-350° C for $HfBr_4$.

For the chlorides, Kadkhodayan *et al.* observed that $ZrCl_4$ was more volatile than $RfCl_4$ [Kadkhodayan 93, 96], but the volatility temperatures and adsorption enthalpies reported for Zr and Rf are extremely close– 175° C for both $ZrCl_4$ and $RfCl_4$, and adsorption enthalpy values of -74 ± 5 kJ/mol and -77 ± 6 kJ/mol, respectively. The difference in assigned volatility order between the chlorides and bromides may be a result of overlapping errors rather a true difference in chemical behavior.

All of the bromide species studied were observed to be sligthly less volatile than their corresponding chloride species (MCl_4). This is in good agreement with both theory [Pershina 92c, Canterford 68] and previous experimental work [Gäggeler 92, Knacke 91, Türler 92b, 96b] using OLGA II, shown in Figure 5-22 (below). Recent experimental results comparing the volatilities of the group 4 oxychlorides ($MOCl_2$) with those of the tetrachlorides also support the conclusion that the compounds observed in this research were the tetrabromides; Türler *et. al* have observed $^{165}HfOCl_2$ and $^{261}RfOCl_2$ to be

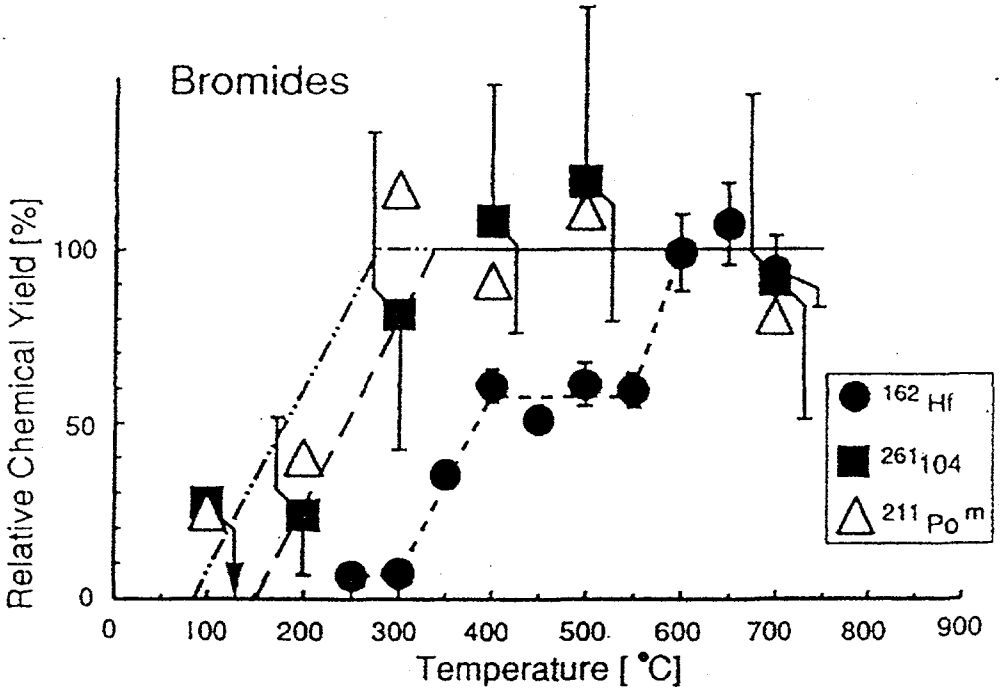

Figure 5-21: Results of OLGA II experiments with Bromides of Po, Hf, and Rf.

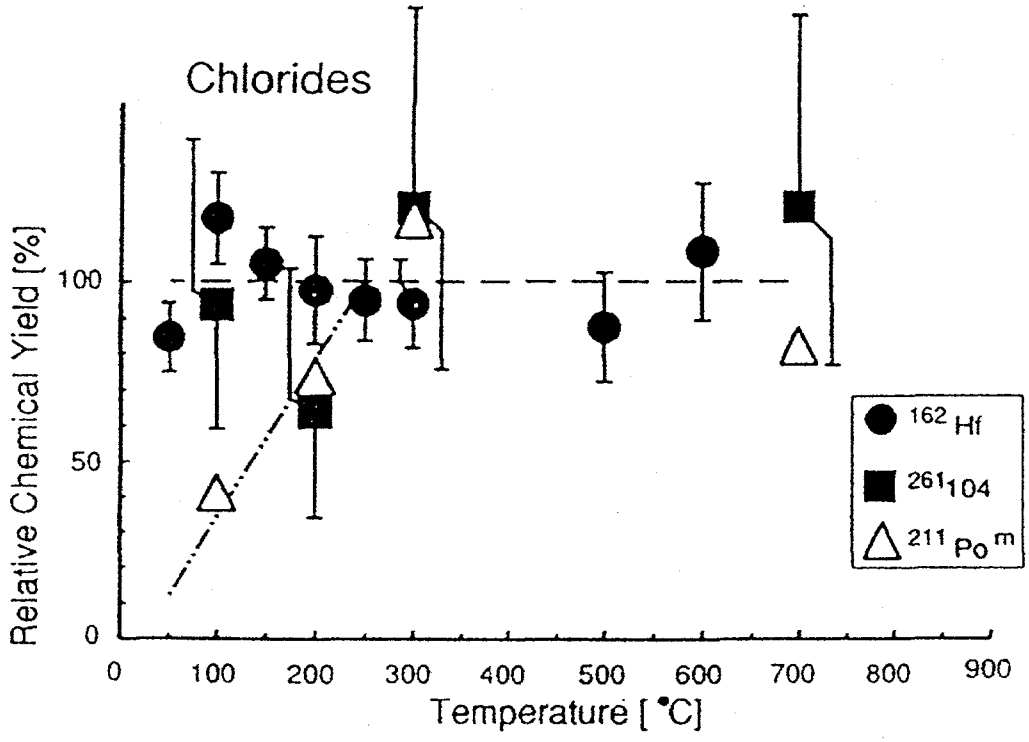

Figure 5-22: Results of OLGA II experiments with Chlorides of Po, Hf, and Rf.

volatile only at temperatures in excess of 350° C [Türler 97b]; according to both data and theory, oxybromides of the group 4 elements should be less volatile than the oxychlorides; however, the volatilities of the species observed here are well below this temperature.

Our results also agree with predictions based on the relativistic calculations of V. Pershina for the temperature dependance of equilibrium vapor pressure (P_{mm}) for the chlorides given in section 2.2; $RfCl_4$ was predicted to have a higher vapor pressure (higher volatility) than $HfCl_4$.

Table 5-1. Volatility Temperatures and adsorption enthalpy values for the group 4 tetrabromides obtained in this work. All experiments were performed with HBr as the brominating agent and KBr as the transport aerosol material. Errors in all adsorption enthalpy values are based on the error analysis given in Section 2.5 of this work.

Compound	Volatility Temp. (°C)	ΔH_a^0 (kJ/mol)
$^{85}ZrBr_4$	250	-108±5
$^{165}HfBr_4$	260	-113±5
$^{167}HfBr_4$	260	-113±5
$^{261}RfBr_4$	175	-87±7

5.3.2 Group 5 Results

Due to the variation in the observed chemical forms of the group 5 elements it is difficult to draw any specific conclusions on the continuation or discontinuation of periodic trends in group 5. However, some general conclusions can be made: under similar experimental conditions, Nb was observed to form the pentahalide, $NbBr_5$; Ta was observed to be stable only as the oxyhalide, $TaOBr_3$; and Ha was observed to form both chlorides and oxychlorides. Table 5-2 shows the results for the group 5 halides studied in this work. Previous experiments with bromides of the group 5 elements using OLGA II are shown in Figure 5-23. They show a Nb-bromide compound with the same volatility as observed in this work, a highly volatile Ta-bromide species which was assigned the chemical form $TaBr_5$, and a Ha-bromide species with a volatility temperature around 300° to 400° C, which supports the theoretical predictions that the bromides of the tranactinide elements will be less volatile than the chlorides.

As with the group 4 compounds, the group 5 bromides and oxybromides were observed to be slightly less volatile than their corresponding chloride and oxychloride forms, a result which is predicted by theory and previous experimental studies [Pershina 92c, Canterford 68, Gäggeler 92, Knacke 91, Türler 92b, 96b].

Table 5-2. Volatility temperatures and adsorption enthalpy values for the group 5 halides studied in this work. All experiments were performed with HBr as the brominating agent and KBr as the transport aerosol material, except for the ^{262,263}Ha experiment which used Carbon aerosols in He as a carrier, HCl as the chlorinating agent and KCl as the reclustering aerosol.

Compound	Volatility Temp. (°C)	ΔH_a^0 (kJ/mol)
$^{87m}NbBr_5$	175	-88±6
$^{88m}NbBr_5$	200	-103±5
$^{166}TaOBr_3$	525	-153±8
$^{262,263}HaCl_5$	≤200	≥-97
$^{262,263}HaOCl_3$	>300	-117±3

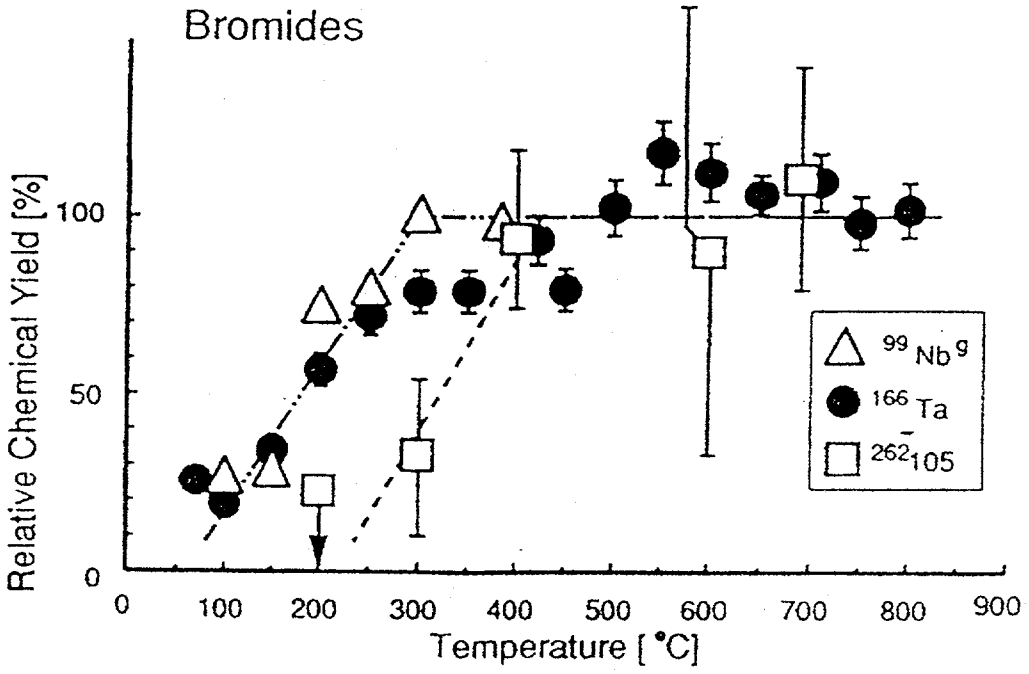

Figure 5-23 Results of OLGA II experiments with Bromides of Nb, Ta, and Ha.

5.3.3 Group 6 Results

We are unable to arrive at any conclusions for trends in the group 6 bromides based on the data observed using HEVI, as the Sg-bromides have yet to be studied using this system and the results of the studies of Mo are highly questionable. The best value for the volatility temperature for the ^{88}Mo-bromides is 200° to 350° C and the chemical form is unknown. Table 5-3, below, gives a summary of our observations of the group 6 elements to date.

Table 5-3. Volatility temperatures and adsorption enthalpy values for the group 6 halides studied in this work. All experiments were performed with HBr as the brominating agent and KBr as the transport aerosol material.

Compound	Volatility Temp. (°C)	ΔH_a^0 (kJ/mol)
^{88}Mo-bromides	200-350	
$^{171}WBr_6$	≥140	≤-77
$^{172}WBr_6$	175	-92±8

6. Summary and Conclusions

6.1 Summary of results of this work

The volatility temperatures of the group 4 compounds $ZrBr_4$, $HfBr_4$, and $RfBr_4$, the group 5 compounds $NbBr_5$, $TaOBr_3$, and $HaCl_5$, and the group 6 compound WBr_6, have been measured using the Heavy Element Volatility Instrment (HEVI) and the On-Line Gas Apparatus (OLGA III). Adsorption enthalpies have been calculated for these species using a Monte Carlo simulation code based on a microscopic model of isothermal gas chromatography. Preliminary studies for the Mo-bromides have also been completed. Our results agree well with results of previous and ongoing research on these compounds and the corresponding chloride compounds of the same elements, as well as the volatilities expected based on observations of macroscopic equilibrium pressure.

The volatility temperatures of the compounds FrBr and $BiBr_3$ have been measured, and adsorption enthalpy values have been calculated from these volatilities. FrBr was additionally used to study the presence of high yields of both volatile and nonvolatile compounds at low temperatures in HEVI.

The best estimates of volatility temperatures and adsorption enthalpies for all compounds studied here are given in Table 6-1. Adsorption enthalpy values by group have also been plotted in Figures 6-1 through 6-4 for both the bromides and chlorides. Figure 6-1 shows the results for the group 4 elements based on this and other research. Our results for the group 4 tetrabromides show the same trends as seen in the chlorides, with $RfBr_4$ showing a volatility similar to that of the $ZrBr_4$, both being more volatile than the homolog $HfBr_4$. The group 4 bromides have a lower volatility than their respective

chlorides, which is in good agreement with the theoretical predictions of Pershina [Pershina 96a, 97] based on her molecular orbital calculations of overlap potentials.

Figure 6-2 shows the results for the group 5 chlorides and bromides. Though it is unclear whether Ha, like Rf, shows a reversal of the periodic trend expected from its lighter homologs, it can be seen that our results agree well with previous and current research on both the group 5 chlorides and bromides. As with the group 4 elements, the group 5 bromides exhibit a lower volatility than their respective chlorides, which again agrees with current theoretical predictions [Pershina 96a, 97]. Though Ta is only seen in our system in the oxyhalide form, $TaOX_3$, both the chloride and bromide systems seem to produce the same molecular forms.

Figure 6-3 shows the current results for the group 5 oxychlorides and oxybromides. Figure 6-4 shows the combined results for all group 5 elements. The oxybromide results from this work agree well with previous chloride results with HEVI. Finally, Appendix 2 shows a summary of all published isothermal gas chromatography experimental results to date, sorted by group.

Table 6-1. Best values for volatility temperatures and adsorption enthalpies for the halides studied in this work.

Compound	Volatility Temp. (°C)	ΔH_a^0 (kJ/mol)
$^{221}FrBr$	550	≤-160
$^{211}BiBr_3$	150	-84±5
$^{85}ZrBr_4$	250	-108±5
$^{165}HfBr_4$	260	-113±5
$^{261}RfBr_4$	175	-87±7
$^{87}Nb^mBr_5$	175	-86±6
$^{166}TaOBr_3$	525	-153±8
$^{262,263}HaCl_5$	≤200	≥-97
$^{262,263}HaOCl_3$	>300	-117±3
^{88}Mo-bromides	200-350	_____
$^{172}WBr_6$	175	-92±8

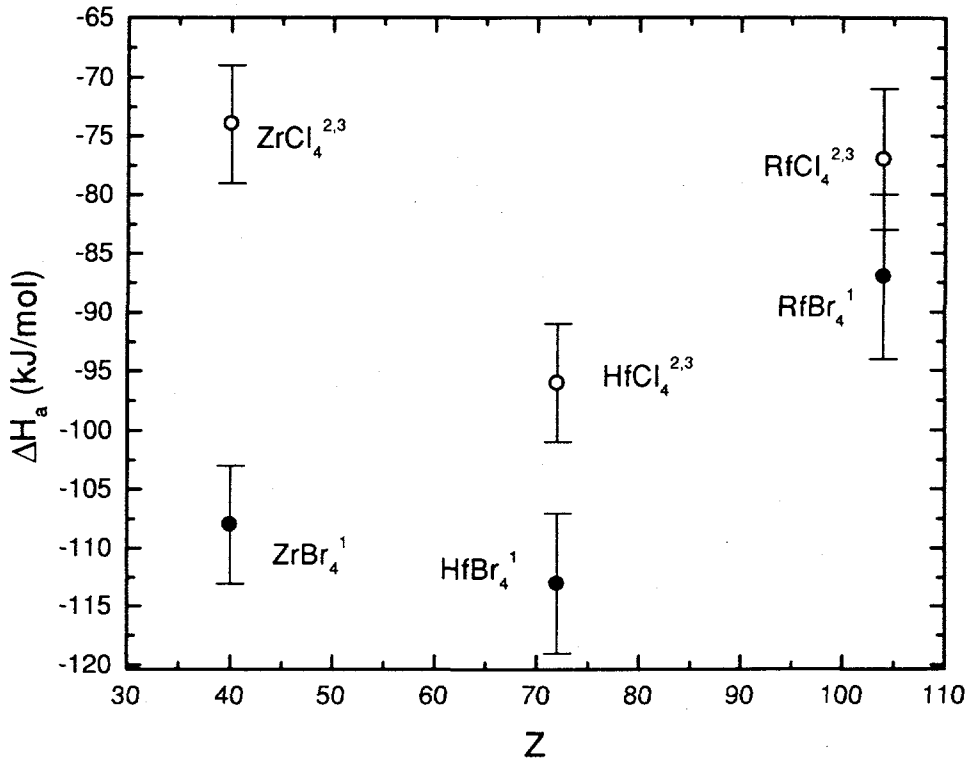

Figure 6-1: Best results of gas chromatography experiments with the group 4 bromides and chlorides. • = Bromides, o = Chlorides. References given are: [1]this work, [2]Kadkhodayan 96, [3]Kadkhodayan 93.

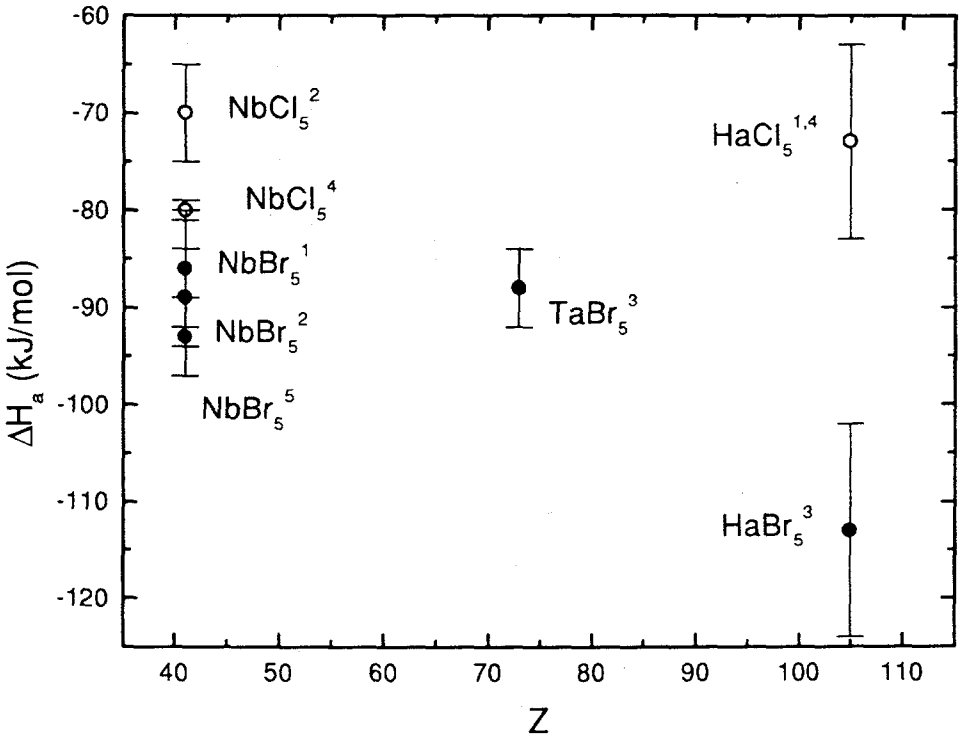

Figure 6-2: Best results of gas chromatography experiments with the group 5 bromides and chlorides. • = Bromides, o = Chlorides. References given are: [1]this work, [2]Kadkhodayan 93, [3]Türler 96a, data from Gäggeler 92 reanalysed, [4]Türler 96b, [5]Nai-Qi 89.

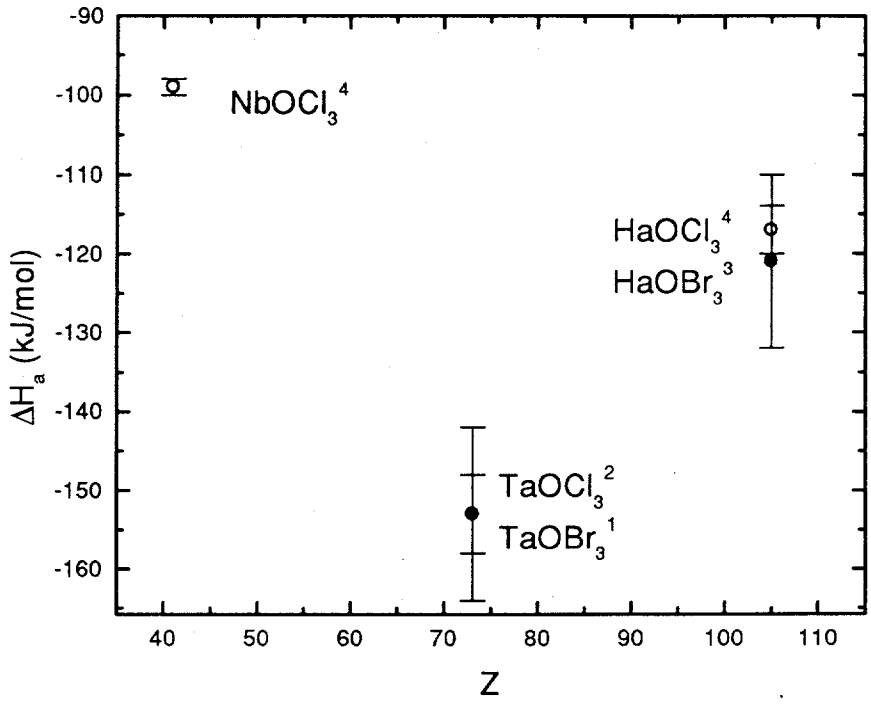

Figure 6-3: Best results of gas chromatography experiments with the group 5 oxybromides and oxychlorides. • = Bromides, o = Chlorides. References given are: [1]this work, [2]Kadkhodayan 93, [3]Türler 96a, data from Gäggeler 92 reanalysed, [4]Türler 96b.

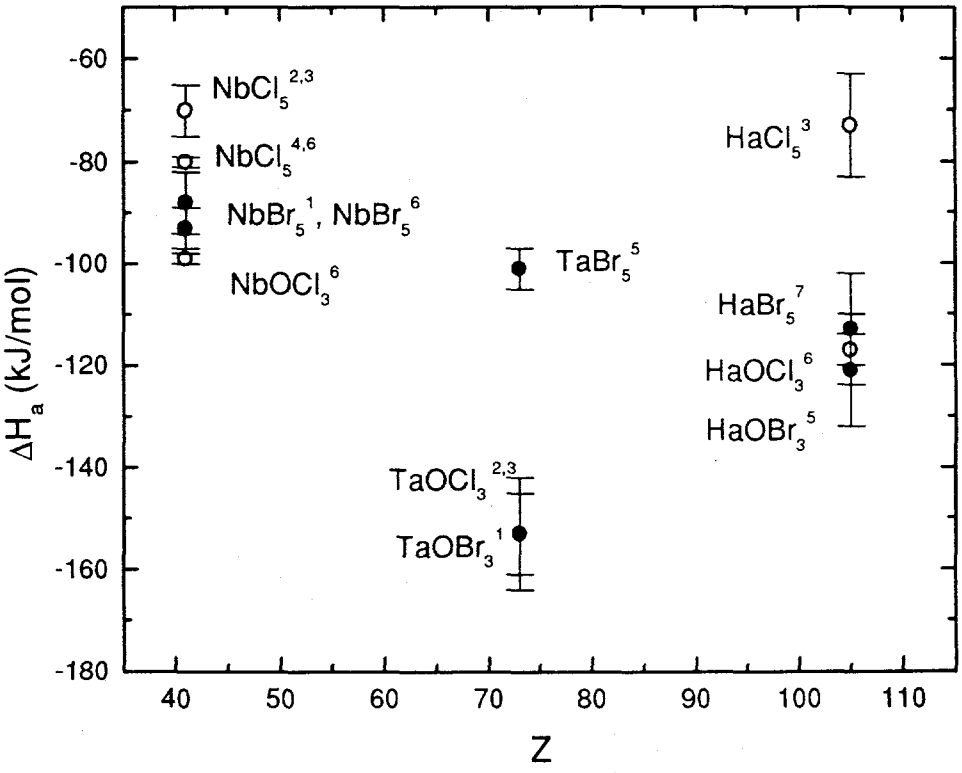

Figure 6-4: Best results of gas chromatography experiments with the group 5 halides and oxyhalides. • = Bromides, o = Chlorides. References given are: [1]this work, [2]Kadkhodayan 96, [3]Kadkhodayan 93, [4]Türler 96a, [5]Türler 96a, data from Gäggeler 92 reanalysed, [6]Türler 96b, [7]Gäggeler92.

6.2 Future Work

Preliminary work with HEVI to convert the gas chromatograph from an isothermal system to a thermochromatography system needs to be continued. This research will ultimately allow a comparison between volatility temperatures observed using the two methods which should permit an evaluation of the systematic errors often inherent in using different instrumental approaches.

The latest experiments performed by Adams et. al. [Adams 98] with HEVI have begun to explore the gas phase properties of the "pseudo-homologs" Th, Pa, U, Np, and Pu. These actinides are known to have stable +4, +5, and +6 oxidation states and are expected to form halogenated compounds similar to those found with the group 4, 5, and 6 elements. Np pentabromides and oxybromides have been studied using HEVI and proposals to study the other light actinides have been made. In addition to determining whether these elements form compounds with volatilities similar to the group 4, 5, and 6 compounds, the large variation in half-lives among isotopes of the same actinide element make these elements ideally suited for the preliminary comparisons of the resultss from isothermal chromatography vs. thermochromatography techniques. The longer-lived isotopes can be used in the thermochromatography studies while shorter-lived isotopes of the same element may be studied on-line with isothermal chromatography.

Ongoing attempts to design chemical systems to study the properties of elements 107 and beyond have pointed to the need for continuing study of the gas phase properties of the transactinide homologs in on-line systems such as HEVI. Experiments on the lighter group 7 homologs, Tc and Re, and the group 8 homologs, Ru and Os, will provide valuable information for designing experiments to study elements 107 and 108.

Continued study of the chemical properties of the transactinide elements with instruments like HEVI provides valuable experience in designing equipment capable of fast, efficient separation, and experiments for the chemical characterization of elements in quantities as small as atoms-at-a-time. In addition these studies should help determine whether the later transactinides show properties similar to their homologs, or whether, as with the actinides, a new place for them based on their chemical properties must be created in the periodic tables of the future.

Appendix I: Monte Carlo Simulation code.

```
'-------------------------------------------------
'MONTE CARLO SIMULATION OF ISOTHERMAL CHROMATOGRAPHY
'USING A MICROSCOPIC MODEL PROPOSED BY I. ZVARA
'
'AUTHOR: ANDREAS TÜRLER
'
'VERSION 1 FOR HEVI
'01/31/92
'-------------------------------------------------
SCREEN 0
CLS

'Declare variables and constants

DIM T(13, 59)
DIM LOSS(13)
DIM MADEIT(13)
CONST Pi = 3.141592653589#  'Nothing else but Pi
CONST M2 = 4.0026           'Molar mass of Helium (amu)
CONST d2 = .147             'Density of Helium
CONST R = 8.31432E+07       'The gas constant (cgs)
```

```
'Read in the actual measured temperature profiles
OPEN "b:\heviprof.txt" FOR INPUT AS #1
FOR X = 0 TO 58 STEP 1
INPUT #1, T(0, X), T(1, X), T(2, X), T(3, X), T(4, X), T(5, X), T(6, X), T(7, X), T(8, X),
T(9, X), T(10, X), T(11, X), T(12, X)
NEXT X
CLOSE 1

'Read in information about molecule
INPUT "Half-life of the nuclide (sec)                    "; T.5
INPUT "Number of molecules for each temperature          "; I
INPUT "The flow rate of He through the column (Torr*l/sec STP)   "; Q
INPUT "The molecular weight of the species, i.e. TaBr5 (amu)     "; M1
INPUT "The density of the species, values from CRC Handbook     "; d1
INPUT " The period of oscillations of the molecule (1.0E-12)     "; p0
INPUT "The enthalpy of adsorption to start with          "; DHaSTART
INPUT "The enthalpy of adsorption to stop with           "; DHaSTOP
INPUT "The step width                                    "; DHaSTEP

Q = Q/760*1000

OPEN "b:\hevi.dat" FOR OUTPUT AS #2
PRINT #2, "Monte Carlo Simulation for HEVI     ";DATE$, TIME$
```

```
PRINT #2, "================================"
PRINT #2,
PRINT #2, "Half-life of the nuclide (sec)              "; T.5
PRINT #2 "Number of molecules for each temperature              "; I
PRINT #2 "The flow rate of He through the column (Torr*l/sec STP)   "; Q
PRINT #2 "The molecular weight of the species, i.e. TaBr5 (amu)     "; M1
PRINT #2 "The density of the species, values from CRC Handbook      "; d1
PRINT #2 " The period of oscillations of the molecule (1.0E-12)     "; p0
PRINT #2 "The enthalpy of adsorption to start with              "; DHaSTART
PRINT #2 "The enthalpy of adsorption to stop with               "; DHaSTOP
PRINT #2 "The step width                                        "; DHaSTEP
PRINT #2,
PRINT #2,

'Loop for different values of Dha
FOR Dha = DHaSTART TO DHaSTOP STEP DHaSTEP
PRINT #2, "Adsorption Enthalpy (kJ/mol)                 "; DHa
PRINT  #2,
PRINT  "Adsorption Enthalpy (kJ/mol)    "; Dha, Time$

'Loop for different temperatures
FOR TX = 1 TO 12
   LOSS(TX) = 0          'The number of nuclides which didn't make it exit
```

```
   MADEIT(TX) = 0        'The number of nuclides which made it to the exit

PRINT "Temperature (ϕC)       "; (TX + 1) * 50

'Loop for I molecules
FOR L = 1 TO I
xi = 0                   'The distance variable in the column (cm)
tt = 0                   'The accumulated time (jump and sit) (s)

'Provide a primer for the random number generator
   RANDOMIZE TIMER

'Generate a random td (Decay Time)
'Since RND actually can be 0 use 1-RND as random number
   td = -T.5/LOG(2) * LOG(1 - RND)

DO

'Generate a random Ni (Jump Length)
'First calculate the Diffusion Coefficient using the Gilliland's equation
   D298 = .0043 * (298.15) ^ 1.5 * SQR(1 / M1 + 1 / M2) / (((M1 / d1) ^ (1 / 3) + (M2 /
d2) ^ (1 / 3))) ^ 2
   D = D298 * ((T(TX, CINT(xi)) + 273.15) / 298.15) ^ 1.75
```

```
'Then calculate N mean
   Nm = 11 * Q (T(TX, CINT(xi)) + 273.15) / 273.15 / (48 * Pi * D)
'Generate random Ni
'Since RND actually can be 0 use 1-RND as random number
   Ni = -Nm * LOG(1 – RND)

'Evaluate the coordinate of the molecule
   xi = xi + Ni

'Calculate the flight time
'Assume that the flight time was Ni/Velocity and Velocity = Qi/Pi*r^2
   tf = 0
   IF xi – Ni > 53 THEN
      tf = 2 * Pi * .002025 * (INT(xi – Ni + 1) – (xi – Ni)) / ((Q * (T(TX, INT(xi – Ni)) +
273.15) / 273.15) + (Q * (T(TX, INT(xi – Ni + 1)) + 273.15) / 273.15
      ELSE
      tf = 2 * Pi * .0841 * (INT(xi – Ni + 1) – (xi – Ni)) / ((Q * (T(TX, INT(xi – Ni)) +
273.15) / 273.15) + (Q * (T(TX, INT(xi – Ni + 1)) + 273.15) / 273.15
   END IF
   FOR Z = INT(xi – Ni + 1) TO INT(xi – 1)
      IF Z > 57 THEN EXIT FOR
      IF Z > 52 THEN
```

```
            tf = tf + 2 * Pi * .002025 / ((Q * (T(TX, Z) + 273.15) / 273.15) + (Q * (T(TX, Z
+ 1) + 273.15) / 273.15))
        ELSE
            tf = tf + 2 * Pi * .0841 / ((Q * (T(TX, Z) + 273.15) / 273.15) + (Q * (T(TX, Z +
1) + 273.15) / 273.15))
        END IF
    NEXT Z
    IF xi > 53 AND xi < 58 THEN
        tf = tf + 2 * Pi * .002025 * (xi – INT(xi)) / ((Q * T(TX, INT(xi)) + 273.15 / 273.15)
+ (Q * (T(TX, INT(xi + 1)) + 273.15) / 273.15
    END IF
    IF xi <= 53 THEN
        tf = tf + 2 * Pi * .0841 * (xi – INT(xi)) / ((Q * (T(TX, INT(xi)) + 273.15 / 273.15)
+ (Q * (T(TX, INT(xi + 1)) + 273.15) / 273.15))
    END IF
    tt = tt + tf

'Check if the nuclide has decayed ?
    IF tt > td THEN
        LOSS(TX) = LOSS(TX) + 1
        EXIT DO
    END IF
```

```
'Check if the molecule has left the column ?
   IF xi > 58 THEN
      MADEIT(TX) = MADEIT(TX) + 1
      EXIT DO
   END IF

'Generate a random time the molecule spent adsorbed
'Calculate t mean
   tm = p0 * 1E-12 * EXP((-Dha * 1E+10) / (R * (T(TX, CINT(xi)) + 273.15)))
   'Calculate vi (mean number of collisions)
   IF xi > 53 THEN
      vi = .045 / (Q * (T(TX, CINT(xi)) + 273.15) / 273.15) * SQR(2 * Pi * R * (T(TX,
CINT(xi)) + 273.15) / M1)
   ELSE
      vi = .29 / (Q * (T(TX, CINT(xi)) + 273.15) / 273.15) * SQR(2 * Pi * R * (T(TX,
CINT(xi)) + 273.15) / M1)
   END IF

'Generate a random ta
'Since RND actually can be 0 use 1-RND as random number
   ta = -vi * tm * Nm * LOG(1 - RND)

'Update total time
```

```
tt = tt + ta

'Check if the nuclide has already decayed?
  IF tt > td THEN
    LOSS(TX) = LOSS(TX) + 1
    EXIT DO
  END IF
  LOOP WHILE tt <= td AND xi <= 58
  NEXT L
 PRINT #2, (TX + 1) * 50, MADEIT(TX), LOSS(TX), (MADEIT(TX) / I) * 100
NEXT TX
PRINT #2,
PRINT #2,
NEXT DHa
CLOSE #2
```

Appendix 2:

Results of all published isothermal gas phase chromatography results for the group 4, 5 and 6 bromides and chlorides, listed by group. Dates of experiments are given where known.

Miscellaneous

Species	-ΔHa(kJ/mol) & Volatility	Halogen agent, aerosol.	Instrument and Date	Reference
$^{211}BiCl_3$	69±4 100°	HCl, MoO_3	HEVI	Kadkhodayan 93[1]
^{218}Po	85, 125°	None	OLGA 3, 2/95	Gärtner 95b
$^{218}PoCl_2$ or $^{218}PoCl_4$	98, 180°	HCl	OLGA 3, 2/95	Gärtner 95b
$^{218}PoOCl_2$	119, 275°	HCl/O_2	OLGA 3, 2/95	Gärtner 95b
$^{218}PoOCl_2$ or $PoCl_4$	125, 315°	$Cl_2/SOCl_2/O_2$	OLGA 3, 2/95	Gärtner 95b
$^{211}Po^mCl_4$	74±5 150°	HCl, MoO_3	HEVI	Kadkhodayan 93[1]
$^{221}FrBr$	≤160, 550°	HBr, KBr	HEVI, 9/96	This work
$^{211}BiBr_3$	84±5 150°	HBr, KBr	HEVI, 9/96	This work

Group IV

Species	-ΔHa (kJ/mol) & Volatility	Halogen agent, Aerosol	Instrument	Reference
$^{98}ZrCl_4$	69±6, 120°C	Cl_2/CCl_4, MoO_3	HEVI	Kadkhodayan 93
$^{98}ZrCl_4$	74±5, 120°C	Cl_2/CCl_4, MoO_3	HEVI	Kadkhodayan 96
$^{98}ZrBr_4$	91±6, 198°C	HBr, MoO_3	HEVI	Kadkhodayan 93
$^{95}ZrBr_4$	108±5, 250°C	HBr, KBr	HEVI, 2/97	This work
$^{167}HfBr_4$	<117, >300°C	HBr, KBr	HEVI, 6/96	This work
$^{166}HfBr_4$	113±5, 300°C	HBr, KBr	HEVI, 11/96	This work
$^{167}HfBr_4$	113±5, 300°C	HBr, KBr	HEVI, 11/96	This work
$^{165?}HfCl_4$	96±5, 225°C	HCl/CCl_4, MoO_3	HEVI	Kadkhodayan 93[1]
$^{165}HfCl_4$	230°C	HCl, C &CsCl	OLGA 3	Türler 97b
$^{165}HfOCl_2$	≥400°C	$Cl_2/SOCl_2,O_2$ (20ml/m), C&CsCl	OLGA 3	Türler 97b
$^{261}RfCl_4$	77±6, 124°C	HCl, MoO_3	HEVI	Kadkhodayan 93[1]
$^{261}RfCl_4$	150°C	HCl, C &CsCl	OLGA 3	Türler 97b
$^{261}RfOCl_2$	410±10°C	$Cl_2/SOCl_2,O_2$ (20ml/m), C&CsCl	OLGA 3	Türler 97b
$^{261}RfBr_4$	87±7, 175°C	HBr, KBr	HEVI, 2/93	This work

[1]Also conforms to values given in [Kadkhodayan 96].

Group V

Species	$-\Delta H_a$ (kJ/mol) and Volatility	Halogen agent, aerosol	Instrument and Date	Reference
$^{99g}NbCl_5$	70±1, 130°	Cl_2/CCl_4, MoO_3	HEVI	Kadkhodayan 93
$^{99g}NbCl_5$	80±1, 150°	HCl, C	Olga 3 1993	Türler 96b
$^{99g}NbBr_5$	89±5, 210°	HBr, MoO_3	HEVI	Kadkhodayan 93
$^{87}Nb^mBr_5$	86±6, 175°	HBr, KBr	HEVI, 2/97	This work
$^{88}NbBr_5$	103±5, 225°	HBr, KBr	HEVI, 6/96	This work
$NbBr_5$	93±4	HBr		Nai-Qi 89
$^{99g}NbOCl_3$	99±1, 250°	HCl, C	Olga 3 1993	Türler 96b
$^{166}TaBr_5$	88±4, 190°	HBr/BBr_3, KCl	Olga 2	Gäggeler 92[2]
$^{167}TaOCl_3$	153±11, 450°	HCl/CCl_4, MoO_3	HEVI	Kadkhodayan 93
$^{166}TaOBr_3$	153±8, 525°	HBr, KBr	HEVI, 11/94	This work
$^{262}HaCl_5$	73±10, 160°	Cl_2/CCl_4, MoO_3	HEVI	Kadkhodayan 93
$^{262,263}HaCl_5$	≥97, 200°	HCl, C	Olga 3 1993	Türler 96b
$^{262,263}HaOCl_3$	117±3, 300°	HCl, C	Olga 3 1993	Türler 96b
"^{262,263}Ha w/HBr"	113±11, 320° 121±11, 320°	HBr/BBr_3, KCl	Olga 2	Gäggeler 92, Gäggeler 92[2]

[2]Values shown are from [Türler 96b] but reanalysed from the data from this reference.

Group VI

Species	$-\Delta Ha$ (kJ/mol) and Volatility	Halogen agent, aerosol	Instrument and Date	Reference
$^{104}MoO_2Cl_2$	90, 175°	O_2/Cl_2, C	OLGA 3, 2/95	Türler 95a
$^{167}WO_2Cl_2$	100, 240°	O_2/Cl_2, C	OLGA 3, 2/95	Gärtner 95a
$^{168}WO_2Cl_2$	96, 225°	$Cl_2/SOCl_2,O_2$ (2ml/m)	OLGA 3	Gäggeler 97
$^{265,266}SgO_2Cl_2$	115±20, 250-325°	$Cl_2/SOCl_2,O_2$ (2ml/m)	OLGA 3	Gäggeler 97

References

[Adams 98] Adams, J, private communication.

[Alonso 73] Alonso, J., Gmelin Handbuch der Anorganischen Chemie, Band 7b, Part A1, Verlag Chemie, GmbH Weinheim/Bergstrasse, 1973.

[Atkins 86] Atkins, P. W., Physical Chemistry, Oxford University Press, New York, p 770-777 (1986)

[Aumann 74] Aumann, D. C., Müllen, G., Nucl. Instr. Meth. **115**, 75 (1974).

[Averill 73] Averill, F. W., Ellis, D. E., J. Chem. Phys. **58**, 2088 (1973).

[Barner 78] Barner, H. E., Scheuerman, R. V., Handbook of Thermochemical Data For Compounds And Aqueous Species, John Wiley & Sons, New York, 1978.

[Belov 75] Belov, V. Z., Zvarova, T. S., Rhalaevskii, M. R., tr. from Radiokhimiya, **17**, No.1, 86 (1975).

[Bethe 29] Bethe, H., Ann. Phys. (Leipz) **3**, 133 (1929).

[Brüchle 86] Brüchle, W., Agarwal, Y. L., Armbruster, P., Brügger, M., Dufour, J. P., Gäggeler, H., Hessberger, F. P., Hofmann, S., Lemmertz, P., Münzenberg, K., Poppensieker, K., Reisdorf, W., Schädel, M., Schmide, K.-H., Schneider, J. H. R., Schneider, W. F. W., Sümerer, K., Vermeulen, D., Wirth, G., Ghiorso, A., Gregorich, K., Lee, D., Leino, M., Moody, K. J., Seaborg, G. T., Welch, R. B., Wilmarth, P., Yashita, S., Frink, C., Greulich, N., Herrmann, G., Hickmann, U., Hildebrand, N., Kratz, J. V., Trautmann, N., Fowler, M. M., Hoffman, D. C., Daneils, W. R., von Gunten, H. R., Dornhöfer, H., J. Less Comm. Metals, **122**, 425 (1986).

[Canterford 68] Canterford, J. H., Colton, R., Halides of the Second and Third Row Transition Metals, John Wiley & Sons, London, 1968.

[Eichler 78] Eichler, B. (listed as B. Aikhler), Mal'tseva, N. S., tr. from Radiokhimiya, **20**, 89, Jan-Feb (1978).

[Eichler 82] Eichler, B., Zvara, I., Radiochimica Acta **30**, 233 (1982).

[Eichler 94] Eichler, B., Türler, A., Jost, D. T., Gäggeler, H. W., PSI Condensed Matter Research and Material Sciences Progress Report 1993, Annex IIIA Annual Report, Villigen, p. 97 (1994).

[Eichler 96] Eichler, R., Gäggeler, H. W., Eichler, B., Türler, A., PSI Heavy Elements Annual Report, Villigen, p. 38 (1996).

[Ellis 84] Ellis, D. E., Goodman, G. L., Int. J. Quantum Chem., **25**, 185 (1984).

[Evans 72] Evans, J. E., Lougheed, R. W., Coops, M. S., Hoff, R. W., Hulet, E. K., Nucl. Instr. Meth. **102**, 389 (1972).

[Firestone 96] Firestone, R., Shirley, V., eds., Table of Isotopes, Eighth Edition, John Wiley & Sons, Inc., New York, 1996.

[Fischer 77] Fischer, C. F., The Hartree-Fock Method for Atoms, John Wiley & Sons, Inc. New York, 1977.

[Freeman 85] Freeman, A. J., Lander, G. H., eds. Handbook in the Physics and Chemistry of the Actinides Vol 2, Elsevier, Amsterdam, p1-27 (1985)

[Fricke 69] Fricke, B., and Greiner, W., Phys. Lett. **30B**, 347 (1969).

[Gäggeler 91] Gäggeler, H. W., Jost, D. T., Baltensperger, U., Weber, A., Kovacs, A., Vermeulen, D., Türler, A., Nucl. Instr. and Meth. **A309** 201 (1991).

[Gäggeler 92] Gäggeler, H. W., Jost, D. T., Kovacs, J., Scherer, U. W., Weber, A., Vermeulen, D., Türler, A., Gregorich, K. E., Henderson, R. A., Czerwinski, K. R., Kadkhodayan, B., Lee, D. M., Nurmia, M., Hoffman, D. C., Kratz, J. V., Gober, M. K., Zimmerman, H. P., Schädel, M., Brüchle, W., Schimpf, E., Zvara, I., Radiochim. Acta **57**, 93 (1992).

[Gäggeler 97a] Gäggeler, H. W., Proc. ACTINIDES-97, Baden-Baden (1997).

[Gäggeler 97b] Gäggeler, H. W., PSI Report, PSI-PR-97-19 (1997).

[Gärtner 95a] Gärtner, M., Gäggeler, H. W., Dressler, R., Jost, D. T., Eichler, B., Türler, A., PSI Annual Report, Villigen, 29 (1995).

[Gärtner 95b] Gärtner, M., Gäggeler, H. W., Hälberli, A., Türler, A., Eichler, B., PSI Annual Report, Villigen, 31 (1995).

[Ghiorso 70] Ghiorso, A., Nurmia, M., Eskola, D., Eskola, P., Phys. Let., **32B**, 95 (1970)

[Glebov 89] Glebov, V.A., Kastztura, L., Nefedov, V.S., and Zhuikov, B.L., Radiochim. Acta **46**, 117 (1989).

[Grant 70] Grant, I. P., Adv. Phys. **19**, 747 (1970).

[Grant 86] Grant, I. P., Aust. J. Phys. **39**, 649 (1986).

[Grant 88] Grant, I. P., Quiney, H. M., Adv. At. Mol. Phys. **21**, 37 (1988).

[Gregorich 91] Gregorich, K. E., Nucl. Instr. Meth., **A302**, 135 (1991).

[Herrmann 82] Herrmann, G., Trautmann, N., Ann. Rev. Nucl. Part. Sci. **32** (1982).

[D Hoffman 80] Hoffman, D. C., Lee, D., Ghiorso, A., Nurmia, M., Aleklett, K., Phys. Rev. C, **22**, 1581 (1980).

[D Hoffman 81] Hoffman, D. C., Lee, D. M., Ghiorso, A., Nurmia, M. J., Alekett, K., Leino, M., Phys. Rev. C, **24**, 495 (1981).

[D Hoffman 96] Hoffman, D. C., Proc. NATO Advanced Study Institute on "Actinides and the Environment", 3-22 (1996).

[D Hoffman 97] Hoffman, D. C, Lawrence Berkeley National Laboratory Report # 40908, Nuclear Science Division (1997).

[S Hofmann 95] Hofmann, S., Ninov, V., Heßberger, F. P., Armbruster, P., Folger, H., Münzenberg, G., Schött, H. J., Popeko, A. G., Yeremin, A. V., Andreyev, A. N., Saro, S., Janik, R., Leino, M., Z. Phys. **A 350**, 281 (1995).

[S Hofmann 96] Hofmann, S., Ninov, V., Heßberger, F. P., Armbruster, P., Folger, H., Münzenberg, G., Schött, H. J., Popeko, A. G., Yeremin, A. V., Andreyev, A. N., Saro, S., Janik, R., Leino, M., Z. Phys. **A 354**, 229 (1996).

[Holstein 97] Holstein, B. R., Am. J. Phys., **65** (6), 519 (1997)

[Horowitz 69] Horowitz, E. P., Bloomquist, C. A. A., Henderson, D. J., Nelson, D. E. J., Inorg. Nucl. Chem. **31**, 3255 (1969).

[Hübener 94] Hübener, S., Eichler, B., Schädel, M., Brüchle, W., Gregorich, K. E., Hoffman, D. C., J. All. Comp. **213**/13, 429 (1994).

[Hudson 92] Hudson, J., The History of Chemistry, Chapman & Hill, New York, 1992.

[Ionova 92] Ionova, G. V., Pershina, V., Johnson, E., Fricke, B., Schädel, M., J. Phys. Chem. **96**, 11096 (1992).

[IUPAC 97] Inorganic Chemistry Division Commission on Nomenclature of Inorganic Chemistry, Pure & Appl. Chem, **69**, 2471 (1997).

[Jost 91] Jost, D. T., Vermeulen, D., Proc. 7th Conf. "REAL TIME '91" June (1991) .

[Kadkhodayan 92] Kadkhodayan, B., Türler, A., Gregorich, K. E., Nurmia, M. J., Lee, D. M., Hoffman, D. C., Nucl. Instr. and Meth. **A317** 254 (1992).

[Kadkhodayan 93] Kadkhodayan, B., Ph.D. thesis, University of California, Berkeley, (1993).

[Kadkhodayan 96] Kadkhodayan, B., Türler, A., Gregorich, K. E., Baisden, P. A., Czerwinski, K. R., Eichler, B., Gäggeler, H. W., Hamilton, T. M., Jost, D. T., Kacher, C. D., Kovacs, A., Kreek, S. A., Lane, M. R., Mohar, M. F., Neu, M. P., Stoyer, N. J., Sylwester, E. R., Lee, D. M., Nurmia, M. J., Seaborg, G. T., Hoffman, D. C., Radiochim. Acta **72**, 169 (1996).

[Kelly 85] Kelly, H. P., Kim, Y. -K., eds. AIP Conf. Proc. No. 136, American Instutute of Physics, New York, 1985

[Knacke 91] Knacke, O., Kubachevski, Hesselman, Thermochemical Properties of Inorganic Subststances II, Springer-Verlag, Berlin (1991).

[Kratz 92] Kratz, J. V., Gober, M. K., Zimmerman, H. P., Schädel, M., Brüchle, W., Schimpf, E., Gregorich, K. E., Türler, A., Hannink, N. J., Czerwinski, K. R., Kadkhodayan, B., Lee, D. M., Nurmia, M. J., Hoffman, D. C., Gäggeler, H. W., Jost, D., Kovacs, J., Scherer, U. W., Weber, A., Phys. Rev. C. **45**, 1064 (1992).

[de Lang 89] de Lang, O. L., Am. J. Phys., **57** (10), 883 (1989).

[Laub 78] Laub, R. J., Pecsok, R. L., Physicochemical Applications of Gas Chromatography, John Wiley & Sons, New York, 1978.

[Lazarev 94] Lazarev, Y. A., Lobanov, Y. V., Oganessian, Y. T., Utyonkov, V. K., Abdullin, F. S., Buklanov, G. V., Gikal, B. N., Iliev, S., Mezentsev, A. N., Polyakov, A. N., Sedykh, I. M., Shirokovsky, I. V., Subbotin, V. G., Sukhov, A. M., Tsyganov, Y. S., Zhuchko, V. E., Lougheed, R. W., Moody, K. J., Wild, J. F., Hulet, E. K., McQuaid, J. H., Phys. Rev. Lett. **73**, 924 (1994).

[Leres 87] Leres, R. G., Lawrence Berkeley National Laboratory report # 24808, Engineering division (1987).

[Lide 96] Lide, D. R. ed., The Handbook of Chemistry & Physics, 77th ed., CRC Press, New York, 1996.

[Lindgren 74] Lindgren, I., Rosen, A., Case Stud. At. Phys. **4**, 93 (1974).

[Löwden 72] Löwden, P.-O., ed. Advances in Quantum Chemistry, Academic, New York, 1972.

[MacFarlane 98] MacFarlane, R. D., McHarris, W. M. C., accepted by Nuc Spec. Reac. Vol. A, p244 (not yet in print).

[Malli 83] Malli, G. L., ed., Relativistic Effects in Atoms, Molecules, and Solids, Plenum Press, New York, 1983.

[Malli 92] Malli, G. L., Can. J. Chem., **70**, 421 (1992).

[Malli 96] Malli, G., Private communication.

[Mazumdar 80] Mazumdar, A., Wagner, H., Kraemer, G., Walcher, W., Bruegger, M., Stender, E., Trautmann, N., Lund, T., Nucl. Instrum. Meth. **174**, 183 (1980).

[McMillan 40] McMillan, E. M., Abelson, P. A., Phys. Rev. **57**, 1185 (1940).

[Meyer 88] Meyer, J., Int. J. Quantum Chem., **33**, 445 (1988).

[Meyer 89] Meyer, J., Sepp, W. –D., Fricke, B., Comput. Phys. Comun. **54**, 55 (1989).

[Moore 39] Moore, F. J., A History of Chemistry, McGraw-Hill, New York, 1939.

[Müllen 75] Müllen, G., Aumann, D. C., Nucl. Instr. Meth. **128**, 425 (1975).

[Mulliken 55] Mulliken, R. S., J. Chem. Phys. **23**, 1833 (1955).

[Nai-Qi 89] Ya Nai-Qi, Jost, D. T., Baltensperger, U., Gäggeler, H. W., Radiochim. Acta **47**, 1 (1989).

[Newman 72] Newman, D. J., Taylor, C. D., J. Phys. **B5**, 2332 (1972)

[Pepper 91] Pepper, M., Burstein, B., Chem. Rev. **91** (5), 719 (1991)

[Pershina 92a] Pershina, V., Sepp, W.-D., Fricke, B., Rosén, A., J. Chem. Phys. **96** (11), 8367 (1992).

[Pershina 92b] Pershina, V., Sepp, W.-D., Fricke, B., Kolb, D., Schädel, M., Ionova, G. V., J. Chem. Phys **97** (2), 1116 (1992).

[Pershina 92c] Pershina, V., Sepp, W.-D., Bastug, T., Fricke, B., Ionova, G. V., J. Chem. Phys. 97 (11), 1123 (1992).

[Pershina 93] Pershina, V., Fricke, B., J. Chem. Phys., **99**, 9720 (1993).

[Pershina 94a] Pershina, V., Fricke, B., Ionova, G. V., Johnson, E., J. Phys. Chem., **98** 1482 (1994).

[Pershina 94b] Pershina, V., Fricke, B., J. Phys. Chem, **98**, 6468 (1994).

[Pershina 94c] Pershina, V., Fricke, B., Kratz, J. V., Ionova, G. V., Radiochem. Acta. **64**, 37 (1994).

[Pershina 94d] Pershina, V., Fricke, B., Radiochim. Acta, **65**, 13 (1994).

[Pershina 94e] Pershina, V., Fricke, B., Ionova, G. V., J. Alloys Compd. **213/214**, 33 (1994).

[Pershina 95] Pershina, V., Fricke, B., J. Phys. Chem., **99**, 144 (1995).

[Pershina 96a] Pershina, V., Chem. Rev. **96**, 1977 (1996).

[Pershina 96b] Pershina, V., Fricke, B., J. Phys. Chem. **100**, 8748 (1996).

[Pershina 97] Pershina, V., Proc. 41st R. A. Welch Conf. on the Transactinide Elements, Houston, Texas, 167 (1997).

[Pitzer 75] Pitzer, K. S., J. Chem. Phys., **63**, 1032 (1975).

[Pyykkö 79] Pyykkö, P., Desclaux, J-P., Acc. Chem. Res. **12**, 276 (1979).

[Pyykkö 84] Pyykkö, P., ed. Int. J. Quantum Chem. **25**(1), 1 (1984).

[Pyykkö 86] Pyykkö, P., Lect. Notes Chem. 41 (1986).

[Pyykkö 88] Pyykkö, P., Chem. Rev. **88**, 563 (1988).

[Rose 78] Rose, S. J., Grant, I. P., Pyper, N. C., J. Phys. B: At. Mol. Phys. **11**, 1171 (1978).

[Rosen 74] Rosen, A., Ellis, D. E., Chem. Phys. **27**, 595 (1974).

[Rosen 75] Rosen, A., Ellis, D. E., J. Chem. Phys. **62**, 3039 (1975).

[Rosen 78] Rosen, A., Int. J. Quantum Chem. **13**, 509 (1978).

[Routti 69] Routti, J.T., Prussin, S. G., Nucl. Inst. Meth., **72**, 125 (1969).

[Rudolph 78a] Rudolph, J., Bächman, K., Steffen, A., Tsalas, S., Mikrochimica Acta [Wien] **I**, 471 (1978).

[Rudolph 78b] Rudolph, J., Bächmann, K., J. Rad. Chem. **43**, 113 (1978).

[Rudolph 79a] Rudolph, J., Bächman, K., J. Chrom., **178**, 459 (1979).

[Rudolph 79b] Rudolph, J., Bächmann, K., Mikrochim. Acta **I**, 477 (1979)

[Rudolph 80] Rudolph, J., Bächman, K., J. Chrom., **187**, 319 (1980).

[Schaedel 88] Schaedel, M., Brüchle, W., Haefner, B., Nucl. Instrum. Methods **A 264**, 308 (1988)

[Schädel 97a] Schädel, M., Brüchle, W., Dressler, R., Eichler, B., Gäggeler, H. W., Günther, R., Gregorich K. E., Hoffman, D. C., Hübener, S., Jost, D. T., Kratz, J. V., Paulus, W., Schumann, D., Timokhin, S., Trautmann, N., Türler, A., Wirth, G., Yakushev, A., Nature **388**, 55 (1997).

[Schädel 97b] Schädel, M., Brüchle, W., Schausten, B., Schimpf, E., Jäger, E., Wirth, G., Günther, R., Kratz, J. V., Paulus, W., Seibert, A., Thörle, P., Trautmann, N., Zauner, S., Schumann, D., Andrassy, M., Misiak, R., Gregorich, K. E., Hoffman, D. C., Lee, D. M., Sylwester, E. R., Nagame, Y., Oura, Y., Radiochim. Acta **77**, 149 (1997).

[Schwyn 88] Schwyn, S., Garwin, E., Schmitt-Ott, A., J. Aerosol. Sci. **19**, 639 (1988).

[Seaborg 46] Seaborg, G. T., Wahl, A. C., Kennedy, J. W., Phys. Rev. **69**, 367 (1946).

[Seaborg 90] Seaborg, G. T., Loveland, W. D., The Elements Beyond Uranium. John Wiley & Sons, Inc. (1990).

[Stober 88] Stober, J., Diploma thesis, ETH Zürich (1988), unpublished.

[Taut 96] Taut, St., Hübener, S., Eichler, B., Gäggeler, H. W., Timokhin, S. N., Zvara, I., PSI Heavy Elements Annual Report, Villigen, p. 41 (1996).

[Tinkham 64] Tinkham, M., Group Theory and Quantum Mechanics, McGraw-Hill, New York, 1964.

[Trautmann 75] Trautmann, N., Aronson, P. O., Bjørnstad, T., Kaffrell, N., Krale, E.,Sharestad, M., Skarnemark, G., Stender, E., Inorg. Nucl. Chem. Lett. **11**, 729 (1975).

[Trigg 97] Trigg, G. L., ed; Heagney, J., Heagney, J., Meyer, H. J., Enc. Appl. Phys. **20** (1997).

[Türler 91a] Türler, A., Gregorich, K. E., Hoffman, D. C., Lee, D. M., Gäggeler, H. W., Lawrence Berkeley National Laboratory Annual Report #31855, Nuclear Science Division (1991).

[Türler 91b] Türler, A., Gäggeler, H. W., Gregorich, K. E., Barth H., Brüchle, W., Czerwinski, K. R., Gober, M. K., Hannink, N. J., Henderson, R. A., Hoffman, D. C., Jost, D. T., Kacher, C. D., Kadkhodayan, B., Kovacs, J., Kratz, J. V., Kreek, S. A., Lee, D. M., Leyba, J. D., Nurmia, M. J., Schädel, M., Scherer, U. W.,

Schimpf, E., Vermeulen, D., Weber, A., Zimmermann, H. P., Zvara, I., Lawrence Berkeley National Laboratory annual report #31442, Nuclear Science Division (1991).

[Türler 92a] Türler, A., Gregorich, K. E., Hoffman, D. C., Lee, D. M., Gäggeler, H. W., PSI Condensed Matter Research and Material Sciesnces Progress Report, 1991, Villigen, p 68 (1992).

[Türler 92b] Türler, A., Gäggeler, H. W., Gregorich, K. E., Barth H., Brüchle, W., Czerwinski, K. R., Gober, M. K., Hannink, N. J., Henderson, R. A., Hoffman, D. C., Jost, D. T., Kacher, C. D., Kadkhodayan, B., Kovacs, J., Kratz, J. V., Kreek, S. A., Lee, D. M., Leyba, J. D., Nurmia, M. J., Schädel, M., Scherer, U. W., Schimpf, E., Vermeulen, D., Weber, A., Zimmermann, H. P., Zvara, I., J. Radioanal. Nucl. Chem. **160**, 327 (1992).

[Türler 94] Türler, A., Eichler, B., Jost, D. T., Gäggeler, H. W., PSI Condened Matter Research and Material Sciences Progress Report 1993, Villigen, p 97 (1994).

[Türler 95a] Türler, A., Eichler, B., Jost, D. T., Piguet, D., Gäggeler, H. W., Mendel, M., Nähler, A., Eberhardt, K., Trautmann, N., PSI annual report 1994, Villigen, p 41 (1995).

[Türler 95b] Türler, A., Eichler, B., Jost, D. T., Piguet, D., Gäggeler, H. W., Hübener, S., Boettger, M., Grantz, M., PSI annual report 1994, Villigen, p 28 (1995).

[Türler 96a] Türler, A., Radiochim. Acta **72**, 7 (1996).

[Türler 96b] Türler, A., Eichler, B., Jost, D. T., Piguet, D., Gäggeler, H. W., Gregorich, K. E., Kadkhodayan, B., Kreek, S. A., Lee, D. M., Mohar, M., Sylwester, E. R., Hoffman, D. C. Hübener, S., , Radiochim. Acta **73**, 55 (1996).

[Türler 97a] Türler, A., Private communication.

[Türler 97b] Türler, A., Presentation, *Actinides 97* session T5-A5, Baden-Baden, October 97.

[Vahle 96] Vahle, A., Hübener, S., Dressler, R., Eichler, B., Türler, A., PSI Heavy Elements Annual Report, Villigen, p. 43 (1996).

[Vogt 96] Vogt, A., Gäggeler, H. W., Türler, A., PSI Heavy Elements Annual Report, Villigen, p. 39 (1996).

[Wigner 59] Wigner, E. P., Group Theory and its Application to the Quantum Mechanics and Atomic Spectra, Academic, New York, 1959.

[Zvara 66] Zvara, I., Chuburkov, Y. T., Caletka, R., Zvarova, T. S., Shalaevsky, M. R., Shilov, B. V., At. Energ. **21**, 83 (1966).

[Zvara 69] Zvara, I., Chuburkov, Y. T., Caletka, R., Shalaevsky, M. R., tr. from Radiokhimiya **11**, 163 (1969).

[Zvara 70] Zvara, I., Belov, V. Z., Korotkin, Y. S., Shalaevskii, M. R., Shchegolev, V. A., Yussonnua, M., Zager, B. A., Reports of the United Institute of the Nuclear Reasearch [in Russian], R12 -5120, Dubna (1970)

[Zvara 76] Zvara, I., Belov, V. Z., Domanov, V. P., Shalaevskii, M. R., tr. from Radiokhimiya, **18,** No.3, 371, May-June (1976).

[Zvara 85] Zvara, I., Radiochimica Acta **38**, 95 (1985).